UNIVERSITY OF SOUTHAMPTON

FACULTY OF SCIENCE

School of Ocean and Earth Sciences

The Minimum Length-Scale of Oceanic Phytoplankton Distributions

by

Paula McLeod

Thesis submitted for the degree of Doctor of Philosophy

March 2004

Graduate School of the

Southampton Oceanography Centre

This PhD dissertation by

Paula McLeod

has been produced under the supervision of the following persons

Supervisor/s:

Dr. Adrian P. Martin,

Prof. Michael J.R. Fasham FRS.

Dr. Kelvin. J. Richards

Chair of Advisory Panel:

Prof. Harry L. Bryden

Member/s of Advisory Panel:

Prof. J.G. Shepherd FRS.

Examiners:

Prof. John Brindley

Dr. Meric Srokosz

The Blind Men and the Elephant
John Godfrey Saxe

It was six men a Hindustan,
To learning much inclined,
Who went to see the Elephant,
(Though all of them were blind):
That each by observation
Might satisfy his mind.

The FIRST approached the elephant,
And happening to fall
Against his broad and sturdy side,
At once began to bawl:
"Bless me, it seems the elephant
Is very like a wall."

The SECOND feeling of his tusk,
Cried, "Ho! What have we here
So very round and smooth and sharp?
To me 'tis mighty clear
This wonder of an Elephant
Is very like a spear."

The THIRD approached the animal,
And happening to take
The squirming trunk within his hands,
Then boldly up and spake:
"I see" quoth he, "The Elephant
Is very like a snake."

The FOURTH stretched out his eager hand
And felt about the knee,
"What most this mighty beast is like
Is mighty plain" quoth he;
"'Tis clear enough the Elephant Is very like a tree."

The FIFTH who chanced to touch the ear
Said "Even the blindest man
Can tell what this resembles most;
Deny the fact who can,
This marvel of an Elephant is very like a fan."

The SIXTH no sooner had begun
About the beast to grope,
Than, Seizing on the swinging tail
That fell within his scope,
" I see," cried he, "The Elephant
Is very like a rope."

And so these men of Hindustan
Disputed loud and long,
Each in his own opinion
Exceedingly stiff and strong,
Though EACH was PARTLY in the right
AND ALL WERE IN THE WRONG!

UNIVERSITY OF SOUTHAMPTON

ABSTRACT

FACULTY OF SCIENCES
SCHOOL OF OCEAN & EARTH SCIENCES

Doctor of Philosophy

MINIMUM LENGTH-SCALE OF OCEANIC PHYTOPLANKTON DISTRIBUTIONS

by Paula McLeod

Starting from the simplest approximations a hierarchy of numerical models is developed with the intention of improving understanding of how biological and physical mechanisms interact in producing observed structure in plankton patches. Specifically how small scale mixing, strain and growth combine in determining the minimum equilibrium length-scale of phytoplankton filaments.

We expand upon a previous study of an exponentially growing tracer in a uniform strain flow to investigate the behaviour of a logistic tracer, a more appropriate approximation of bulk phytoplankton population dynamics. A new equation to describe the minimum expected length-scale is derived. The effect of explicit nutrient representation is also considered. This is not found to affect patch size, although a striking effect on cross-sectional profile is observed under certain conditions.

We test the derived formula in a more realistic and hence more complex physical environment (a two-dimensional turbulent flow). We investigate inert and logistic growth tracer dispersal and consider the effectiveness of the previously derived formula for predicting minimum length-scales. In addition to inert and logistic growth tracer models we also consider a more sophisticated ecosystem model and assess the propriety of using a logistic tracer for investigations of mesoscale phytoplankton patchiness.

An aside is taken to determine the best measure of strain when investigating plankton patch dynamics. A comparison is made of techniques used in comparable previous studies of tracer dynamics and recommendations made for future investigations. Errors resulting from mis-sampling of the tracer field are also considered. These results are intended to provide recommendations when considering oceanic tracer dispersal and calculation of mixing parameterisations.

The 'best case' scenario is investigated throughout hence all results provide a robust upper limit of what is possible observationally.

List of Tables

All tables are contained in a section towards the end of the thesis.

Chapter 4

Chapter 5

Chapter 6

Chapter 7

List of Figures

All figures are contained in a section towards the end of the thesis.

Chapter 1

Chapter 2

Chapter 3

Chapter 4

Chapter 5

Chapter 6

Chapter 7

Acknowledgements

First and foremost I wish to acknowledge Dr. Adrian Martin. Constant guidance, encouragement and inspiration has resulted in the completion of a set of works which is useful and of which I can be proud. Repeated readings and guidance as to use of the English language has ensured I can convey this to others.

I also wish to acknowledge Prof. Harry Bryden and Prof. Mike Fasham for their guidance and encouragement throughout the PhD. Additional thanks to Dr. Kelvin Richards for helping me embark on this PhD and determine a topic of investigation in an expansive subject area.

There have been many people at SOC that I have benefited greatly from discussion with. The most prominent of those who I have worked with are Katya Popova and John Allen. There have been many other with whom I have discussed various matters, and received sound advice from. Peter Challenor, and Paulo Cippolini have been of most help in devising analysis techniques, James Harle for explaining how to put them into practise.

Outside of direct scientific advice there have been even more people who I should acknowledge. To prevent an expansive list I shall acknowledge those at the edges of the time line: from James through to Sophie Pendlebury and all the people in-between.

The thesis as a whole was funded by a NERC studentship: GT04/99/MS/262. NERC also inadvertently funded two cruises as part of the Marine Productivity Thematic, a fantastic opportunity. Generous funding from the US-JGOFS committee allowed attendance of a greatly beneficial conference trip.

My parents, Christine and Ian McLeod, have been a constant source of support, perspective and extra funding! They created a foundation for an interest in science, an inquisitive yet guarded attitude (some say awkward), and a definite tenacity to whatever I start.

I should acknowledge the advice of my Gran, Hetty McLeod. For reminding me throughout that there is life outside of a PhD, until among her final words to me insisting that I finish no matter what else. I did.

Last but by no means least, Bob Keogh. He helped me through my first sea-going experience and has not stopped since. To say thank-you is not enough. His support and encouragement is beyond invaluable and has ensured I have reached this point with a smile.

CHAPTER 1: General Introduction

Patchiness or spatial heterogeneity is an undisputed, ubiquitous feature of oceanic plankton distributions (e.g. Bainbridge, 1957; Fasham, 1978; Mackas *et al.*, 1985). Scales of observed structure range from centimetres to hundreds of kilometres (Haury *et al.*, 1978). The characteristics of patchiness, such as spatial extent, intensity and biodiversity, can be critical factors in determining a population's dynamics, crucial to the creation and persistence of ecological stability, or the ability to absorb perturbations (Simberloff and Wilson, 1969; Steele, 1974; Smith *et al.*, 1996).

Within the following work simple ecosystem models are investigated in order to improve understanding of the nature of the bio-physical interactions responsible for the size and shape of phytoplankton patches. The nature of tracer dispersal (both inert and reactive) is investigated in a series of numerical models. A hierarchical approach is followed, building upon complexity as understanding is improved. This ensures that the "best case scenario" can be investigated throughout. We start with the simplest model and at each stage of evolution introduce a single new process. In this way the influence of each process can be accurately quantified. This method also allows a "best case" scenario to be followed throughout, taking the approach that minimises error even if this is unfeasible *in-situ*. In this way it is possible to provide a robust upper limit of what is possible observationally.

Within the scope of the thesis attention is restricted to filamental structures: a simple yet commonly observed aspect of mesoscale phytoplankton patchiness. What they are and why they are chosen for investigation is explained below.

1.1 Explanation and Justification

Adopting the Mallorian ethic no further warrant is required but existence. Upon closer inspection a fundamental flaw in reasoning is discovered:

"This is the only irrefutable reason for climbing Everest that I know of... but it didn't work with Mom"

George Leigh Mallory, 1923.

The necessity for further justification is apparent. A brief insight into the motivation for studies of mesoscale phytoplankton distributions is provided prior to an overview of studies of specific relevance to this thesis.

1.1.1 The importance of phytoplankton

Knowledge of the distribution of phytoplankton, the microscopic plants described as the "grass of the ocean", is of vital importance for global concerns such as fisheries and climate studies. With phytoplankton lying at the base of the oceanic food chain knowledge of their distribution is of particular importance in assessing the food supply, and so in part the survival chances, for young fish (Parsons *et al.*, 1984). An equally essential role of phytoplankton is in the determination of biogeochemical fluxes, with much current interest centred on Carbon Dioxide (CO_2). Through primary production (the production of new biomass from inorganic matter) phytoplankton have a large impact on CO_2 concentration in the surface ocean and hence the atmosphere by fixing CO_2 into biological "particles". Chemical and biological aggregation of these particles result in larger particles which can sink to the deep ocean (below the euphotic zone past where primary production no longer occurs) until they are biologically transformed or they reach the ocean bottom. The two stage carbon sequestration (growth and sedimentation) by plankton, known as the "biological pump", has the potential to remove large quantities of carbon from the atmosphere-surface ocean and to ensure its extraction to a relatively inert store for geological timescales. The magnitude and location of the downwards fluxes is dependent

firstly upon the coagulation of the biological particles (Jackson and Burd, 1998), which has primarily bio-chemical controls (Jackson and Burd, 2002), but also upon the physical scale of the phytoplankton patches (Waite and Johnson, 2003). Attention here is restricted to the latter: obtaining an understanding of the controls on the spatial extent of phytoplankton patches.

1.1.2 The importance of mesoscale patchiness

Most ecological environments are sub-divided or patchy (Cassie, 1963; Hassel *et al.*, 1991) and the ocean is no exception. Planktonic patchiness or heterogeneity in both the temporal and spatial planes has been widely documented since the earliest days of oceanic exploration, (see e.g. Bainbridge (1957) for a summary of early literature). Spatial heterogeneity is a crucial factor in a population's dynamics and may be critical to the creation and maintenance of ecological stability, or the ability to absorb perturbations (Simberloff and Wilson, 1969). Temporal scales of phytoplankton patchiness vary from the order of minutes to millennia, while spatial scales range from basin wide to a few centimetres (Haury *et al.*, 1978; Bennett and Denman, 1985). Observed plankton heterogeneity results from heterogeneity in both the underlying physical field and from variable biological processes. The balance of mechanisms responsible for the observed heterogeneity vary with scale.

The mesoscale, of order 1-100 kilometres spatially and of order days temporally, is perhaps the most variable of scales when considering open ocean dynamics in terms of observed distributions and their longevity. The existence of mesoscale physical features (notably eddies, fronts and regions of high strain) is evident in many remotely sensed images of sea surface temperature and more relevantly in Chlorophyll *a*, the principal phytoplankton biomarker (Jeffrey and Mantoura, 1997). The stirring induced by the highly variable velocities observed in such regions is known to have a major effect on the

distributions of water mass tracers, such as temperature, and also on phytoplankton. An example of the patchiness induced by such mesoscale processes is shown in figure 1.1. Of ecological relevance, spatial heterogeneity in phytoplankton patches has the potential to greatly increase production with estimates ranging up to six times the level resulting from initially homogeneous distributions (McGillicuddy *et al.*, 1998; Siegel *et al.*, 1999; Martin *et al.*, 2002; Brentnall *et al.*, 2003). At mesoscale spatial scales, phytoplankton can be regarded as passive: they are moved as dictated by the dynamics of the local flow. It should be remembered however that phytoplankton are reactive. Although moved by the water mass there are additional biological mechanisms responsible for plankton patchiness. The co-variability of temperature and chlorophyll spatial spectra (Denman, 1976) was taken for some years as evidence of the physically determined distribution of phytoplankton distributions. However developments in technology and modelling has provided much evidence that mesoscale effects are more complex in origin: bio-chemical processes do indeed have the potential to exert significant influence on observed structure. Furthermore, simple modelling studies indicate that the combination of phytoplankton growth, small scale mixing and advection has the potential for a greater influence on mesoscale phytoplankton distributions than growth or advection can alone. Stirring of phytoplankton or other chemical tracer fields generates different heterogeneity to that expected from stirring of an inert tracer or from reactive dynamics in the absence of stirring (Abraham, 1998; Neufeld *et al.*, 2000). The interaction of variable growth and strain, in particular, has a significant impact upon the biogeochemical properties of water masses, and hence plankton communities, associated with frontal regions, eddies and the intervening regions of high strain (Strass, 1991; McGillicuddy *et al.*, 1998; Oschlies and Garcon, 1998; Abraham *et al.*, 2000; Martin *et al.*, 2001a).

The effects of and evidence for the effect of mesoscale physical controls on phytoplankton distributions have received considerably more attention than the brief introduction given here. For a wider view there are several reviews of observations of

planktonic heterogeneity and the approaches taken to determine and to understand the mechanisms responsible for its appearance (see for example (Bainbridge, 1957; Steele, 1978; Martin, 2003). There are a large array of features and possible causal processes documented for plankton patchiness. Here it is chosen to focus on perhaps what is one of the simplest. What controls the equilibrium width of plankton filaments seen in so many observations (see figure 1.1)? Although a seemingly simple question, the topic is an interesting one for two reasons. First, such features can be seen in one sense as "building blocks" for mesoscale patchiness. They are a fundamental feature of such distributions and yet stlll, it will be argued, poorly and often mistakenly understood. Second, it will be demonstrated that the balance between the three phenomena of biological growth, small-scale mixing (parameterised as effective diffusivity) and gradients in the advecting velocity field yields a rich variety of behaviour even in so simple a setting. This conveys a clear and stark message to be extremely careful to avoid the frequent simplistic interpretation often applied to much more complex situations.

1.1.3 The importance of length-scale

We have already mentioned that length-scale of phytoplankton heterogeneity may have implications for estimates of surface ocean export fluxes (Waite and Johnson, 2003). Knowledge of expected minimum length-scales is also required for guidance as to the minimum required resolution of larger scale general circulation models wishing to resolve mesoscale heterogeneities, given that it has been shown that features of this scale have a significant impact upon the magnitude of biogeochemical fluxes. It is known that the interaction and relative domination of biological and physical processes in producing observed structure varies with scale (Wroblewski *et al.*, 1975). In keeping with our developing intention of investigating the simplest case and hence interaction of the fundamental processes of stirring, mixing and growth on the scale of plankton patchiness

attention is also restricted to another simplest case: the effect of these processes on a single phytoplankton patch. In the terms of our investigations this will be a single perturbation of tracer (or phytoplankton) concentrations above the background concentration throughout the majority of the spatial domain. It is the minimum length scale of this to which we will restrict attention and refer to in terms of "patch size".

The term minimum length-scale is perhaps misleading. More accurate in the context of these studies is the term equilibrium length-scale. The minimum and equilibrium length-scales are referred to interchangeably throughout for simplicity of reference. The equilibrium length-scale is set by the balance of strain, seeking to narrow a patch, with small-scale mixing and growth seeking to broaden it. The equilibrium length-scale is achievable provided that the structure forms within the biological and physical timescales of the phytoplankton population and its environment. The frequency with this is likely to occur (and be recognised as equilibrium) is somewhat debateable but will be assumed an achievable state for the purposes of the investigations to be carried out.

1.2 Specific Considerations

1.2.1 The KiSS studies and recognition of a critical length scale

With regards investigation of a critical or equilibrium patch size the earliest theoretical approach considered the balance of turbulent diffusion and exponential growth (Skellam, 1951; Kierstead and Slobodkin, 1953). The so-called KiSS papers (after the authors initials) identified a critical length scale, $L_{C1}=\pi\sqrt{(\kappa/\mu)}$ where κ is the coefficient of effective diffusivity and μ the net growth rate of phytoplankton population within the patch (growth outside of the patch is assumed to be zero). If any patch is smaller than this then the population will decay to extinction, whereas if a patch size exceeds the critical length scale it will continue to grow in time. The KiSS model therefore predicts a minimum scale

required for a patch of phytoplankton to persist. The simplicity of the model allows ample scope for elaboration to both the biological (e.g. Platt and Denman, 1975; Wroblewski *et al.*, 1975; Wroblewski and O'Brien, 1976) and physical (e.g. Okubo, 1978; Petrovskii, 1999b, 1999a) representations. These extensions to the KiSS model predict the critical length scale to fall in the range of hundreds of metres up to tens of kilometres. Perhaps the most useful message of these investigations is the sensitivity of the models to the biological parameterisation used. For example non-linear terms in the biological representation allow for long-term persistence of the population (Wroblewski *et al.*, 1975; Petrovskii, 1999b), even if the patch is below the classical critical length-scale.

The use of diffusion as a parameterisation of turbulent dispersal of tracer is a vast over-simplification of the dispersion expected by ocean currents. Strain in particular is not represented and yet the importance of this in generating heterogeneity and controlling tracer patch morphology is well recognised (Ottino, 1989). The aim of this thesis is to investigate rigorously the behaviour resulting from explicitly taking strain into account when considering the fate of a plankton patch.

1.2.2 Minimum length scale of inert tracer distributions

Bearing in mind the, above-mentioned, proven sensitivity of results to the biological parameterisation used, attention is turned first towards the determination of the scale of inert tracer patches.

The evolution of an inert tracer field in a straining flow goes through three distinct regimes (Garrett, 1983). For small length scales ($L << \sqrt{(\kappa/\lambda)}$, where κ is the effective diffusivity for small scales and λ the strain rate) a patch falls below the influence of the strain effects and disperses predominantly through effectively diffusive processes. Once the patch is sufficiently large it is influenced by the mesoscale field, which tends to strain the patch into a filament. The filament width is expected to have Gaussian cross-section of

spatial variance $\sigma^2=\kappa/\lambda$. The Gaussian cross-section results from the normal distribution of the concentration probability spectrum about its mean position as noted by Garrett (1983). For larger scales, streaks merge and mesoscale processes act effectively diffusively in influencing the growth of the patch. The predicted time taken for merging or homogenisation of the tracer field depends upon both the assumed large-scale and small-scale diffusive parameters and the local straining rate. It is the ratio of the effective diffusivity to the strain rate that determines the critical length-scale, $L_{C2}=\sqrt{(\kappa/\lambda)}$, at which strain effects start to dominate dispersal. The strain-dominated regime is the focus of this thesis in particular the minimum-equilibrium width at which strain effects, acting to increase tracer gradients, are partially balanced by dispersion, acting to smooth tracer gradients.

The above theory of inert tracer dispersal is supported by *in-situ* monitoring of an inert tracer (Ledwell *et al.*, 1993, 1998). In Ledwell's (1993) series of investigations a number of patches of sulphur hexafluoride (SF_6) were released on an isopycnal surface at approximately 300m and their dispersal along and across isopycnal surfaces was monitored over a period of 30 months. Lateral tracer profiles were found to maintain an approximately Gaussian structure which tended to an equilibrium width. Using Garrett's theory of tracer dispersal in a turbulent flow, values of isopycnal and diapycnal diffusivity were estimated from the width and relevant strain rate. For diapycnal calculations the assumed strain rate is the vertical velocity shear. For lateral considerations, strain rate is calculated from the rate of change of each patch length. A complimentary numerical investigation by Sundermeyer and Price (1998) supports the findings of Ledwell *et al.* (1998). In the work of Sundermeyer and Price (1998) the mixing and stirring of simultaneously deployed Lagrangian particles and a inert tracer was considered through observations and numerical simulation. The theory of Garrett is again supported by results with the caveat that a scale factor of 2 (reduction in strain rate) was required to match the *in-situ* observations when calculating strain rate from the rate of change of patch length.

The application of this scale factor to this particular method of calculating strain rate under the particular temporal and spatial variations in the strain field is noted, and the implications will be discussed later in the thesis. The issue of strain rate, in particular how it is best quantified and how best to "recalibrate" model results to match those derived *in-situ* will be discussed in detail in Chapter 5.

The existence of a minimum-equilibrium length scale for oceanic inert tracer distributions has been proven observationally and numerically. Whether this is correctly related to the local rates of strain and effective diffusivity is less easy to test. The nature of effective diffusivity, a parameterisation of under resolved straining processes, inherently prevents this: it is not a property which can be directly measured *in-situ*. The closest to this has been the extensive analysis of Okubo investigating "apparent diffusivity" of *in-situ* dye release (Okubo, 1971). He derived a relationship between apparent or effective diffusivity and the length-scale of investigation (L) of $\kappa \propto L^{\gamma}$, where $\gamma \sim 4/3$. However there is an order of magnitude error inherent in this estimate. The value of effective diffusivity approximated in this way will depend upon, amongst other aspects, the local velocity field (in particular the local strain rate and de-correlation length scale), the background sea state and stability, and current meteorological conditions. These effects are likely to significantly increase the error in estimating effective diffusivity in the surface ocean but the last two may be reduced along a subsurface isopycnal layer, as investigated in the aforementioned tracer studies of Ledwell (1998). In summary, a theoretical formula relating the minimum equilibrium length scale of inert tracer distributions to the local effective diffusivity and strain rate has been derived and the existence of a minimum length scale has been proven though *in-situ* studies.

1.2.3 Minimum length scale of reactive tracer distributions

The first study to address the competition between growth and diffusion in a pure straining flow was Martin (2000). The width of an exponentially-growing tracer filament in a strain dominated environment is found to converge to a Gaussian of the same cross-sectional variance as an inert tracer, $\sigma^2=\kappa/\lambda$, (Martin, 2000). This prediction of a minimum width for phytoplankton filaments has been "verified" by recent iron fertilisation experiments. The Southern Ocean Iron Release Experiment (SOIREE) (Boyd *et al.*, 2000) produced a plankton patch that was drawn into a filament, visible in satellite imagery of the area (Abraham *et al.*, 2000). Assuming the phytoplankton behaved as an exponentially-growing tracer the same approach as Ledwell *et al.* (1998) was used to calculate a value for effective diffusivity for the region (Abraham *et al.*, 2000). Abraham (2000) used the newly provided theory of phytoplankton length-scales to estimate effective diffusivity from the effective strain rate (calculated from rate of change of patch length) and the equilibrium patch width.

The existence of minimum equilibrium length scale towards which phytoplankton patches will tend was verified to some extent by the SOIREE study. Whether the formula is correctly relating equilibrium width to the regional strain rate and effective diffusivity is an open question, largely due to significant uncertainties in estimates of strain and effective diffusivity. Furthermore, there are indications that the simple model of an exponentially growing reactive tracer may not always be appropriate, as realised initially (Martin, 2000). The filament induced in the SOIREE experiment is not of Gaussian cross-section. There is a flatter, "table top" shape observed (Boyd and Law, 2001b). This shape is not in accordance with the theory of Martin (2000). It appears likely that by not including important aspects of phytoplankton population growth such as resource limitation, predator grazing, or resource depletion (Banse, 1991) vital aspects of the biological dynamisms responsible for observed *in-situ* structure are being overlooked. It is the aim of this thesis to redress this.

1.3 What is 'The Thesis'?

1.3.1 Philosophy

It is sought to further the understanding of the interaction of biological and physical processes in controlling the minimum equilibrium length-scale of observed mesoscale phytoplankton distributions. To gain understanding of these interactions a numerical approach is taken. By considering a hierarchy of numerical models, starting from the simplest approximations, it is possible to:

- at each stage identify the precise mechanisms responsible for observed structure;
- identify, and quantify, errors resulting from consideration of a more complex field; and
- in the event of reproduction of observed structure explain its presence and formulative history.

It is intended to be rigorous throughout the investigation in minimising and quantifying possible sources of error. This means that any results will be a 'best estimate'. In the event of application of derived relationships to *in-situ* studies where it is not possible to be so precise (for reasons that will be explained) errors will therefore be considerably increased. The magnitude of these additional observationally incurred errors is not something which is considered within the context of the thesis. Rather the aim is to determine the best results that could be obtained in an ideal world as an upper limit on expectations.

1.3.2 Aims

To further the understanding of controls on minimum equilibrium length-scale of phytoplankton distributions a hierarchal approach will be taken. In accordance with this we will conduct a series of investigations building gradually upon the complexity of the

representation of the dynamics of both phytoplankton and the flow in which it is embedded.

The first step is to further the results of Martin (2000) by investigating the effect of a finite population limit on phytoplankton patch width. Hence a single change has been applied to the simplest model. This will be achieved by investigation of a logistic growth tracer in a pure strain flow with background diffusion parameterising small scale mixing processes. The logistic growth term imposes a limit to which population concentrations will tend, provided that the population can grow sufficiently fast to avoid extinction through dilution by mixing. The constant, spatially homogeneous, pure strain flow will provide the simplest environment in which to investigate the dynamics of logistic growth "phytoplankton" under the influence of differential advection. This is the scope of Chapter 2.

Following this, in Chapter 3, the additional effect of resource depletion will be considered by explicitly modelling the nutrients upon which "phytoplankton" are dependent for growth. The same physical environment, a constant purely straining flow, will be used for consistency and to allow clearest comparison of results with Chapter 2.

The next stage involves testing the findings of Chapter 2 and 3 in a more complex flow where strain is neither uniform nor constant. This will make use of a two-dimensional turbulence model. This will allow investigation of the reactive tracer distributions subjected to the combined effects of a temporally and spatially varying strain rate and also rotation. The details of the model and the tools necessary for its analysis are laid out in Chapter 4.

A single tracer release will be investigated with the intention of maintaining our attention on the minimum-length scale of a single phytoplankton patch/filament. Initially this will be using an inert tracer to quantify the changes in physical effects involved in progressing to the more realistic flow. The relaxation of the assumption of a uniform constant pure strain flow will be shown to result in much greater spatial variability and greatly increased difficulties in predicting the length scale of phytoplankton distributions

within it. Of relevance to this is the current ambiguity concerning how to quantify strain as experienced by a tracer patch. This is the object of Chapter 5. In Chapter 6 we then consider the dispersion of a reactive tracer with an imposed population limit in the turbulent flow and whether the logistic growth model is a sufficient description of phytoplankton population dynamics. The latter will be achieved through comparison of the widths observed in logistic growth tracer distributions with those formed when using a more complex phytoplankton ecosystem model (this more sophisticated model is once more described in Chapter 4).

Remembering that a numerical investigation remains purely academic until applied to the real world, throughout the thesis and in particular in Chapter 7 recommendations will be made as to how theoretical results relate to what is practical to observe. First, how the analysis techniques used throughout our investigations can be applied to *in-situ* studies will be described along with what limitations there are. Second the additional errors resulting from sampling methodology will be discussed in Chapter 7 together with possible means of reducing them.

Once again, throughout all investigations we will ensure that all possible sources of error are minimised. Thus all presented results can be taken as a best case scenario, the relationships described will apply in an ideal environment and approximated errors will only stand to increase under non-ideal sampling and/or analysis.

CHAPTER 2: Minimum length scale for growth limited oceanic plankton distributions.

The works contained in this chapter have been published in Ecological Modelling:

McLeod et al. (2002): 'Minimum length-scale for growth-limited oceanic plankton distributions'. Ecological Modelling ***158*** *p111-120*

2.1 Introduction

The motivation for investigating controls on plankton patchiness, and in particular expected equilibrium length-scales of patches, has been explained in chapter 1. The reasons for starting with simple parameterisations of both the planktonic ecosystem and the turbulent surface ocean dynamics have been rationalized. We start from a level of understanding that phytoplankton, when described as an exponentially growing tracer, has an asymptotic width controlled by the ratio of rates of mixing to strain in the same manner as found for an inert tracer (Martin, 2000; Garrett, 1983). Although exponential growth can be considered a suitable first order approximation of phytoplankton population growth in the absence of resource limitation it is prudent to further investigate acknowledged aspects of phytoplankton ecosystem dynamics. An implicit representation of resource or nutrient limitation is considered by use of a logistic growth term to describe reactive tracer dynamics (Strogatz, 1994).

2.2 Methods

Consider the evolution of the distribution of a reactive tracer, such as phytoplankton, in a fluid environment. We describe this by:

$$\frac{DP}{DT} = \kappa \nabla^2 P + \mu P\left(1 - \frac{P}{P_0}\right) \qquad 2.1$$

where P is the tracer concentration, D/DT is the total derivative, κ is an effective diffusivity which parameterises physical processes at scales smaller than the model resolution, and μ is the maximum net growth rate of the tracer. The final term in equation 2.1 is a greatly simplified parameterisation of biological processes. Otherwise known as logistic growth it has a threshold population limit, P_0, to which the population will tend and above which the population is unable to sustain itself. This is the simplest parameterisation of growth limiting factors such as grazing and nutrient limitation. It can be noted that as $P_0 \to \infty$ the system tends to that describing an exponentially growing tracer. The growth rate, μ, is considered homogeneous, i.e. any variation, either spatially or temporally, is assumed to be at scales larger than the structure produced by the flow. It should be noted that we only take ambient waters to have zero concentration of phytoplankton for convenience. Simply replacing the growth term $\mu P\left(1 - \frac{P}{P_0}\right)$ with $\mu(P - P_b)\left(1 - \frac{P}{P_0}\right)$ allows any constant uniform background concentration, P_b, without changing any of the dynamics or following results. This substitution does not alter the equilibrium states of the population ($P=0$, $P=P_0$) but does allow for the perturbation upon a non-zero background population level.

We will assume that the flow is two-dimensional and divergence free, a reasonable assumption for the ocean away from strong fronts and at scales greater than ~1km where vertical motions are negligible in comparison with lateral processes (Batchelor, 1967). Any such flow can be resolved locally into a pure strain and a rotation. Straining processes are primarily responsible for the formation of filaments (Ottino, 1989). Consequently, for the sake of simplicity, we restrict attention to a pure straining flow, $\underline{\mathbf{u}}=(-\lambda x, \lambda y)$, where λ is the

straining rate. In such a flow field the tracer will be drawn out in the y direction into a ribbon-like structure or filament. Thus a one-dimensional approximation to equation 2.1 can be justified, as the across-filament gradients (in the x direction) will far exceed those along the filament. To aid analysis further equation 2.1 can be non-dimensionalised firstly by normalising the concentration with respect to the population limit, $C = \frac{P}{P_0}$, and secondly by substituting $t = \frac{1}{\lambda}\tau$, and $x = \sqrt{\frac{\kappa}{\lambda}}\phi$.

Thus

$$\frac{\partial C}{\partial \tau} = \phi\frac{\partial C}{\partial \phi} + \frac{\partial^2 C}{\partial \phi^2} + \beta C(1-C). \qquad 2.2$$

The remaining parameter, $\beta = \mu/\lambda$ is an inverse Damköhler number (Damköhler and Heumann, 1982) being a measure of the ratio of reaction to flow time scales. Typical net growth and strain rates in the ocean both vary in the range 0.01-1 day^{-1}. We therefore choose to examine β in the range 0.01-100. From now on an asterisk will be used to denote dimensional parameters.

Our model is a combination of two well-studied systems. As such one may expect the solution of equation 2.2 to tend towards the solution of each component in certain limits.

Consider first the limit of large β ($\geq O(1)$), we shall explain our definitions of "large" and "small" later. Without advection equation 2.2 reduces to the well-known Fisher's equation (Murray, 1993). Fisher's equation, which combines diffusion with a logistic growth term, possesses travelling wave solutions, which can take the form of propagating fronts (Fisher, 1937). For an initially localised 'seed' population these fronts have a minimum velocity,

$U_{min}=2\sqrt{\beta}$ ($U^*_{min}\equiv 2\sqrt{(\kappa\mu)}$, in dimensional form) (see e.g. Murray, 1993). The velocity of these fronts increases with decreasing steepness of the front. We conjecture that with the inclusion of an opposing advective velocity the fronts will stop where the opposing flow is of similar magnitude to that of the frontal propagation.

Considering the flow field $u=\phi$ ($u^*=\lambda x$) and frontal velocity $U_F \sim\sqrt{\beta}$, and assuming that the fronts propagate symmetrically from the origin this results in a final expected non-dimensional width of the logistic filament:

$$W_L \sim \sqrt{\beta}\,, \left(W_L^* \sim \frac{\sqrt{\kappa\mu}}{\lambda} \right) \qquad 2.3a$$

The functional form of this differing significantly from that for an exponentially-growing (or inert) tracer:

$$W_I \sim 1\,, \left(W_I^* \sim \sqrt{\frac{\kappa}{\lambda}} \right) \qquad 2.3b$$

The width of an exponentially growing (or inert) tracer (eqn. 2.3b) is dependent upon a balance diffusion (acting to widen the patch) and strain (acting to narrow the patch) (Garrett, 1983; Martin, 2000). Considering equation 2.3a the final width for a logistic growth tracer, W_L, is now dependent on the growth rate of the tracer and is more sensitive to strain rate. It is the combination of all three bio-physical parameters acting upon the tracer patch which determine its equilibrium width. Growth and diffusion acting to widen the tracer patch are balanced by strain acting to narrow the patch.

Next consider the limit of small β ($\lhd 1$). For small C equation 2.2 approximates the Martin (2000) model. The tracer concentration will remain low on the condition that the growth rate, β, is sufficiently small. There the use of a growth term without logistic correction results in a Gaussian of width W_I (eqn. 2.3b), the magnitude of which increases or

decreases exponentially with time depending on the relative magnitudes of the growth and strain rates (Martin, 2000).

In summary, for small β stretching should dominate, preventing the concentration from reaching its limiting value (1), and the solution is expected to tend towards that for an inert or exponentially-growing tracer i.e. a Gaussian of width W_I. For large β biological effects should dominate and the solution is expected to tend to that for Fishers equation in the presence of opposing advection.

To find, and quantify, the limits on the behaviour of the system we solve equation 2.2 numerically. The advection scheme is solved by flux-corrected upstream differencing (Smolarkiewicz, 1984), chosen for its positive definite transport, stability and diffusive correction (Smolarkiewicz and Grabowski, 1989). For simplicity the reactive component is solved by a 4^{th} order Runge-Kutta scheme (Rood, 1987).

2.3 Results

The inclusion of the factor (1-C) in the growth term radically changes the behaviour of the system compared to one with unlimited exponential growth. As expected the behaviour of the system is very dependent on the value of β. Figure 2.3.1 shows the tracer distribution for four different values of β which characterise the different regimes of the system. The four regimes are of three geometric classes with another differentiated through temporal variation. The distinct geometric solutions mean that spatial variance is no longer a consistent indicator of spatial extent. Henceforth we define the width, W, as the distance between the 'noses' of the fronts. We define the 'nose' as 0.01% of the maximum tracer concentration as it gives the most consistent results. Consistency implies the independence

of the width measurement on geometric effects, compliant with our motivation for calculation of width as opposed to spatial variance. In figure 2.3.2(b) we show the variation of final width with parameter value.

The first regime is found for values of $\beta \leq 1$ the distribution decays to zero as a Gaussian of width 8.6 (figure 2.3.1(a)). The width of the distributions is constant for $\beta < 1$ (figure 2.3.2(b)) i.e. the width is independent of growth rate, reproducing the result of Martin (2000) for an exponentially-growing tracer in a convergent flow field. In this regime the domination of biological effects by the flow is sufficient that the tracer concentration never reaches the threshold where fronts begin to form.

For $\beta \geq 10$ we find the second distinct geometric regime where a propagating front develops (figure 2.3.1(c) and (d)). The nose of the front stops where the advective current balances the propagation velocity (figure 2.3.2(a)). As expected the asymptotic filament width varies as the square root of the parameter β (figure 2.3.2(b)). However there is an additional constant correction to equation 2.3 suggesting that the frontal behaviour is modified by the advective field beyond simple additive effects. The asymptotic frontal gradient is seen to increase with β, figure 2.3.2(c). We suggest that this is because for a higher growth rate the population is better able to sustain itself closer to the stopping point. For a lower growth rate the current has a greater effect on the population 'pushing' it away from the equilibrium point resulting in a gentler front. The speed of frontal propagation is dependent upon the frontal gradient. This effect results in our third regime, distinguished through its time varying behaviour. The steady state solution is the same as for lower values of β (>10). However, there exists a critical growth rate, β_c, such that for $\beta > \beta_c$ instead of stopping directly at the steady state point fronts 'overshoot' before

subsequently converging (figure 2.3.1d). The precise value of β_c is initial condition dependent although it increases as the difference between the initial condition and the steady state solution decreases. The magnitude of overshoot increases generally with β for a range of given initial condition. Results (not shown) suggest that for a sufficiently high growth rate gentle fronts propagate outwards faster than the advective field is able to adjust the frontal gradient and hence propagation velocity. The fronts eventually become steeper, reducing the frontal velocity with the consequence that the filamental width decreases until the expected width, at the velocity balance, is reached.

Our fourth regime corresponds to the transition region where there exists a non-zero asymptotic solution is neither exactly Gaussian nor a propagating front (figure 2.3.1b). We choose to delineate this regime and to differentiate between the Gaussian and propagating front regimes by using Kurtosis, $K = \frac{\mu_4}{\sigma^4}$, a measure of the 'peakiness' of a distribution, where μ_4 is the fourth moment about the mean and σ^2 is the distribution variance. The Kurtosis of a Gaussian is 3. In its extreme a frontal solution may be thought of as a box or double step function, which has K = 1.79. Here a frontal solution is defined by its Kurtosis being within 10% of that of an extreme frontal solution, i.e. K $<$1.97. The Kurtosis of the steady state solution is show in figure 2.3.3(b) as a function of β. The three geometric regimes may also be distinguished through their maximum asymptotic height, figure 2.3.3(a). A frontal solution has a limiting concentration $\cong$1 whilst Gaussian solutions tend to zero. Referring to figure 2.3.3(a,b) the transition regime therefore spans $1 \leq \beta < 10$ and 1.8 $<$Kurtosis $<$2.7, where the maximum concentration of the distribution neither decays to zero nor reaches its limiting value. In its steady state the concentration reaches a limit where, at the centre of the filament, net growth is matched by losses due to diffusion, remembering that the advective contribution is zero at the centre of the domain.

The velocity and width distributions, figure 2.3.2(a),(b), have a two-part linear regression:

$$V_f = 4.3\max(1,0.4(\sqrt{\beta}-1.6)+1) \qquad 2.4$$

$$W = 8.6\max(1,0.4(\sqrt{\beta}-1.6)+1) \qquad 2.5$$

$$\left(W^* = 8.6\sqrt{\frac{\kappa}{\lambda}}\max\left\{1,0.4\left[\sqrt{\frac{\mu}{\lambda}}-1.6\right]+1\right\}\right)$$

where V_f is the velocity at the "nose" the points between which the width, W, is measured. A very good fit to data is observed. The leading non-unity coefficients are dependent on the definition of width. Our formula for the width changes from constant to increasing as $\sqrt{\beta}$ at the point where $\beta=1+\varepsilon$, and $\varepsilon\approx1.5$. In the transition regime the asymptotic width is under predicted, but the maximum error is less than 10% of the predicted width.

The time taken to reach steady state is also of interest. The behaviour of the concentration at the centre of the filament can be modelled by:

$$C(t) \sim C_0 + C'\exp\left(-\frac{t}{\eta}\right) \qquad 2.6$$

where C_0 is the final concentration and η the decay timescale is given to good approximation by $\eta = \frac{1}{|\beta-1|}$ (figure 2.3.3(c)). The approximation is purely empirical. The apparent singularity at $\beta=1$ shows the transition between an exponentially decaying solution and a non-zero steady state being achieved.

The time for the filament width to reach its equilibrium value is more difficult to quantify. For $\beta\leq1$ the time scale is 0.5, or a decay rate of 2. This agrees once again with that found by Martin (2000) for an exponentially-growing tracer. For $\beta>1$ the decay timescale is initial condition dependent. The time taken for the distribution to achieve its steady state solution

decreases with increased proximity of the initial condition to the asymptotic solution. We are interested in the longest expected convergence time for a plankton distribution. We therefore choose to describe convergence times for the smallest practicable initial condition (width 2 boxes, C_{max}=0.01). For $\beta < 5$ (approximately Gaussian) steady state is achieved within ~0.28 model time units. Assuming $\lambda \sim 1x10^{-5}$ s^{-1}, as a typical upper ocean strain rate, this corresponds to ~0.5 day. For the propagating front solutions the mean convergence time is 0.22 model time units. Assuming $\lambda \sim 1x10^{-5}s^{-1}$ again this corresponds to ~0.25 day. However $\lambda = 10^{-5}$ s^{-1} is the predicted maximum straining rate. For the smallest expected strain rate, $\lambda = 10^{-7}$ s^{-1}, this would be 25 days, but a mean value is 3 days corresponding to $\lambda = 10^{-6}$ s^{-1}. Both mentioned time scales are dependent on the assumed straining rate. As the Lagrangian integral timescale for a mesoscale ocean flow varies from 2-10 days (Griffa *et al.*, 1995), this suggests that not all filaments will achieve the predicted steady state width during the life span of the straining process.

2.4 Discussion

The predicted width of a reactive tracer with logistic growth differs from that predicted for an inert or exponentially-growing tracer by $L_R/L_I = \max(1, 0.4\sqrt{\beta} + 0.36) = \Gamma(\beta)$, where L_R is the width of a reactive tracer filament and L_I the width of an inert or exponentially growing filament. For a given λ using the expected width of an inert filament to calculate κ for a growth-limited reactive tracer leads to an overestimate of κ by a factor of Γ^2 for $\beta > 2.5$.

Choosing typical values of $\kappa \sim 1$ m^2s^{-1} and $\lambda \sim 10^{-6}$ s^{-1} results in a predicted inert filament width of 8.6km. The predicted width of a growth-limited reactive filament, in the same environment, is the greater of 8.6km or $8.6x[0.4(\sqrt{(\mu/\lambda)} - 1.6) + 1]$ km. In practice filament

width is limited above by oceanic integral length scales which vary considerably with location and particularly with 50-80 km for mid-latitude location (Stammer, 1997). However for the values above to increase the reactive filament to the order of the integral length scale of the mesoscale field requires $\beta \sim 62$. The largest discrepancy between exponentially-growing and growth-limited phytoplankton that could be expected will occur in bloom conditions in low energy regions. Here we may expect $\beta \sim 20$ giving a factor of 2 difference. Although $\beta \sim 20$ may be realistic for short periods, such values are unlikely to be sustained for periods larger than a few weeks as net growth rates rapidly decrease with the onset of decreased nutrient availability and increased predation.

It should be remembered that effective diffusivity varies with scale. If we use Okubo's (1971) empirical formula $\kappa = 0.0103 L^{1.15}$ $cm^2 s^{-1}$, with growth and straining rates of similar order such that $\beta = 3$, and μ and λ are in the range 10^{-5}-$10^{-7} s^{-1}$ then our formula predicts filament widths in the range 0.8-80 km accordingly. As previously discussed in chapter 1 it should be noted that all estimates of filament width using Okubo's formula have an associated error of up to an order of magnitude due to the sensitivity of the parameterisation of diffusivity to sea and weather conditions (Okubo, 1971).

To date the only application of the expected width of a tracer filament to observational data has been to derive a value for the local effective diffusivity. The expected width of an exponentially-growing tracer was applied to a plankton filament formed during the recent SOIREE experiment (Boyd *et al.*, 2000; Abraham *et al.*, 2000). The values described by Abraham *et al.* suggest $\beta = 1.5 \pm 1$. The formulae for growth-limited and unlimited exponentially-growing tracers do not differ for this value. However caution must be urged as for higher values of β the predicted solutions differ dramatically. Comparison of results

through derived values of diffusivity is not recommended as there no independent means of assessing the correct value of effective diffusivity. A better means of comparison of model results, both between models and with observations, is through the structure or Kurtosis of the filament cross-section. However this requires high-resolution information on tracer concentration, such as low-level remote sensing or fine scale in-situ surveys. Issues relating to fine scale *in-situ* surveys are discussed in chapter 7.

The structure observed in a reactive tracer field, such as plankton, is often markedly different from that of an inert tracer, (Denman and Platt, 1976; Seuront *et al.*, 1999) . We have shown that one reason may be a different functional form for the expected asymptotic width of any filaments formed.

$$W^* = 8.6\sqrt{\frac{\kappa}{\lambda}}\max\left(1, 0.4\left(\sqrt{\frac{\mu}{\lambda}} - 1.6\right) + 1\right) \qquad 2.7$$

For relatively large growth rate or small strain rate, such that $\mu/\lambda > 2.6$, the predicted structure differs significantly from that predicted for an inert or exponentially-growing tracer. Observed mesoscale filament widths are expected to vary from less than 1km up to the integral length-scale of the straining field. These filaments are expected to have a mean convergence time of ~3 days, based on an the mean convergence time of filaments within the model using a mean strain rate of $10^{-6}s^{-1}$. Numerical results suggests there are factors likely to disrupt the formation of filaments on larger scales: grazing modifying the distribution; variation of the current field and growth rate on temporal and spatial scales less than those required for the asymptotic solution to be achieved.

An interesting feature of our results is that the biological processes assumed can have a marked effect on the filamental structure. This is in contrast to the case of an exponentially-growing tracer where filament width is independent of growth rate. Perhaps

counter-intuitively imposing a limit on the population size such that fronts of plankton propagate out from the centre of a convergent flow results in a wider final distribution than if growth was unrestricted. The width of tracer patches is described by equation 2.7. For a sufficiently high growth rate the asymptotic width is greater than that of an inert or exponentially growing tracer. However this is dependent upon a frontal solution being formed. As the population limit tends to infinity the time taken for these fronts to form will also tend to infinity, nevertheless the asymptotic width remains as that described by equation 2.7.

Having derived a formula for predicting the minimum width of phytoplankton distributions this can now be tested by explicit simulation of such tracers in two-dimensional turbulent fields. Prior to this it is wise to assess modifications resulting from a more complex biological representation- the explicit inclusion of processes such as nutrient limitation and grazing.

CHAPTER 3: The structure/behaviour of growth-limited plankton filaments- with explicit nutrients.

3.1 Introduction

Investigation of the typical length-scale of phytoplankton distributions have found that, when described by an exponentially growing tracer, the width of phytoplankton distributions are determined by the same balance of rates of mixing and strain as for inert tracer (Martin, 2000). Although in the absence of grazing a healthy phytoplankton population with sufficient light and nutrients will grow exponentially (Banse, 1991) this is expected to be a phenomenon of finite duration. Predator grazing and resource limitation will eventually curb the net population growth rate. This effect was considered by means of a logistic growth term in chapter 2. A modification to the formula was derived describing the added dependence of the spatial distribution of a growth-limited population on the applied growth rate, with an increased dependence on strain rate (equation 2.7).

The next stage in the progression is to explicitly represent to the effect of nutrient availability on population growth. Although logistic growth is considered a reasonable first-order description of the effect of nutrient limitation, it is also expected that a biological population will eventually exceed the capacity of its environment. As a consequence nutrient deprivation will eventually reduce the effective growth rate. This is the motivation for explicitly including nutrients. For simplicity death rate is not considered to increase.

3.2 Methods

The evolution of a pair of reactive tracers, such as phytoplankton and nutrient, in a fluid environment can be described by:

$$\frac{DP}{DT} = \kappa\nabla^2 P + \mu\left(\frac{N}{N+K}\right)P - \mu\frac{P^2}{P_0} \quad 3.2$$

$$\frac{DN}{DT} = \kappa\nabla^2 N - \mu\left(\frac{N}{N+K}\right)P \quad 3.3$$

where P is the phytoplankton concentration, N is nutrient concentration, D/DT is the total derivative, κ is an effective diffusivity parameterising physical processes at scales smaller than the model resolution, μ is the maximum net growth rate of the tracer, K is the half-saturation constant (the nutrient concentration at which half-the maximum growth rate is achieved), and P_0 is the threshold population limit. The diffusivity of N and P are assumed to be the same. Differing diffusivity between biological compartments have been used in studies of phytoplankton ecosystem dynamics to represent the potential for differing aspects such as motility (e.g. Matthews and Brindley, 1997). Due to the spatial scales being considered ($>O(1km)$), and for simplicity, within the thesis the same diffusion rate is assumed for all biological parameters.

As stated in the previous chapter the flow is assumed to be two-dimensional and non-divergent. As we are primarily interested in filamental structures attention is restricted to a purely straining flow, centred on the domain midpoint. As a tracer in such a flow field will be drawn out into a long, thin filament a one-dimensional approximation is justified as in Chapter 2:

$$\frac{\partial P}{\partial t} = \lambda x\frac{\partial P}{\partial x} + \kappa\frac{\partial^2 P}{\partial x^2} + \mu\left(\frac{N}{N+K}\right)P - \mu\frac{P^2}{P_0} \quad 3.4$$

$$\frac{\partial N}{\partial t} = \lambda x\frac{\partial N}{\partial x} + \kappa\frac{\partial^2 N}{\partial x^2} - \mu\left(\frac{N}{N+K}\right)P \quad 3.5$$

where λ is the straining rate of the flow.

To further aid analysis the system can be non-dimensionalised through the following normalisations:

$$\tau = \lambda t, \phi = \sqrt{\frac{\lambda}{\kappa}}x, C = \frac{P}{P_0}, N' = \frac{N}{K}, \beta = \frac{\mu}{\lambda}$$

Resulting in the model equations:

$$\frac{\partial C}{\partial \tau} = \phi \frac{\partial C}{\partial \phi} + \frac{\partial^2 C}{\partial \phi^2} + \beta\left(\frac{N'}{N'+1}\right)C - \beta C^2 \qquad 3.6$$

$$\frac{\partial N'}{\partial \tau} = \phi \frac{\partial N'}{\partial \phi} + \frac{\partial^2 N'}{\partial \phi^2} - \beta\left(\frac{N'}{N'+1}\right)N_s C \qquad 3.7$$

Where $N_s = P_0/K$ is the ratio of the population limit to the nutrient half saturation coefficient. N_s acts as a scaling between the rate of nutrient consumption by phytoplankton and actual rate of nutrient depletion. For this reason it is chosen to cover two orders of magnitude. Other parameters are chosen to cover an extreme range of typical nutrient concentration, growth and strain rates (Sundermeyer and Price, 1998; Abraham *et al.*, 2000):

$$N_s = [0.1\ 1\ 10]$$

$$\beta = [0.01\ 0.1\ 1\ 2.5\ 5\ 7.5\ 10\ 20\ 30\ 100]$$

$$N_0' = [0.01\ 0.1\ 0.5\ 1\ 5\ 10\ 50\ 100\ 500\ 1000]$$

Nutrient concentrations are initially homogenous throughout the domain with a concentration N_0'. A source is included as a boundary condition $N'(0,\tau) = N'(\phi_{max},\tau) = N_0'$. This is the equivalent to assuming that the filament is surrounded by a region of uniform concentration, N_0'. The manner in which the nutrients are introduced to the domain leads to a constant inwards flux, at a rate dependent upon the strain rate. At equilibrium this is balanced by losses due to consumption (by the phytoplankton) and divergence of the flow.

The dynamics of the system are not expected to differ significantly from those described in Chapter 2. The modification to include an explicit representation of the effects of nutrient depletion acts upon the effective growth rate, β, only. This will result in a reduction of the effective growth rate, $\beta N'/(1+N')$, when nutrients are limiting, $N' << (N'+1)$. The death rate

is unaffected by nutrient availability. As before a two-part system is expected: for growth rates comparable to or less than strain rate a Gaussian solution; for growth rates significantly higher than strain rate a propagating front solution. For high phytoplankton growth rates nutrient depletion may reasonably be expected to occur. With this, modification to the shape and dynamics of the fronts due to inhomogeneous growth rates across the patch extent must also be expected.

3.3 Results

Explicit representation of nutrient variability can have a striking impact on the asymptotic tracer profile. An example of this is shown in figure 3.3.1 depicting the asymptotic structure of phytoplankton and nutrient distributions for a high effective growth rate, $\beta=30$, $N_s=1$ and a range of boundary nutrient concentrations. From the previous chapter's results, for this value of β a propagating front solution is expected resulting in a table-top cross-sectional profile. For very high nutrient availability the expected asymptotic structure is observed. For low availability a Gaussian solution is observed. For moderate background nutrient availability a double peaked asymptotic profile is observed. This is a clear example of biological dynamics determining observed structure. Nutrient limitation is reducing the population growth rate at the centre of the domain, but not so at the edge exposed to the influx of nutrients. This leads to the distinctive double peak where the phytoplankton growth rate at the centre of the domain is significantly less than that at the edge of the patch. As proposed, the across patch heterogeneity of phytoplankton effective growth rate can result in a markedly different structure to that which may be expected when nutrients are not included.

Whilst considering the behavioural regimes of the system the effect of the nutrient scaling, N_s, is not mentioned explicitly. There is a discussion of this later and figures relate to all three values of N_s for which runs are conducted .

Figure 3.3.2 shows the maximum asymptotic concentration, P_{max}. Which generally increases with N_0' and β. However explicit representation of nutrient availability is resulting in a local reduction of population growth rate and population size as seen in figure 3.3.1. For $N_0' << 1$ population growth is severely limited throughout the domain. This results in a change of behavioural regime to that expected for a non-nutrient limited logistic tracer. For $\beta < 1$ a decaying Gaussian solution is expected and observed. For $1 < \beta < 2.5$ and steady state Gaussian solution is expected, but a decaying Gaussian is observed. For $\beta > 2.5$ the solution is expected to tend towards a propagating front solution, this being achieved for all $\beta > 10$. However a Gaussian solution is observed for all β with $N_0' < 0.1$. A non-zero steady state solution, of form dependent on β as described above, is achieved for $0.1 < N_0' < 100$, $\beta > 10$. For high N_0' no change to the expected asymptotic structure is observed as there is no significant reduction to effective growth rate as $N'/(N'+1) \approx 1$.

Figure 3.3.3 shows Kurtosis, a measure of "peakiness". As mentioned in the previous chapter a Gaussian solution has a Kurtosis of 3, and propagating front or table top solution has a Kurtosis of 1.8. In the instance of a double peak Kurtosis is further reduced. As the tracer is in a convergent flow field symmetric about the centre of the domain the solution is expected to be symmetrical in the same way. If the maximum concentration lies away from the centre of the domain then the population must be locally nutrient deprived at the centre, with any new influx of nutrient being consumed by the outlying population before reaching the centre of the domain, i.e.:

$$\frac{\beta N'}{N'+1}(centre) < \frac{\beta N'}{N'+1}(edge).$$

Figure 3.3.4 shows the difference between the maximum tracer concentration and that at the domain centre- the position most isolated from nutrient supply. This is a simple approximation of the peak height. For $\beta > 10$ a double peak is generally observed, for a non-zero steady state solution, $N_0' > 0.1$. For a sufficiently high growth rate nutrients are consumed before reaching the centre of the patch. This region becomes nutrient depleted and experiences a reduction in population growth rate sufficient that losses exceed new growth and the population declines. For the highest growth rates, $\beta \sim 100$, this can tend to population extinction at the domain centre.

The asymptotic width of solutions (figure 3.3.5) is not significantly altered by explicit representation of restriction of growth rate due to nutrient limitation. The same approximation for asymptotic width of a tracer profile applies:

$$W = 8.6\max\left(1, 0.4\left[\sqrt{G} - 1.6\right] + 1\right) \qquad 3.8$$

$$\left(W^* = 8.6\sqrt{\frac{\kappa}{\lambda}}\max\left(1, 0.4\left[\sqrt{\frac{\mu \tilde{N}}{\lambda\left(\tilde{N}+K\right)}} - 1.6\right] + 1\right)\right)$$

However the width is not so simply estimated from the maximum growth rate, β, but dependent upon the effective growth rate $G=\beta[N^*/(N^*+1)]$, where N^* is a locally representative nutrient concentration. When considering patch dynamics there is a question as to over what spatial extent N^* should be calculated. Either by taking a simple mean or by considering maximum concentration over the width of the phytoplankton patch a good estimate of the actual width is calculated (in the dimensional form of equation 3.8 $\tilde{N}$ is the

mean nutrient concentration across the filament). On the condition of a non-zero steady state being achieved the error is less than 10% in the worst case and significantly less than this for the rest (figure 3.3.6). The error is calculated as the difference between measured width and that predicted by equation 3.8. The variation of asymptotic width and Kurtosis with $\sqrt{G}$ are shown in figure 3.3.7 and 3.3.8 respectively. The relationship between actual width and that predicted from equation 3.8 deteriorates for higher effective growth rates.

Results relating to varying nutrient scaling, N_s, have been presented while describing the behaviour of the system, although there has been no necessity to mention this explicitly. The general relationships described do not alter with the scaling. The exact values of β and N_0' at which particular features are observed do. The maximum phytoplankton concentration is largely unaffected by N_s. However for N_s=10 the population limit is reached for a higher nutrient availability for $\beta \sim 10$, compared to that for lower values of N_s (figure 3.3.2). The double peak is somewhat more sensitive to the scaling. For decreasing N_s the double peak is first formed at an increasingly higher growth rate (figure 3.3.3 & 3.3.4), as the rate of nutrient depletion decreases. The width of the patch is largely unaffected by rate of nutrient depletion, as verified by a fit of equation 3.8 (figure 3.3.5). The patch core, isolated from nutrient influx by the outlying population, is sensitive to the rate of nutrient depletion as a result of the sensitivity of phytoplankton growth rate to nutrient availability. Although a change to shape is dependent upon the nutrient concentration. Patch width appears to be solely controlled by nutrient availability at the edge of the patch.

The time taken to reach steady state, both with respect to the width and the maximum phytoplankton concentration is also of interest. The inter-dependence of effective growth-

rate and nutrient concentration make this a somewhat complicated consideration. A lower local nutrient concentration results in a lower local effective growth rate, resulting in a longer time to convergence. However a smaller population places less of a demand on resources allowing nutrient concentrations to tend towards the limit, N_b', thereby increasing the effective growth rate. A higher growth rate would decrease convergence time but a higher population places more of a demand on available resources decreasing nutrient concentrations and hence growth rate.

Next consider the rate of adaptation of the maximum phytoplankton concentration. Although steady state solutions are being achieved the simple relationship between maximum (or apparent) phytoplankton growth rate and decay time scale derived in chapter 2 is no longer observed. However it has been noted that if the population concentrations are not in a steady state across the filament this will not necessarily affect the steady state with respect to the width.

Finally consider the time within which a width-wise steady state is achieved. Convergence times are affected by the proximity of the initial condition to the asymptotic solution. From a practical consideration we are interested in whether a patch will achieve its asymptotic structure within the integral time-scale of the flow. Estimated Lagrangian integral timescales for general mesoscale ocean flows vary from 2-10 days (Griffa *et al.*, 1995). The width-wise convergence times were not found to differ substantially from those observed for the simple logistic tracer. With this consideration in mind the previous qualitative result for time varying behaviour is not significantly altered: some filaments will achieve steady state within this time-scale; others will not.

3.4 Discussion

The explicit representation of nutrient availability does not significantly alter the dynamics controlling the asymptotic width of a phytoplankton patch in a pure strain environment. However from a modelling perspective the definition of effective growth rate and the region over which is calculated becomes less easily determined. This is a problem equally applicable to observational studies.

The formula derived in chapter 2 is still applicable to the expected width of oceanic plankton distributions:

$$W = 8.6\sqrt{\frac{\kappa}{\lambda}}\max\left[1, 0.4\left(\sqrt{\frac{\mu^*}{\lambda}} - 1.6\right) + 1\right] \qquad 3.9$$

where κ is the effective diffusivity, λ is the measured strain rate of the environment, and μ^* is the nutrient dependent effective growth rate, $\mu^* = \mu\frac{N^*}{K + N^*}$, and N^* is the mean nutrient concentration across the phytoplankton patch.

The cross-sectional profile is, however, modified by resource depletion compared to the asymptotic shape found in a situation without nutrient limitation. A non-regular, or double peak, profile of an observed plankton filament is suggested as an indication of a nutrient limited population with a source external to the patch, an example would be between upwelling areas as may be found between eddies.

The model considered an instant response to nutrient availability. Surrounding water are taken to have a zero tracer concentration for convenience only. Non-zero background concentration can be considered by simple modification of the reactive terms. None of the results nor dynamics of the system are altered by this modification but nutrient

concentration is now maintained by an additional source related to the level of the background concentration.

3.5 Conclusions

Explicit representation of the effect of nutrient concentration on growth rate of a phytoplankton population has no effect on the minimum expected length-scale in a strain dominated environment, provided calculations are made based on the effective population growth rate taking into account local nutrient concentrations and not the maximum possible phytoplankton growth rate. The cross-sectional structure of a patch can however be modified, by the inclusion of explicit nutrient dynamics, due to the local limitation of population growth rate.

Ultimately it is wished to test any model findings with *in-situ* data. Analysis of high-resolution underway datasets of concurrent measurements of phytoplankton and nutrient concentrations in relation to the local flow dynamics would allow this to be investigated observationally. Due to difficulties with obtaining reliable *in-situ* synoptic datasets of sufficient spatial resolution the next stage of investigation is to test the previously derived formula with more complex physical and ecosystem models. The formula is initially investigated in a more complex physical environment. It is also prudent to test the propriety of a logistic tracer as a parameterisation of phytoplankton population dynamics.

CHAPTER 4: Introduction and method description for 2D investigations.

4.1 Introduction

In chapters 2 and 3 the behaviour of a logistic tracer in a one-dimensional pure strain flow has been investigated. A formula relating the minimum equilibrium width to the rates of mixing (effective diffusivity), strain and growth has been derived (equation 2.7). Further investigation has shown that explicit representation of nutrient availability does not impinge upon the functional form of the equation with the proviso that the growth rate is now the nutrient dependent apparent growth rate as opposed to the maximum applied growth rate (equation 3.9). Although one-dimensional pure strain is suitable for initial investigation of the minimum equilibrium length-scale of tracer distributions, in a uniform purely straining flow essential features of oceanic physical dynamics are excluded. Specifically the effects of temporally and spatially varying strain and rotation are neglected. This is the motivation for the progression to a two-dimensional turbulence model. Our first aim is to test the previously derived formula in a more realistic physical environment. With the progression to two-dimensions it is also possible to test the propriety of a logistic tracer as a parameterisation of phytoplankton ecosystem dynamics. This is assessed through comparison of results relating to logistic tracer dynamics with those relating to a more sophisticated ecosystem model.

With the progression to a more complex physical environment it is necessary to initially consider the dynamics of an inert tracer once again. This is to enable quantitative distinction between the effects of physical and reactive dynamics. An inert tracer is taken as a "benchmark" as modifications to the size and shape of a patch of such tracer are purely the result of the physical environment it experiences. This can then be taken into

consideration when analysing the size and shape of structure observed in the distribution of logistically growing and more complex, interacting biological tracers. Hence the complementary contributions of physical and biological processes can be isolated.

4.2 Methods.

In chapters 6 and 7 there are three different experiments carried out with the same model. Prior to explanation of these experiments the physical model, used for all experiments, is described followed by the biological model(s) used. Following an explanation of the experiments to be conducted necessary the analysis techniques that have been devised are introduced.

4.2.1 Model description.

The evolution of tracers in a two-dimensional (horizontal) quasi-geostrophic turbulence model is considered. This may be thought of as considering tracer distributions along an isopycnal surface or in a surface mixed layer with negligible vertical effects. The two-dimensional turbulence model is a good first order approximation to upper ocean circulations. We find large and small, cyclonic and anti-cyclonic, rotational features with intervening regions of high strain. The dynamics both of a single reactive tracer and of a simple ecosystem model in the same physical environment are considered.

a. Physical Model

The temporally and spatially varying, non-divergent, velocity field used to advect all tracers is obtained from a numerical model of vorticity. The un-scaled physical dynamics are purposely kept the same for each model runs. As a consequence the advective flow field is

identical for all runs described. This ensures that results between runs for different diffusivities, tracer dynamics, and tracer initialisation are directly comparable. Any observed differences in the tracer distributions are therefore solely due to changes in the aforementioned, user defined, properties.

The two-dimensional quasi-geostrophic turbulence field is obtained by numerical integration of:

$$\frac{Dq}{Dt} = F + D_1\nabla^8 q + D_2\nabla^{-2} q \qquad 4.1$$

The equation describes the temporal and spatial evolution of potential vorticity in a forced, barotropic, quasi-geostrophic flow, where:

$$q = \nabla^2\psi - \frac{\psi}{R^2} + f \qquad 4.2$$

is the potential vorticity. R is the ratio of the Rossby radius of deformation to the domain size and f is the Coriolis parameter. This is related to the velocity field via the streamfunction, ψ, as:

$$u = -\frac{\partial\psi}{\partial y}, v = \frac{\partial\psi}{\partial x}. \qquad 4.3$$

For mid-latitudes a Rossby radius of roughly 100km is assumed. Hence $1/R^2 \approx 25$ for a domain size of 512km. The resulting turbulent flow is inhabited by coherent rotational structures, eddies, with strong shear in the intervening region, (figure 4.2.1(a)), characteristic of geostrophic turbulence. The physical model is run to a statistical steady state prior to its use in runs with biological tracers. Statistical steady state means that when considering a plot of energy against wavenumber the area under the plot, and its slope, remain constant. Energy is calculated from the integral over all angles of the Fourier transform of the velocity field, calculated for each wavenumber. The model domain is doubly periodic with 256x256 grid cells of size 2x2km resulting in a 512x512 km domain.

For this spatial scaling the eddies are of diameter 40-80 km, which corresponds well with mid-latitude observations. As will be explained in the description of the biological model a differing time scaling, relating the time scale of the physical field to that of the reactive tracers, is used in the two sets of experiments described below. This results in peak velocities of approximately 40 cm s^{-1} for inert and logistic tracer investigations. For the NPZD model the time scaling increases peak velocities are approximately 100 cm s^{-1} (figure(4.2.1(b)). Further details of the turbulence model can be found in Babiano *et al.* (1987).

The vorticity equation is solved using a pseudospectral scheme with forcing, F, to maintain constant energy levels in mode 10, and high (D_1) and low (D_2) frequency damping to i) represent energy dissipation at short and long wavelengths respectively, and ii) ensure the potential vorticity conforms with observed spectra. The damping coefficient are constant at all times and for all runs. They are to ensure a realistic energy spectrum and to prevent the "building up" up energy at long length scale and enstrophy at short length scales. The values of the coefficients are fixed having been determined by Martin *et al.* (2002) to produce an appropriate parameterisation of long and short length-scale dissipative processes. The pseudospectral scheme is used for computational efficiency. However it is not suitable for reactive tracer advection. The sinusoidal nature of the Fourier transform precludes its use as reactive tracer transport must be positive definite. Therefore biological tracer advection is carried out using a finite difference scheme (Smolarkiewicz and Margolin, 1998) with explicit diffusion (Smolarkiewicz and Grabowski, 1989). Smolarkiewicz's schemes are used for their robust and accurate nature. In addition to this there are corrections for the overly diffusive nature of any finite difference scheme, and also to prevent propagation of errors resulting from sharp tracer gradients.

Effective diffusivity, parameterising the rate of mixing and sub-grid scale stirring, was scaled to unity during non-dimensionalisation in the previous one-dimensional model.

In that instance when calculating expected length-scales, dimensional values were estimated using Okubo's formula related effective diffusivity to length-scale (Okubo, 1971). Although the two-dimensional physical field is again non-dimensionalised prior to solution it is necessary to pick a range of model effective diffusivities which are equivalent to realistic values. The same range of values for effective diffusivity is used for the majority of investigations. For the tracer (inert and logistic) runs $35.4 \leq \kappa \leq 89.0$ m^2s^{-1}. For the NPZD runs, due again to the differing biological time scaling, this corresponds to $107 \leq \kappa \leq 214$ m^2s^{-1}. This range is chosen as previous testing has found diffusivity, tested through propagation of a Fisher front in a purely diffusive environment, to be accurately reproduced for this range of values (Martin *pers. comm*). The values are considered appropriate for the grid spacing within the model considering the order of magnitude error associated with the values (Okubo, 1971).

The initialisation of tracer fields will be discussed below in the context of the experiments to be carried out. In addition to this a number of perfect virtual Lagrangian drifters are initialised throughout the domain. These can be positioned at any point in continuous space, not just within a cell as with tracers. This has the great advantage of allowing high spatial resolution within areas of particular interest- the cells within which tracers are initialised. These drifters are initialised with one at the centre of each cell throughout the domain with an increased 5x5 per cell resolution (regular 200m spacing) in the cells within which tracers are initialised plus those 3 cells extending each side to ensure good local coverage.

b. Biological Model

There are a plethora of marine ecosystem models in use to simulate the many different biological processes in the marine environment.

In an attempt to understand population dynamics using the simplest case first two individual tracers are used prior to use of an ecosystem model

i) *inert tracer*: to interpret dynamics purely resulting from the physical processes. To investigate reactive dynamics and ensure results are comparable with the one-dimensional studies it is necessary to first understand any differences, in tracer dispersal, solely due to the physical model dynamics. This provides a foundation on which reactive effects can be considered. Furthermore an inert tracer has been shown to be suitable for predicting phytoplankton patch size for low growth rates (Martin 2000).

ii) *logistic tracer*: thought to be suitable for representing a phytoplankton bloom. A population limit is specified. Below this concentration tends exponentially towards this limit as described in chapter 3. As the limit is approached net growth rate decreases with quadratic mortality exceeding linear growth if the population threshold is exceeded. The one-dimensional studies showed filament width to be independent of population limit, therefore this limit is kept constant between all logistic tracer runs.

iii) *Nitrate-Phytoplankton-Zooplankton-Detritus*: a four compartment ecosystem model as described below.

Nitrate-Phytoplankton-Zooplankton Detritus (NPZD) model

The phytoplankton model used is that of Martin *et al.* (2001), a slightly modified version of that developed by Oschlies and Garcon (1999) which in turn adopts many functional forms and parameter values from the Fasham (1990) seven compartment ecosystem model. It is used due to its robustness and ability (embedded in a locally suitable physical model) of reproducing seasonal cycles in both oligotrophic and non-oligotrophic regions without

changes to the parameter set (Oschlies *et al.*, 2000). As with the two-compartment ecosystem (model) investigated in chapter 3 the same applied effective diffusivity is used for all compartments.

In the absence of physical processes, mixing and stirring, the evolution of the individual biological tracers within the four compartment model are given by:

$$\frac{dN}{dt} = s(N_o - N) - V_P\left(\frac{N}{k_N + N}\right)P + \mu_D D + \gamma_2 Z \qquad 4.4a$$

$$\frac{dP}{dt} = V_P\left(\frac{N}{k_N + N}\right)P - \left(\frac{g\varepsilon P^2}{g + \varepsilon P^2}\right)Z - \mu_P P \qquad 4.4b$$

$$\frac{dZ}{dt} = \gamma_1\left(\frac{g\varepsilon P^2}{g + \varepsilon P^2}\right)Z - \gamma_2 Z - \mu_Z Z^2 \qquad 4.4c$$

$$\frac{dD}{dt} = (1-\gamma_1)\left(\frac{g\varepsilon P^2}{g + \varepsilon P^2}\right)Z + \mu_P P + \mu_Z Z^2 - \mu_D D - w_s\frac{D}{h} \qquad 4.4d$$

where N, P, Z, and D are concentrations of Nitrate (N_{NPZD}), Phytoplankton (P_{NPZD}), Zooplankton (Z_{NPZD}) and Detritus (D_{NPZD}) respectively. The other parameters are as described in table 4.1. Values, unless explicitly mentioned, are those of Oschiles and Garçon (1999), determined by a optimisation exercise (Fasham, 1995) to give good agreement with North Atlantic chlorophyll and nitrate levels when embedded in a basin circulation model. The modification to the Oschiles and Garçon (1999) model is the nitrate source term, $s(N_0\text{-}N)$, representing nutrient upwelling from "deep". In addition to local N_{NPZD} value, this is dependent on the vertical transport parameter, s, and the Nitrate value in the underlying water (here regarded as below the mixed layer), N_0. Two different values are used for the "deep" value for Nitrate: N_0=2 and N_0=15 mmol N m^{-3}. These estimates correspond to mid-latitude North Atlantic nitrate concentrations (Fasham, 1995). The values are chosen to represent the effect of higher (winter max.) and lower (summer min.) nutrient availability on the phytoplankton population growth rate and so enable investigation of the phytoplankton patch size under different ecosystem conditions. The other parameter to be altered in the experiments is the prey capture rate, ε. This is set at 0.2

and 1.0 (mmol N m^{-3})$^{-2}$ d^{-1} to represent smaller and larger predators respectively. Combinations of N_0 and ε are used to create 4 different scenarios or biological regimes (B.R.) for investigation.

B.R.(i): N_0=15 mMol N m^{-3}, ε=1 (mMol N m^{-3})$^{-2}$ d^{-1}

B.R.(ii): N_0=2 mMol N m^{-3}, ε=0.2 (mMol N m^{-3})$^{-2}$ d^{-1}

B.R.(iii): N_0=15 mMol N m^{-3}, ε=0.2 (mMol N m^{-3})$^{-2}$ d^{-1}

B.R.(iv): N_0=2 mMol N m^{-3}, ε=1 (mMol N m^{-3})$^{-2}$ d^{-1}

The varying biological regimes allow for investigation of the structure produced in P_{NPZD} with differing achievable growth rates. The applied maximum phytoplankton growth rate, V_p, remains the same for all runs at 1 d^{-1}. Investigations of the N-P system in chapter 3 showed that the definition of growth rate that we should use is the nutrient dependent effective growth rate which corresponds here to:

$\mu^* = V_P\left(\frac{N^*}{k_N + N^*}\right)$, where N^* is the mean concentration of N_{NPZD} across the filament width, this means there will be a different effective growth rate for each width measurement of the filament. As guidance the range of effective growth rates for each biological regime are listed below.

B.R.(i): $0 < \mu^* < 5\text{x}10^{-2}$ day^{-1}

B.R.(ii): $3\text{x}10^{-8} < \mu^* < 5\text{x}10^{-4}$ day^{-1}

B.R.(iii): $3\text{x}10^{-5} < \mu^* < 7\text{x}10^{-3}$ day^{-1}

B.R.(iv): $2\text{x}10^{-6} < \mu^* < 5\text{x}10^{-3}$ day^{-1}

4.2.2 Experiments

Tracer release experiment

An idealised tracer release experiment is conducted with inert and logistic tracers in a two-dimensional (horizontal) turbulence model (see section 4.2.1a for description). The structure produced in these tracers is considered and compared to the physical properties of the environment is which it has evolved (rates of mixing and strain). The tracer is initialised in a small patch of 3x3 grid cells, ≡ 6x6 km. The model is run for 6000 iterations, approximately 33 days. The full tracer field is output approximately once every 600 iterations or 3.3 days. The physical field, of which we require a greater temporal resolution for calculation of strain rate, is outputted every 60 iterations (0.3 days). The model is run for a range of diffusivities $35.4 \leq \kappa \leq 89.0$ m^2s^{-1} and maximum growth rates of 0 (inert), 0.1, 0.5 and $1d^{-1}$. The values of applied effective diffusivity and maximum growth rate are chosen to represent a reasonable range of observed values. The population limit, shown in chapter 2 and 3 not to impact upon the minimum equilibrium width, is kept constant for all runs at 1 mMol m^{-3}.

There is primary interest in the minimum equilibrium length-scale of the resulting tracer distributions throughout the run. In chapter 2 filaments were found to have a mean convergence time of 3 days for a strain rate of $10^{-6}s^{-1}$. Predominantly filamental structure, an indication of strain dominated dispersal, is identified. The width of the tracer patch is then used together with a measure of the local strain rate to calculate a value for effective diffusivity according to equation 2.7/3.9. The calculated value is compared with that applied throughout the run for all runs covering the above range of effective diffusivities. This results in a discrete and pre-defined range over which to carry out a regression and hence allows quantitative assessment of the quality of the formula for relating patch width to rates of mixing, strain and reaction. The technique used to find the width of the filament

in the 2D model is described in section 4.2.3a. An in-depth investigation of methods used for calculation of strain is presented in Chapter 5.

Fertilization experiment

This experiment uses a similar method to the individual tracer release investigations. Initially the flow and mixing are frozen and the NPZD biological fields run to homogeneous equilibrium for the parameter values used. The parameters and their applied values were described previously in section 4.2.1b and listed in table 4.1. The P_{NPZD}, Z_{NPZD} and D_{NPZD} domains are then initialised homogenously at the equilibrium value. The N_{NPZD} field is initialised at the equilibrium value apart from a small (3x3 grid cells) patch which is 'spiked' with the deep value, N_0. The flow is then unfrozen and the full model is then evolved for 6000 iterations. Preliminary investigations found that interesting biological transient was completed, with concentration perturbations becoming undetectably low, before the field had developed interesting spatial structure through physical dispersal. To avoid the need for alteration of biological parameters, requiring an extensive tuning and sensitivity analysis as well as being somewhat biologically unjustified, the time scaling between physical and biological models is reduced by a factor of 3 compared with that used for the preceding individual tracer experiments. This is chosen to allow the biological field to maintain realistically observable values of tracer heterogeneities in the time taken by the flow to tease out a filament. The order of three reduction in scaling is equivalent to an increase in the rate of physical processes: i.e. velocity and hence strain rate. The new scaling results in peak velocities of up to $1 m s^{-1}$, still a reasonable value for frontal regions such as between eddies as found here. The model run now lasts approximately 10 days, with daily outputs of the tracer field and ten times daily outputs of the physical field.

The cross-sectional structure of filaments produced in each of the biological fields is considered, the width calculated and this used with the local (with respect to the width measurement) strain rate to calculate a value for effective diffusivity (using equation 2.7/3.9). This is then compared with the applied value as with the prior individual tracer studies. One minor change is that only the P_{NPZD} field is used for determining the position for extraction of data. The other fields are extracted at the same positions to ensure that profiles can be compared directly. The P_{NPZD} field is chosen as it is the dynamics of phytoplankton distributions in which we are ultimately interested. The goal of this stage of investigation is to describe the minimum expected length-scale of phytoplankton distributions and to consider the difference between a parameterisation of phytoplankton dynamics (logistic tracer) with that seen in a more sophisticated ecosystem model (P_{NPZD}).

Interference experiment

This presence of a single filamental structure is a rare event, normally indicative of tracer release or fertilization experiments (Ledwell *et al.*, 1993; Boyd and Law, 2001a). In addition to analysis of a single patch or filament there is necessity to consider the generally intricate patterns observed in natural oceanic phytoplankton distributions (e.g. figure 1.1). It is wished to also consider the effect of multiple filaments, impinging upon each other, when attempting to measure minimum equilibrium length-scales of inert tracer and phytoplankton distributions. The original filament, analysed in the previous experiments, is still present but it is now obscured by a more complex tracer field. A complex field is generated in two ways:

i) *Multiple release*: in addition to the single release already described additional multiple discrete 6x6km patches are initialised throughout the domain.

ii) *Release above a background level*: the single 6x6km patch is initialised above a non-zero background level, extending a little way either side of the patch.

The areas selected for interference with the filament are identified through back-tracking of drifter trajectories. As previously mentioned drifters are initialised throughout the domain. Those which are within the filament at any stage of its evolution are identified and their initial position used for initialisation of the tracer (and N_{NPZD}) fields. For the multiple release setup ten additional positions are picked on qualitative grounds such that an interesting, multi-filamental, field ensues. For the release above a background level each individual cell, for which a drifter initialised within was in or close to the original filament by day 21, is initialised at half the deep level (0.5 for the inert tracer, $N_0/2$ for the N_{NPZD} field). The positioning of the cells ranges between 5-50 cells away from the original tracer release location. Results relating to the interference experiments are presented in chapter 7- survey of tracer fields.

4.2.3 Analysis techniques.

In addition to the model setup the techniques used for analysis of the tracer profile require careful consideration. Approaching tracer investigations from a numerical perspective we are in the beneficial position of having accurate and synoptic knowledge of the tracer field. It is sought to minimise all extra possible sources of error.

a. Finding the width of a filament

To avoid a convoluted description the steps for measuring width are listed below with elucidation where necessary. The same width-finding technique is used for analysis of all two-dimensional tracer fields. There is a slight exception in the case of the ecological model where analysis of the N_{NPZD}, Z_{NPZD} and D_{NPZD} fields uses the same cuts/transects used for the P_{NPZD} analysis. This is to ensure that results for all components of the ecological model are directly comparable.

i) ***A suitable tracer distribution is identified*** a tracer patch not isolated within an eddy core is used. For ease of analysis one is chosen not extending across the domain boundaries. In keeping with our intentions of investigating the "best case scenario" it is chosen to investigate filamental structure, indicative of strain dominated tracer dispersal, when our formula for predicting minimum-equilibrium width of tracer distributions is expected to be most accurate.

ii) ***The tracer field is contoured at a chosen threshold level.*** The one-dimensional study showed 0.01% of maximum tracer concentration to give consistent results for width measurements, removing geometric effects impinging upon width measurement, and is used again for inert and logistic tracer studies. For the NPZD analysis a higher threshold is used, 1% of maximum P_{NPZD} concentration, as this is deemed to be a more reasonable detection limit for comparison with observational capabilities.

iii) ***A suitable section of filament identified.*** Areas showing refilamentation and/or interference within the main filamental structure, and obvious eddying are avoided as these are structure determined by processes on a different scale to that which we are considering. Again this is justified through our motivation of investigating the "best case scenario". This complication is investigated in chapter 7.

iv) ***The tracer gradient at each point along the section is calculated.*** These gradient calculations are the starting points for the lines of extraction, as the gradient determines the direction in which the cut is taken. The tracer gradient, calculated at each point along the chosen section of the threshold boundary of the tracer, will be orthogonal to the tracer isopleths.

v) ***A cut is taken across the tracer patch in the direction orthogonal to the boundary isopleths.*** The cut is continued until the tracer concentration once more reaches the threshold value.

vi) ***At each grid cell along the cut the tracer concentration is extracted.*** Strain rate also extracted in the same positions as the tracer concentrations (details of derivation of the strain field are presented in chapter 5). For the NPZD case having determined positions of the P_{NPZD} cross-section all tracer concentrations and production values are extracted for the same positions.

vii) ***A curve is fitted to the extracted tracer distribution.*** For an inert tracer a Gaussian is fitted. For the logistic tracer and NPZD model both a Gaussian and a double hyperbolic tan (DTANH) function are fitted. That which results in the lowest error between the data and the fit is taken as the solution. The curve is fitted according to minimisation of the least squares error between the data and the curve. The propriety of fitting simple curves and the number of actual tracer profiles being well described by these curves is discussed in section 4.3.2.

viii) ***The fitted curve is used to estimate the width of the filament for this cut.*** Although different thresholds were used for detection of the tracer boundary in step (ii) all fitted curves (for inert, logistic and ecosystem tracers) use a threshold of 0.01% of the maximum tracer concentration along the cut to estimate width to ensure consistency.

Having accurately measured the width of the tracer filament a value of effective diffusivity is calculated according to equation 2.8 or 3.9, as appropriate, using the best local estimate of strain rate for this cut. This issue of what constitutes our "best" estimate of local strain rate is discussed in-depth in chapter 5.

b. Calculation of effective diffusivity

Effective diffusivity is calculating according to the formula for predicting minimum length-scale (equation 2.8, 3.9 as appropriate). The calculated value is then compared with the applied value. The accuracy of the relationship is quantitatively assessed through a linear regression of effective diffusivity calculated for all runs, at all times of suggested strain dominated dispersal, for a particular tracer against the range of applied effective diffusivity for which the tracer was investigated. The ability of the formula to predict minimum equilibrium width can then be criticised based on

i) *Accuracy*- the deviation of the coefficients of regression from a 1:1 fit

ii) *Precision*- degree of linearity in the fit. This is based on the R^2 value which provides a measure of the percentage variability within the data explained by the linear regression used. This is considered with the proviso of a good confidence of fit, or *p* value which describes the probability of reproducing the relationship from a random dataset. The root residual mean square (RMS) error, a measure of the error between the actual model output and the values predicted via our formula (equation 2.8/3.9), is also used as a measure of the mean magnitude of deviation between measured values of width, and estimates of them made using knowledge of the applied effective diffusivity.

Based on these criteria the previously derived formulae for predicting minimum equilibrium length-scale can be judged on their ability to predict minimum length scales in a more realistic scenario. From this recommendations can be made as to their application in further modelling or *in-situ* studies. Modification to any scaling factors can be made based on the deviation from a 1:1 relationship providing a good linear relationship is still found. A generally poor relationship will suggest that the formula is not fully representing processes controlling patch width and that further investigation of the reactive processes which must be represented within the formula is necessary.

c. Estimating Local Strain rate

The strain rate is extracted from the strain field simultaneous to width finding in the method described above. However the particular method for calculating strain requires careful consideration as a number of different methods have been used in studies of tracer dynamics. The various approaches and the methods for determining the most appropriate method of measuring strain rate are considered in chapter 5.

4.3 Preliminary Results

Prior to presenting specific results for reactive tracers in chapters 6 and 7 some brief insights into inert tracer dynamics within a turbulent field are presented to explain our reasoning behind choices made in subsequent chapters. Errors as a result of inaccuracy in measurements, curve fitting and unrepresentative model output are also considered.

4.3.1 Tracer Dispersal

Unsurprisingly the structure observed in an inert tracer is dependent upon the range and strength of the physical processes by which it has been affected. Figure 4.3.1 shows an example of two extreme outcomes.

Tracer A has been initialised within a large eddy which remains stationary for the period considered. Eddies are often observed to stationary for periods of months (Martin *et al.*, 1998) and it is more than reasonable that this feature remains stationary within the modelled period of 30 days. Around vortices there is a transport boundary trapping physical tracers within the core (e.g. Wiggins, 1988; Martin *et al.*, 2001b). The tracer effectively diffuses within the transport boundaries but remains isolated from the rest of the field within the core of the eddy. Although interesting, the dynamics of tracers trapped

within eddies forms a different subset of tracer investigations not considered within the context of this thesis.

Tracer B has been initialised within a strong straining region. The physical dimensions of the patch are controlled by the competition between mixing, stirring and reactive dynamics (when considering a reactive tracer, not applicable for inert tracers) as opposed to closed transport barriers. The theoretical regimes described by Garrett's (1983) theory may be seen. The patch initially disperses primarily as a result of effectively diffusive mixing. As it reaches a sufficient length scale to experience strain in the flow it is drawn out into a long, thin filament. As the length scale increases further re-filamentation occurs, the beginnings of which can be seen in the profile of tracer (B) onwards from day 8, resulting in an increasingly convoluted profile which will lead eventually to the predicted homogenisation of the tracer field. It is the dynamics of the mode of tracer dispersal, in the second, strain dominated period, in which we are interested. This is the period when the one-dimensional formula derived in a uniform pure strain flow should best apply.

Figure 4.3.2 shows comparison plots for an inert tracer, logistic tracer (maximum growth rate=1 d^{-1}), and P_{NPZD} tracer of the NPZD model in a strain dominated flow (full analysis can be found in chapter 6). This provides an illustration of the influence of reactive effects acting in conjunction with the physical dynamics of the flow in which they are contained. Structure can be remarkably different for the inert and reactive tracers- such as for the logistic tracer where dispersal due to propagation of reactive fronts of tracer are clearly dominating over physical controls on structure in this instance. For the P_{NPZD} tracer additional biological constraints are suppressing biological dynamics preventing the propagation throughout the domain as seen for the logistic growth tracer. The P_{NPZD} structure is very similar for to that of the inert tracer where, aside from differences in concentration, it is difficult to visually discern any differences between structure in the inert

and reactive (P_{NPZD}) tracers. As will be shown in chapter 6 there are however subtle yet significant differences which can easily be missed.

4.3.2 Consideration of effect of error in width and strain on κ_{calc}

Considering first an inert tracer, or low growth rate reactive tracer for which the asymptotic structure is Gaussian, the calculated effective diffusivity depends on width, W, and strain rate, λ, as $\kappa \sim W^2\lambda$. A very crude estimate of error in the calculated effective diffusivity, κ_{calc}, is similarly dependent: $\varepsilon\kappa \sim \varepsilon W^2 . \varepsilon\lambda$, where ε denotes the error.

This assumes that the largest errors in W^2 and λ occur simultaneously. Any error in strain rate will have a similar magnitude of effect on the calculated diffusivity. Typical variability in the strain rate is found to be of order $10^{-6}s^{-1}$ for a mean strain rate of $1x10^{-5}$ s^{-1} so this will have a 10% effect on calculated diffusivity. This is assumed to be the expected order of magnitude error of effective diffusivity. The width has a greater potential for influencing the magnitude of the error as the solution is dependent on the square of width. An error of 1km (1/2 a grid cell) has the potential for a 7% error in diffusivity, for a typical width of 30 km.

For a high growth rate logistic tracer, where the asymptotic solution is described by a DTANH function the effective diffusivity is now dependent upon the effective growth rate, μ, and has increased dependence upon the strain rate, $\kappa \sim (W^2\lambda^2)/\mu$. Very crudely once again this has similar effect on the maximum estimate of error, $\varepsilon\kappa \sim (\varepsilon W^2 . \varepsilon\lambda^2)/\varepsilon\mu$. Typical phytoplankton growth rates are of similar magnitude to typical oceanic strain rates, meaning a 10% error in estimating growth rate will have approximately 10% effect on calculated diffusivity. The dependence of error in diffusivity on the square of error in strain rate actually acts to decrease its effect. An error of order 10^{-6} on a mean strain of order $10^{-5}s^{-1}$ now has a maximum impact of 1% error on effective diffusivity.

This sensitivity of error in effective diffusivity emphasises the necessity for consistent and accurate measurement of width, strain and growth rates. Methods relating to accurate measure of strain rate are presented in chapter 5. The appropriate measure of growth rate was considered in chapter 3. For the following analysis of a logistic tracer the growth rate for consideration is the maximum applied value. For the NPZD investigations it is the nutrient dependent apparent growth rate that should be used, as in chapter 3. This will be further discussed in chapter 6 in the context of results. Regarding width, every effort is made to ensure accuracy in the methods used here by minimisation of errors in curve fitting and a high threshold R^2 for considered solutions (0.95 for the tracer experiments, 0.80 for the NPZD compartments as explained in section 4.3.2). Consistency is provided by use of the same analysis methods throughout all investigations. One possible source of error here is the difference in boundary threshold for finding width, remembering that all curves are solved to the same threshold (0.01% of maximum) in accordance with our definition of width. This has been investigated by comparing the mean and standard deviation of width of an inert tracer patch measured at threshold of 0.001, 0.01, 0.1, and 1% of the maximum tracer concentration. For a threshold greater than 0.01% there is no significant change in width for the different threshold values, although there is a slightly increased variance of width with threshold. This suggests that is it preferable to use the lowest possible threshold to reduce error on width, but a higher threshold can be used if necessary for identification of the filament, such as in the NPZD investigations where a lower threshold was considered observationally unreasonable. A lower threshold, 0.001% of maximum, results in a mean width within the error bars of the other threshold but it is greater by approximately 5km. A threshold of 0.01% of maximum tracer concentration is the lowest bound that can be considered for consistency between mean and variation of width measurements, an indication of error.

4.3.2 Error in fitting curves to data

Due to the sensitivity of error in effective diffusivity on the error in measurement of filament width we restrict attention to high quality fitted curves. Only cuts where the R^2 value is greater than 0.95 will be used for calculation of effective diffusivity. This applies to all tracer at all times.

For the inert tracer an acceptable curve fit to transect is reached for all transects taken. Of these an R^2 of greater than 0.95 is achieved for at least 50% of solutions. Table 4.2(a) lists the number of individual width measurements calculated for each tracer at each time, the number of these achieving a width solution, and the number for which the threshold R^2 value is achieved. For the logistic tracer again a solution is achieved for all transects (table 4.2(b)-(d)). For the run with lowest general quality of fit an R^2 of greater than 0.95 is achieved for more than 40% of solutions. The percentage of satisfactory solutions does not consistently depend upon diffusivity or growth rate. This can be taken as a reassurance that any observed trends in width or calculated diffusivity are not a result of geometric effects- the fitted curves do not describe data less accurately due to growth or mixing effects.

For the P_{NPZD} compartment of the NPZD model the chosen solutions of Gaussian curve or double hyperbolic tan (DTANH) function no longer consistently describe the across filament profile accurately (table 4.2(e)-(h)). Examples of the fits are shown in figure 4.3.3. For all biological regimes and times 0-70% of transects are sufficiently well described by a Gaussian or DTANH function that they can be considered for quantitative analysis of the variation of width. Again there are no consistent trends upon applied diffusivity or biological regime (a reflection of maximum growth rate).

4.3.3 Confidence in the regression

Having considered a regression of calculated to applied effective diffusivity the confidence in the regression is estimated. The regression analysis assumes the errors are normally distributed about the predicted value. It is very reasonable to expect of high degree of non-linearity in the variability associated with the data. However a first order approximation of the error is obtained by assuming a normal (Gaussian) distribution. For all tracer runs a "*p* value" less than 0.001 is calculated (Lindley and Scott, 1996) meaning there is a less than 0.1% chance of reproducing the regression with a random data set. For the NPZD runs there is, on occasion, a lower sample size due to the smaller number of satisfactory fits when fitting curves to filament cuts (table 4.2). Even at worst though there is less than a 1% probability of reproducing the distribution with a random dataset . This is taken as reassurance that the regressions of calculated to applied effective diffusivity are statistically sound. This does not necessarily mean there is a good fit, or that the formula is validated or negated. It does however mean that there can be a reasonable degree of confidence in results. Findings are not a chance occurrence, they are a definite consequence of the physical and ecosystem model dynamics. Whether we have been extensive enough in our model consideration is considered within the context of the experiments (chapters 5, 6 and 7).

4.4 Aims for remaining chapters

Investigation of tracer dynamics continues by building upon previous one-dimensional results (chapter 2 and 3) through considering the dynamics of a reactive tracer in a two-dimensional turbulent field.

In chapter 6 the formulae derived in chapters 2 and 3 for predicting the minimum length-scale of tracer distributions in a pure strain flow are tested. The validity of

investigating a logistic tracer as a proxy for phytoplankton dynamics is also questioned by considering the dynamics of a simple ecosystem model in the same physical environment.

In chapter 7 an attempt is made to enable comparison with observational results by considering the difference between an accurately, and synoptically, known simple tracer field and i) that likely to be observed in a ship based study, ii) the type of convoluted field known to more commonly be found in general phytoplankton distributions.

Prior to this we take an aside in chapter 5 to consider a seemingly obvious factor- the measure of strain rate. Although clearly defined methods of calculating this exist they vary through comparable studies and there is currently no obvious "best" definition. It may vary with context and it is therefore important to ascertain which, if any, estimate of strain rate is best used for the purposes of investigating tracer filament morphology.

CHAPTER 5: The 'Best' Measure of Strain.

5.1 Introduction

Prior to quantifying the minimum length-scale of tracer filaments in a two-dimensional model (see chapter 4 for model description and chapter 6 for results) an aside is taken to consider the options available for quantifying strain effects. As discussed throughout the thesis the minimum length scale of tracer distributions has been found to depend upon the local rates of mixing and strain. Although these rates can be defined mathematically in a number of ways the appropriate choice may depend on the context in which it is to be used.

Mixing is generally accepted as a term to describe both the actual mixing of fluids, a molecular process, and the effect of repeated stretching and folding (straining processes) at scales smaller than those which can be explicitly resolved (here 2km). Effective diffusivity is an accepted parameterisation of mixing rates, used to describe these sub-grid scale advective processes. Although it is not a quantity which can be measured directly *in-situ* mixing rates have been subject to in-depth investigation (Okubo, 1971).

Strain rate is clearly mathematically defined as the gradient of the velocity field. This is an instantaneous value describing the strain effect upon a fluid element at a point in space and time. When considering tracer dynamics a parameterisation is required of the cumulative effects of the spatially and temporally varying strain experienced by a tracer patch over its spatial extent and history. There have been a number of different techniques used to quantify strain in comparable theoretical and observational studies of tracer patch dynamics. This chapter considers which measure is most appropriate for investigations of the nature considered.

Observational constraints mean that sea-faring investigators by necessity limit themselves to whatever information is available but investigation via a numerical simulation allows exploration in an idealised environment where desired fields can be known globally and synoptically, where there is accurate knowledge of applied parameterisations (the value of effective diffusivity), and where possible sources of error in sampling can be minimised.

To investigate strain rates, the dispersal of an inert tracer in the two-dimensional turbulence model, described in chapter 4, is considered. An inert tracer is used as any observed distributions are solely due to the flow history the tracer patch has experienced. Although reactive tracers are considered in subsequent chapters there are incompletely understood reactive-physical dynamical interactions associated with these. Hence inert tracer dispersal is taken as our gauge for understanding the physical environment. High resolution Lagrangian drifter deployment and simultaneous output of the tracer and velocity fields allows various descriptions of strain to be calculated and the relationship between the tracer patch width and these used to assess the accuracy and practicality of each description of strain for use in investigation of oceanic tracer dispersal.

5.2 Methods

We are seeking to derive the "best" measure of "effective" strain rate- a quantitative measure of the effect of temporally and spatially varying strain rate on tracer dispersal. For this the dispersal of an inert tracer is considered. Knowing that the width of inert tracer patches is well described by the dispersal theory of Garrett (1983) and that this is supported by observation (Ledwell *et al.*, 1993) we justify determining our "best measure of strain" according to this theory.

An inert tracer is initialised, with high resolution Lagrangian drifters, in a high strain region of the physical model and the field evolved as described in chapter 4. The width of the tracer patch is calculated and this used with the various methods used for calculating strain rate for estimating the value of the effective diffusivity. A number of runs are conducted for a range of applied values of effective diffusivity. The "best" measure of strain will be that which results in the "best" calculation of effective diffusivity, determined from the highest quality of regression of the calculated and applied effective diffusivities as described in chapter 4. Great care has been taken to minimise all possible sources of error in width measurements. The only source of variation is in the method for calculating strain rate.

The strain rate is calculated at the position of each drifter. The standard initial resolution of these drifters is one per grid cell (2km spacing) with 5x5 per gridcell (400m spacing) in each cell that tracers are initialised and for three cells deep surrounding such cells to ensure good local coverage. These ideal drifters are unaffected by frictional effects, which result from droguing with *in-situ* drifters. Velocity at each drifter position in time is recorded. Strain rate is calculated either from the velocity gradient (strain tensor) at the position of each drifter at each time, or from the movement of each drifter over the previous time step. The strain fields are gridded, using linear interpolation, to produce a strain field for each method at each time allowing direct comparison with the tracer field so that the strain can be extracted at exactly the same positions as the tracer concentrations. The exceptions to this are methods 13 and 14 which provide a single estimate for effective strain rate to be used for tracer analysis at all positions and times. Using prior knowledge of inert tracer dispersal, as described above, it is possible to assess the best measure of strain for our purposes.

5.2.1 Determining 'Best' measure of "Effective" Strain

Explicit solution of the equations describing dispersal of an inert tracer in a pure strain environment (Garrett, 1983) shows that the variance of the tracer cross-section, σ^2, is related to the diffusivity, κ, and strain rate, λ, by:

$$\sigma^2 = \frac{\kappa}{\lambda} . \qquad 5.1$$

Equation 5.1 states that the width of an inert tracer patch is given by a balance of the two processes acting upon the patch, diffusion acting to widen the patch and smooth tracer gradients, and variable advection (strain) acting to narrow the patch and increase tracer gradients. When considering a dimensional argument, we are concerned with dimensions in space (L) and time (T). We are dealing with diffusion, κ of dimensions [L^2/T], and strain, λ of dimensions [1/T], and are seeking a length-scale, l of dimensions [L]. The dimensional argument leads to the conclusion that $l \sim \sqrt{(\kappa/\lambda)}$ and analysis by Garrett (1983) shows the coefficient of proportionality to be one.

By repeating the tracer dispersal experiment for a number of different diffusivities a dataset covering a prescribed range of values is obtained. The regression of $\sigma^2\lambda$ (κ_{calc}) to κ_{app} (calculated to applied diffusivity) can then be calculated using the plethora of available options for determining λ. By determining which version of λ provides the best fit for the above regression the best strain for the continuing studies of tracer dispersal can be determined.

A number of methods are considered including both instantaneous strain rates and estimates of the strain history of the tracer patch. In addition to determining the theoretically most accurate way of measuring strain effects the most practical method available for calculating strain rate in an *in-situ* study is determined.

5.2.2 Description of "Effective" Strain Rate

Prior to describing the different methods used for quantifying effective strain rate, the definition of strain rate and the effect that it is wished to parameterise in this instance are qualitatively described.

Need for Effective Strain Rate

Strain rate is mathematically defined as the gradient of the velocity field at a position in space and time. However an instantaneous measure of strain rate is not sufficient for the purposes of this study. A measure of the cumulative effect of spatially and temporally varying strain rate as experienced by a tracer patch is required. One measure of strain history is represented in the Lyapunov Exponents of a flow.

Cumulative measure of strain history- Lyapunov Exponents

Consider the trajectories of two initially infinitesimally separated fluid elements $\mathbf{x} = \begin{pmatrix} x(t) \\ y(t) \end{pmatrix}$ and $\mathbf{x} + \delta\mathbf{x} = \begin{pmatrix} x(t) + \delta x(t) \\ y(t) + \delta y(t) \end{pmatrix}$. Provided δx and δy are small the change of separation due to differing advective histories is given by:

$$\frac{d}{dt}\begin{pmatrix} \delta x \\ \delta y \end{pmatrix} = \mathbf{S}(t)\begin{pmatrix} \delta x \\ \delta y \end{pmatrix} \qquad 5.2$$

where $S(t)$ is the strain tensor of the velocity field.

In a two-dimensional, non-divergent flow ($v_y = -u_x$), the strain tensor can be resolved into purely straining and rotational components (Ottino, 1989) and expressed as:

$$\mathbf{S} = \begin{pmatrix} u_x & u_y \\ v_x & -u_x \end{pmatrix} = \underbrace{\begin{pmatrix} u_x & \frac{u_y + v_x}{2} \\ \frac{u_y + v_x}{2} & -u_x \end{pmatrix}}_{Symmetric:Strain} + \underbrace{\begin{pmatrix} 0 & \frac{u_y - v_x}{2} \\ \frac{-u_y + v_x}{2} & 0 \end{pmatrix}}_{Anti-symmetric:Rotation\ /\ Eddy\ effects} \qquad 5.3$$

$$\mathbf{S} = \quad A \quad = \quad B \quad + \quad C$$

The extension to a divergent field is straightforward but not relevant here.

For the two fluid elements their separation velocity depends upon the eigenvalues of the strain tensor, λ. These can be found by solving $|A - I\lambda| = 0$, where $I = \begin{pmatrix} 1 & 0 \\ 0 & 1 \end{pmatrix}$ is the identity matrix.

For small times the trajectory separation then satisfies $|\delta\mathbf{x}| = \delta\mathbf{x}(0)e^{\lambda t}$. In a non-divergent flow there will be exponential stretching along one directional axis (axis of maximum positive strain), and exponential contraction along the other. In general the two axes will not be orthogonal. The cumulative effect of strain can therefore be characterised by the finite time Lyapunov exponent (FTLE).

$$\lambda(\mathbf{x}(t), t) = \frac{1}{t}\log\left(\frac{\delta\mathbf{x}(t)}{\delta\mathbf{x}(0)}\right) \qquad 5.4$$

with the largest Lyapunov Exponent referring to the axis experiencing maximum stretching, or the dominant strain direction. In a non-divergent strain flow the exponents will be equal in magnitude but opposite in sign: there will be exponential growth of the tracer length-scale in the direction of the positive eigenvector, exponential contraction in the other. In the absence of mixing (here effective diffusion) the width of a tracer patch will continue to decay exponentially. However when mixing is present, as in the models considered here, a balance is reached between contraction due to strain and expansion due to diffusion, as shown in chapter 2.

When considering strain effects over small time intervals more care must be taken, as transient events may not be resolved, so a slight modification to the calculation of FTLE's is adopted (Pierrehumbert and Yang, 1993).

The matrix **M** is formed satisfying

$$\frac{\partial \mathbf{M}}{\partial t} = \mathbf{S}(t).\mathbf{M} \tag{5.5}$$

subject to the initial condition $\mathbf{M}(0) = I$, where I is the identity matrix. **M** can then be solved for θ, where $\begin{vmatrix} \mathbf{M}_{11} - \theta & \mathbf{M}_{12} \\ \mathbf{M}_{21} & \mathbf{M}_{22} - \theta \end{vmatrix} = 0$.

The newly desired modified Lyapunov exponent (MFTLE) is given by:

$$\lambda = \frac{1}{t}\log(\theta) \tag{5.6}$$

where θ is the eigenvalue of **M** with largest modulus.

On a practical note Lyapunov exponents are calculated by considering the cumulative effect of stretching on initially orthogonal unit vectors, $\mathbf{x}_0 = \begin{pmatrix} 1 \\ 0 \end{pmatrix}$ $\mathbf{y}_0 = \begin{pmatrix} 0 \\ 1 \end{pmatrix}$, for each time step. At subsequent times these vectors remain of unit length, by renormalisation after each time step, but lie in the direction of the axes of stretching. As the velocity field varies on temporal scales greater than a single time step (~0.1 hour) the deformation of the unit vectors can be approximated by a Taylor expansion limited to the first order:

$\mathbf{x}_t = \mathbf{x}_0 + \left[dt \cdot \left(u_x \mathbf{x}_0 + u_y \mathbf{y}_0\right)\right]$, $\mathbf{y}_t = \mathbf{y}_0 + \left[dt \cdot \left(v_x \mathbf{x}_0 + v_y \mathbf{y}_0\right)\right]$. The magnitude of the Lyapunov exponent for one time step, λ_i, is calculated from the change in size of the unit vectors:

$$\lambda_i = \frac{1}{dt} \cdot \log\left(\sqrt{\mathbf{x}_t^2 + \mathbf{y}_t^2}\right) \tag{5.7}$$

$$(\text{as } |\mathbf{x}_0| = |\mathbf{y}_0| = 1)$$

This is a measure of strain over the previous time interval or instantaneous Lyapunov exponent. The FTLE's, being a cumulative measure representing the strain history experienced by a particle, are expressed as $\lambda = \frac{\sum_{i=1}^{N} \lambda_i}{N}$, the modified exponents as

$$\lambda = \sum_{i=1}^{N} \frac{1}{t_i} \log \theta_i \qquad 5.8$$

where θ is calculated as shown above and t_i, the length of one time step, is the same for all times.

5.2.3 Methods for calculation of strain

It should be remembered that the most mathematically correct descriptions are seldom practical observationally and as a result concessions must be made. This may well create a fundamental mismatch between numerical and observational studies. We consider a selection of descriptions of strain in an idealised environment where every effort can be made to minimise sources of error.

We first describe all the different measures of strain considered before investigating which is the most appropriate and/or practical for studies of oceanic tracer dispersal.

λ_p, λ_f: Eigenvalues of the flow

The eigenvalues of the strain tensors corresponding to the two-dimensional, non-divergent (v_y=-u_x) velocity field are calculated. Eigenvalues relating to both the whole flow and to the pure strain component are considered. The positive eigenvalue (corresponding to exponential separation) is taken throughout

i) Whole flow: 5.9

$$|A - I\lambda| = 0, \Rightarrow \lambda = \pm\sqrt{u_x{}^2 + v_x u_y}$$

$$\lambda_1 = \sqrt{u_x{}^2 + v_x u_y}$$

ii) Strain component: 5.10

$$|B - I\lambda| = 0, \Rightarrow \lambda = \pm\sqrt{u_x{}^2 + \left(\frac{u_y + v_x}{2}\right)^2}$$

$$\lambda_2 = \sqrt{u_x{}^2 + \left(\frac{u_y + v_x}{2}\right)^2}$$

Where A and B are as described in equation 5.3. Eigenvalues of the strain component of the flow are also known as the diagonalised strain tensor (Haidvogel and Keffer, 1984) and form the strain component of the Okubo-Weiss mixing parameter (Okubo, 1970; Weiss, 1991).

λ_3:Gradient of Velocity Field

The stretching experienced by a tracer element is a result of differential advection within its boundaries. One of the simplest quantifications of this uses the magnitude of the velocity gradient at a point as:

$$\lambda_3 = \sqrt{u_x{}^2 + v_y{}^2} \qquad 5.11$$

The gradient is calculated at each particle position. This provides an instantaneous measure of strain at each position. This method of calculating strain is considered in the Garrett (1983) theory describing tracer dispersal in a turbulent environment, previously referred to.

λ_4-λ_{12}: *Lyapunov Exponents*

The theory and method relating to calculation of Lyapunov exponents has already been presented above. A variety of specific realisations are tested.

$\lambda_{4\text{-}8}$: *Instantaneous Lyapunov Exponents*

$$\lambda_t = \frac{1}{t}\log\left(\sqrt{\mathbf{x}_t^{\,2} + \mathbf{y}_t^{\,2}}\right) \qquad 5.12$$

The effect of stretching on the unit vectors due to

i) the whole flow, $\lambda_{4,5}$ (A in equation 5.4)

ii) rotational effects (anti-symmetric component of the strain tensor), λ_6, (C)

and

iii) pure strain (symmetric component of the strain tensor) , $\lambda_{7,8}$ (B)

are considered using the value over a single time step.

The above three cases are considered to assess the relative effects of the components on the observed stretching for a given time step. Rotational stretching is expected to be negligible, the whole flow and pure strain to be very similar.

$\lambda_{9\text{-}12}$: *Finite Time Lyapunov Exponents*

These are calculated only for the whole flow tensor (A). This is because the cumulative effects of stretching and rotation will be combined over time. Both the effect on units vectors:

$$\lambda_{9,10} = \frac{\sum_{t=1}^{N} \lambda_t}{N} \qquad 5.13$$

and the modified exponents:

$$\lambda_{11,12} = \sum_{t=1}^{N} \frac{1}{\delta t} \theta_t \qquad 5.14$$

are considered.

λ_{13}: *Rate of Change of Length*

A widely used "holistic" method of calculating *in-situ* strain rate for the purpose of tracer dispersal and fertilization experiments is from rate of change of patch length (Ledwell *et al.*, 1993, 1998; Abraham *et al.*, 2000; Sundermeyer and Ledwell, 2001). Put simply, a crude approximation to the cumulative strain experienced by a tracer patch can be obtained through considering the rate of change of length of the tracer patch. This seemingly simple measurement is, however, non-trivial. As is shown later, when we determine which estimate is to be carried forward, the value of strain is highly dependent upon the method used for measuring length and the accuracy with which it is carried out.

Two methods for finding the length of a filament are considered:

i) Maximum Tracing along filament.

The maximum tracer concentration within the whole filament is found. Surrounding grid cells are then searched for the next greatest value. This becomes the next reference cell. Surrounding boxes are then searched for the next greatest value, and so on until no available cells exceed the threshold concentration. A progression along the filament is encouraged by invoking the additional rules that:

(i) There shall be no return to a previously occupied cell.

(ii) There shall be no immediate doubling back. When a step is taken the subsequent one cannot result in a sharp reversal of direction.

(iii) There shall be no progression to a cell of higher concentration. This causes some problems with later stage convoluted filaments requiring user input to ensure completion of the along filament measurement.

An over-riding advantage of this method is that it is reasonably objective, there is very little requirement for user input in determining the length of a filament.

ii) Maximum tracing along rows/columns of domain.

Each row and column of the tracer grid is searched to find the maximum value in the row/column. Those corresponding to the filament are identified by the user. The filament can then be pieced together using the maxima, by eye, in a manner thought to best describe the filament. Although a highly subjective method this removes problems associated with the previous maximum tracing method in more convoluted filaments where tracer concentration does not decrease smoothly.

In addition, different boundary thresholds (the cut off for determining where a filament ends) are considered. The effect of using a reactive tracer is also considered, where rate of change of length will now depend upon reactive processes in addition to physical dynamics.

Having traced the centre line filament, by whichever method, this line is then subject to a seven points average. A seven point average was deduced to be an appropriate limit in order to smooth the jagged nature of the profile, a result of the discrete nature of the domain. It also reduces errors resulting from the necessity to have some user input, such as how the filament maxima are pieced together or in the case of a non-uniform decrease in concentration along the filament length where the centre line lies. A seven point average was found to remove the undesired effects without filtering out actual variations in the

filament length. It is sought to remove error without disguising physical properties of the filament.

Finally, strain rate is calculated from a least squares linear fit to the variation of log of filament length with time. This is only carried out for periods where length is increasing exponentially, indicating strain dominated dispersal. By analogy with the Lyapunov exponents,

$$L \sim L_0 e^{\lambda t} \Rightarrow \log(L) \sim \log(L_0) + \lambda_{13} t \qquad 5.16$$

Where L is the filament length at time t, initially of length L_0.

The use of half filament lengths was considered and disregarded as we seek a parameterisation of the cumulative effect of temporally and spatially varying strain rate. It is inappropriate to expect a sub-sample of the filament to be representative of properties as a whole.

Having compared the various methods of calculating strain from rate of change of length a representative value is compared with results from the other strain measuring techniques.

Determining the exact methods for measuring rate of change of length

The value of effective strain rate calculated from rate of change of length is highly dependent upon the details of the approach taken to measuring filament length (figure 5.2.1, depicting strain rate calculated from rate of change of patch length measured in a number of different situation and by two different methods). Great care has been taken to ensure lengths are measured as accurately, precisely and objectively as possible. Strain rate is calculated from a least squares linear fit of log of length with time. This is only carried out for the period where length is increasing exponentially. This varies with the applied diffusivity and boundary threshold but is generally days 9-18, which, it should be noted, is

different from the period where drifters within the tracer patch are separating exponentially. The length can be considered as increasing exponentially up to day 21 but the filament is becoming increasingly convoluted towards the end of that period requiring a greater degree of user input to measure the length and so day 21 is generally disregarded. The different periods of exponential stretching of the patch length and exponential drifter separation is discussed below in the section relating to λ_{14}.

Effective diffusivity is found to consistently affect measures of the method of estimating strain based on rate of change of length (fig. 5.2.1(a,b)). A higher diffusivity results in a lower estimate of strain rate. This is found for both methods of length finding.

The maximum tracking approach to finding length consistently results in a higher estimate of effective strain rate than that found from reassembling length from row and column maxima (fig. 5.2.1(b)). Maximum tracking is presumably a more accurate method as there is less necessity for user input and hence is more objective.

Varying the threshold boundary for defining the edge of the filament results in comparable estimates of mean strain, although a larger error/variability on the estimate is found for a higher threshold (fig. 5.2.1(c)).

A reactive (logistic) tracer, of sufficiently high maximum growth rate (0.5 d^{-1}), was found to result in a higher estimate of strain compared with an inert tracer (fig. 5.2.1(d)). The difference is somewhat negligible when compared to errors resulting from different thresholds and diffusivities. However a note of caution must be issued with this that due to the morphology of the filament a logistic tracer requires a greater level of user input for tracking the length of the filament. The inherently subjective nature of this, despite best efforts, will always result in an unquantifiable increase in error.

In summary, the strain rate calculated from rate of change of patch length varies with the analysis method, applied diffusivity, tracer threshold and behaviour of the tracer. This is

perhaps unsurprising but must be considered as a possible source of error when using this method. For the purpose of further analysis the mean value calculated from rate of change of the inert tracer patch length measured by maximum tracking for a mid-range diffusivity (53.4 m^2s^{-1}) at a threshold of 1% of the maximum tracer concentration is used as this will be most indicative of physical dynamics as opposed to tracer dynamics. This results in an effective strain rate of 1.5e-6 ± 2.0e-7 s^{-1}.

In practise investigators would not have this luxury of choosing this most representative measure of strain from rate of change of length. Our measure here is another best case scenario.

λ_{14}: *Separation of drifters*

Having calculated Lyapunov exponents from unit test vectors at the position of drifters we also estimate them directly from separation of the drifter trajectories. This is independent of any property of the drifters other than position and is closer to what can practically be calculated from *in-situ* drifter deployments.

Attention is now restricted to drifters initialised within the tracer patch. The tracer patch initially covers a 3x3 box area. The drifters are initialised in a 5x5 grid within each of these cells, resulting in a 400m resolution within the 6x6km patch.

The separation of each pair of drifters is monitored and then averaged for each initial spacing. This is done at 400m intervals. At later times the mean distance between pairs of drifters initially separated by the same distance is considered and the period when strain dominates is identified, i.e. when the separation of drifters is exponential. A value of effective strain rate is then calculated using a regression of the log of separation with time.

$$\lambda_{14} = \frac{1}{t}\log\left(\frac{\delta x_t}{\delta x_0}\right) \qquad 5.16$$

where δx_t is the separation of drifters, initially separated by δx_0, at time t.

Having considered the dispersal of drifters, and the effect of calculating strain rate over different periods and initial separations a representative value is chosen for comparison with other methods.

Separation of Drifters

The positions of drifters initialised within the tracer patch at three day intervals are shown in figure 5.2.2. Over 6000 model time steps (~30 days) all drifters initialised within the patch stay within the patch. Drifters are initialised at 400m intervals. Strain rate is calculated from the mean rate of separation of pairs of drifters initialised at the same separation distance. The averages are calculated for initial drifter spacing for bins spanning 400m to 6000m (largest separation within the patch) at 400m intervals. The mean separations for initial drifter separations of 400m and 4000m are shown in figure 5.2.3. The period when separation of drifters is exponential is the period where drifters are primarily influenced by strain effects. Figure 5.2.4 shows strain rate calculated from the mean separation of drifters at each initial separation. The three markers for each separation correspond to strain rate calculated over days 15-21, 15-24, and 15-27. Corresponding directly to these is a highest to lowest progression of strain rate respectively. Including periods where the separation of drifters is not exponential results in a lower estimate of strain rate. Note again the difference to the period when the tracer patch length appears to be increasing exponentially (days 9-18). Days 15-21 are consistently the period over which drifter separation is closest to exponential. This is strain dominated period corresponds with the second of Garrett's theoretical three regimes for tracer dispersal. For clarity the results for days 15-21 are replotted in figure 5.2.5. The estimated effective strain rate varies with initial separation of drifter pairs, with three groupings of <2000m, 2400-3600m, and >4000m showing internal

consistency in the estimate of strain rate. The mean strain rate is comparable for separations up to 2km, a slightly smaller standard deviation in strain rate is found for the closest separation of 400m. This supports the logic of using the minimum possible initial separation for calculating strain rate, as it is the closest approximation to the theory of the separation of initially infinitesimally separated fluid elements from which the method is derived. Using the smallest initial separation provides a single value for strain rate (for all runs) of $3.0 \times 10^{-6} \pm 2.0 \times 10^{-8}$ s^{-1}.

5.2.4 Length and time scales of the velocity field

When developing a parameterisation for the effect of a temporally and spatially varying strain rate knowledge is required of the limits over which this can justifiably be calculated. The limits are obtained from the integral or de-correlation length/time scales of the velocity field. It provides an upper limit to the length/time scales above which the velocity field is considered uncorrelated, above which additional dynamical features help control local velocity.

Maximum length-scales

A simple estimate of the upper length-scale for consideration of the velocity field is obtained by consideration of the length-scale of eddies. Within the physical models coherent rotational structures (eddies) have a length-scale of 40-80km. Once tracer length-scales exceed this it is reasonable to expect the filament to be experiencing a significantly differing balance of local rates of mixing and strain throughout its extent. Consideration of drifter separation has already indicated that local strain varies on scales an order of magnitude less than this (<6km). The eddy length-scale provides a semi-quantitative measure of the length-scale beyond which it can reasonably be expected to find different dispersal balances throughout the filament.

Maximum time-scales

A representative time-scale of the flow is less simply extracted. For this we measure explicitly the de-correlation time-scale of the flow using the Lagrangian correlation function of velocity, **u**, at all drifter positions.

The Lagrangian correlation functions (LACF's), R_{ii}, are defined as:

$$R_{ii}(\tau) = \frac{\langle \mathbf{u}_i(t)\mathbf{u}_i(t+\tau)\rangle}{\overline{\langle \mathbf{u}_i^{\,2}\rangle}} \qquad 5.19$$

where τ is the time lag from an arbitrary time t and $\mathbf{u}_i$ (i=1,2) represents the x and y components of the Lagrangian velocity. The double subscripts ii=(11,22) denote (x,y) autocorrelation functions. The angled brackets denote an average over all drifters, and overbar an average over all times. The correlation is calculated for all particles, and separations, and averaged over all particles. The maximum time-scale of the flow is estimated from the maximum time lag for which velocities can be considered correlated. The LACF for the flow used is shown in figure 5.2.6. For a 95% confidence limit the integral time scale of the flow is 5 days. This provides an upper limit to the time scale over which the velocity field can be considered correlated for the calculation of any field properties.

Although not explicitly required for consideration of strain the eddy length-scale and correlation function provide a useful measure of the length and time-scales over which field properties can be compared. For subsequent investigations drifters are initialised at 400m intervals up to 2km, particle positions are output three times daily and tracer fields output every 3 days.

5.2.5 Summary of methods

The fourteen methods used for estimating strain rate are summarised in table 5.1. Each method will be considered and the best one for representing the effect of a spatially and temporally varying strain rate on the width of a tracer patch will be established. This will be determined from the strain resulting in the highest quality of fit when calculating a regression of calculated diffusivity, $\sigma^2\lambda$, with the applied value(s) κ_{app} for an inert tracer.

5.3 Results

5.3.1 Mean variation

Perhaps unsurprisingly, different methods of estimating effective strain give different estimates. Methods 1-8 provide an instantaneous value of strain rate. Methods 9-14 are representative of the strain history, with methods 13 and 14 solely dependent on the strain history of the whole tracer patch. Figure 5.3.1 shows an image of the strain fields at the 3000th iteration (~day 15) for methods 1-12. The varying emphasis of dynamical features is evident. All are plotted with the same colour scale to aid visual comparison.

Plots are shown in figure 5.3.2, showing the mean and standard deviation of strain rate calculated over the entire domain and run period (i), and over days 15-21 (ii). The corresponding numerical values are listed in table 5.2. Although days 9-24 are visually identified as the period where the structure appears to be a simple filament (figure 4.3.2), analysis of drifter displacement shows that days 15-21 are the period during which drifters were dispersing predominantly due to strain i.e. separating exponentially (figure 5.2.4). Note that λ_6, the instantaneous Lyapunov exponents (ILE's) associated with the rotational component of flow, is negligible in comparison with the other methods as expected. For the finite time Lyapunov exponents (FTLE's) ($\lambda_{9\text{-}12}$), which are representative of strain

history, the modified exponents show a greater range of values. This supports the motivation for using them, that the effects of small transient features are resolved in greater detail.

Although all methods produce a similar estimate of mean effective strain rate there are clear differences in the way that the field is resolved (figure 5.3.1) resulting in significant variation in the standard deviation of the strain rate between methods. It now remains to identify the most appropriate method for our purposes.

5.3.2 Determining 'Best' Strain

As reiterated throughout, the best strain for our use is that providing the best quality of fit for a regression of calculated to applied effective diffusivity ($\sigma^2\lambda$ to κ).

For each of the methods used for calculating strain the maximum, minimum and average values are considered. The R^2 value for the regression over days 9-24 (visually identified as the period of strain dominated dispersal from the filamental structure) are listed in table 5.3(a). The values relating to the regression over days 15-21 (identified as the period of strain dominated dispersal from separation of drifters) are shown in table 5.3(b). The highest quality of fit results from use of one of the FTLE's (λ_{10}). However this has to be calculated as one of a pair. The partner (λ_9), corresponding to the initially orthogonal unit vector, provides a slightly lower quality of fit. It is not possible to separate the components without prior knowledge of the dynamics and expected relationship. Their mean R^2 still exceeds those for $\lambda_{1\text{-}8}$ but, taken as a pair, there are more precise methods for estimating strain rate.

The MFTLE's ($\lambda_{11,12}$) are the next best contender for "best estimate of effective strain rate". Both components provide an equally good quality of fit, meaning that either

can be used. As it is only the magnitude of strain we are interested in we will use the positive MFTLE at any time. The exponents can be calculated at any time and position throughout the domain (as drifters at which these are calculated are distributed throughout the entire domain) and have been advocated in comparable studies as the most accurate method of quantifying cumulative strain effects (Pierrehumbert and Yang, 1993). A downside is that $\lambda_{11,12}$ lack practicality in an observational sense. Current observational technology does not allow for collection of sufficiently high resolution, spatially and temporally, measurements of velocity. Although this is not an applicable point in numerical studies it is accepted that this means that results obtained in a modelling context here will always be better than can be achieved *in-situ*.

Finite time Lyapunov exponents can not be calculated in the manner above for *in-situ* investigations. On a note of practical reassurance the supposedly cruder methods of calculating strain from rate of change of patch length and from separation of particle trajectories result in a very good quality of fit. It should be remembered that unlike all other methods $\lambda_{13,14}$ provide a single estimate of strain rate to be applied at all times, over the entire filament. For comparison, the mean and standard deviation of the other methods for estimating strain within the filament are listed in table 5.3(c). It becomes apparent that the seemingly good regression for $\lambda_{13\text{-}14}$ is an artefact of using a single measure of strain rate. In this instance scatter in calculated diffusivity is due solely to variation in estimated width. Given the potential sources of unquantifiable error associated with measuring strain rate using rate of change of patch length and the restricted spatial area when using separation of drifters these methods are discounted for further analysis. From a practical perspective it is reassuring to note that a reasonable measure of strain is obtained using these methods. The level of knowledge of the flow required for calculation of finite time Lyapunov exponents will never be available aside from in a modelling context.

By comparing the quality of the regression over different periods, table 5.3(a,b,c), there is evidence of the deterioration, indicated by a lower R^2 value, of the relationship between the rates of mixing, strain and patch width outside periods of strain dominated dispersal (days 15-21) and also when the filament is exceeding the length-scale of rotational features (approximately after day 18). This is a point to be noted. The filament increased exponentially for a longer period than drifters within the patch were experiencing exponential stretching- both indicators of strain dominated dispersal. The drifters do not completely cover the patch. Especially as time progresses. The drifters are experiencing dispersal solely as a result of advection by the flow whereas the tracer is also diffusing (mixing with surrounding water). By considering local strain rate, problems associated with the definition of the length-scale of the field are removed. The effect of consideration of the filament width when its size and shape are not being dominated by strain can be minimised by restricting attention to periods when the patch is predominantly filamental, but by considering local strain rate, such as in $\lambda_{1\text{-}12}$, it is possible to alleviate problems with differing local dispersal regimes along the patch length.

Having chosen the finite time Lyapunov exponents modified for more accurate resolution of small time intervals, $\lambda_{11\text{-}12}$, as the method of calculating strain there is one final aspect to be considered- the gradient of the fit. Having used variance of the inert tracer cross-section as our definition of width a 1:1 fit of calculated to applied diffusivity is expected from previously theoretical and numerical studies. This is evidently not so for any of the methods for estimating effective strain (table 5.4). Knowing that explicit solution of the equation describing dispersal of an inert tracer in a uniform pure strain environment results in $\sigma^2\lambda = \kappa$ then the strain used here could be "corrected" according to the gradient and intercept of the linear regression to give a 1:1 fit. The observed departure from a 1:1 fit can be considered to be due to the high degree of variability in direction and magnitude of strain over the filament and its history affecting the necessarily cumulative measurement of

effective strain rate. In short, the relationship, $\sigma^2=\kappa/\lambda$, only applies for uniform, constant λ. Perhaps it is no surprise that it needs modification if the strain rate varies spatially and temporally. Differing coefficients for the regression result not only from differing methods of calculating effective strain but also the period over which the regression is carried out. Technically the theory only applies to a strain dominated filament. Without hindsight it would not have been possible to determine that drifters within the patch separate exponentially over days 15-18, indicating the dominance of strain effect. When considering dispersal of the tracer patch alone it is reasonable to assume the structure of the patch is primarily influenced by straining processes over day 9-24 and this is the period for which the majority of tracer investigations will be carried out. Therefore a value for corrected strain rate, using the maximum value of one of the MFTLE's is used of:

$$\lambda_{corr} = \frac{|\lambda_{11}|}{2.46} + 0.86 \qquad 5.20$$

This is particular to this method, and for this physical environment. This will alter the value of the strain rate used but not its variability. Whether this is the value that should be used for all subsequent analysis is considered in the following discussion.

5.4 Discussion

Although strain rate is a well defined property the number of differing methods of calculating its effect on the stirring history of a tracer has resulted in the necessity to consider all previously used techniques, prior to choosing the one to be used in the two-dimensional studies. We need to estimate the effective strain rate –encompassing the effects of temporally and spatially varying strain rate on tracer dispersal. The problems in determining strain rate in both model and *in-situ* studies have been touched upon. It has been determined that for investigation of tracer dispersal the best way of calculating strain

is the finite time Lyapunov Exponent modified for short time scales (Pierrehumbert and Yang, 1993), $\lambda_{11,12}$. This ensures that the effects of rapidly varying regions of strain, such as edges of eddies, are accurately represented. The maximum magnitude of the locally extracted strain rate appears to dominate structure of the patch (table 5.3 a,b).

The progression from a pure strain flow, in chapters 2 and 3, to turbulent field, in chapter 4 onwards, appears to necessitate modification of the effective strain rate in order that it relates to width and effective diffusivity as predicted in a simpler environment. The modification is not altering the variability in strain rate or the relationship between rates of mixing, strain and equilibrium width; merely recognising that in a highly complex field there are a spectrum of scales on which physical dynamics vary considerably in space and time. For this particular analysis the empirical scaling given in equation 5.20 has been derived. It should be clearly noted that this correction applies to this specific model and dynamical setup within the studies period only. It is not dissimilar to the $\lambda/2$ correction applied to strain rate in a comparable study of tracer dispersal in order to ensure model dispersal matched observed rates (Sundermeyer and Price, 1998) but this may just be coincidental. For confidence in this apparent agreement an array of runs with different physical flows is required. As we are only to investigate tracer dispersal for the model configured as described in chapter 4 there is no motivation for any more in-depth analysis at this point but it may well prove to be a worthwhile line of future investigation. The uncorrected value of the 'best' method of representing strain effects, $\lambda_{11,12}$, will be used for all subsequent tracer investigations. The scaling mentioned above is linear and can be subsequently applied post analysis in consideration of the scaled relationship, if required in chapter 6.

Practicality:

We have determined the best theoretical method for estimating the cumulative effects of a temporally and spatially varying strain rate for the purposes of investigating tracer dispersal in this two-dimensional turbulent flow. But there remains a mismatch between this and what is actually practical for *in-situ* investigations of tracer dispersal. Having determined the best measure of effective strain obviously all subsequent analyses in the thesis will use this as the definition of effective strain rate. However observational applications of our results must be considered. Many methods have been considered which are practical to calculate from model output. The more severe constraints of *in-situ* sampling have also been considered. All except one of the considered methods of calculating strain require synoptic, global (in terms of the tracer patch), knowledge of the velocity field. This may be calculated from altimetry data, provided data is available from the remote platform at comparable times to sampling of the tracer field. This may not provide data at sufficient spatial resolution ($<O(10)$ km) though. It is not new to urge caution with regards calculation of strain from ADCP surveys, as there is an inherent bias resulting from the finite time required to survey an area and also from the significant spatial bias resulting from sampling strategy. The magnitude of errors resulting from synoptically sampling an ideal field have been shown to be significant. These errors will only increase using asynoptic data.

The observationally practical methods of measuring strain use rate of change of patch length, λ_{13}, and separation of drifters, λ_{14}. They show a comparable estimate of strain rate to the more rigorous yet not observationally practical Lyapunov exponents, and an apparently good relationship when applying a regression of calculated to applied diffusivity for an inert tracer. Further consideration suggests that the apparently good relationship (high R^2) may be due to the small variability associated with these methods as a single value is used for analysis of the whole filament. Analysis has shown a high sensitivity of effective

strain rate calculated from rate of change of patch length to the method used to calculate the length of the patch. This suggests a need for extreme caution with this approach. Multiple drifter deployments simultaneous with tracer release provides a representative and relevant measure of strain with minimal possible sources of errors associated with the ensuing analysis of dispersal. Ideally drifters should be deployed at highest possible resolution. However it has been found for this field that estimates of strain rate do not significantly vary for a resolution less than 2km. Note that this may purely reflect the 2km resolution of the model. In this investigation this constitutes 40 drifter pairs from 25 drifters. This resolution has been determined with hindsight as being appropriate for the flow investigated here and so should be taken only as a guidance figure. It should also be remembered that we have considered perfect drifters, free from effects such a friction, wind, and vertical shear. A modelling context also provides the luxury of unlimited numbers of drifters deployed at any desired spatial resolution prior to enable accurate visualisation of the flow.

It is suggested that for *in-situ* measurement of effective strain rate for tracer dispersal the most representative and accurate method is from the rate of separation of drifters deployed at the highest practicable resolution (clearly this is limited in reality by the costs and logistics of drifter deployment).

5.5 Conclusions

The best measure of strain for the purposes of analysing tracer dispersal in our model of two-dimensional turbulence is the maximum Finite Time Lyapunov Exponents modified to better resolve small time intervals, $\lambda_{11,12}$. This method out-performs a variety of techniques widely used for calculating both strain rate when considering tracer dispersal and dispersion

rates during fertilisation experiments. Despite investigation in an idealised environment errors remain large and caution is urged for those considering using such techniques.

To agree with theory derived in a uniform pure strain environment the value of the effective strain rate, $\lambda_{11,12}$, may be modified by applying a linear scaling, as in equation 5.20. It is thought the modification is due to the under-resolution of the temporally and spatially varying strain rate. To be able to generally apply a correction for different models and dynamical regions within the one used here, an ensemble of runs, covering differing physical setups and forcing, is necessary. This will not necessarily lead to a universal solution but will provide guidance as to whether correction for effective strain rate, to account for the under-resolution of temporal and spatial variation, has is approximately general or specific to the model in which it was derived. Therefore tracer dispersal investigations continue in chapter 6 and 7 using the uncorrected effective strain rate, λ_{11}.

CHAPTER 6: Investigation of tracer morphology in a fully turbulent 2D field.

6.1 Introduction

The previous two chapters have determined methods for the analysis of tracer dispersal (Chapter 4- Methods for two-dimensional tracer investigations) and for the best measure of strain for the purpose of investigating oceanic tracer dispersal (Chapter 5- 'Best' measure of strain). It is now possible to test the formula derived in chapters 2 and 3 for predicting the minimum equilibrium width of a reactive tracer (and hence phytoplankton) distributions. It is sought to further the one-dimensional studies in determining the controls on minimum length-scale of oceanic phytoplankton distributions in a more realistic physical environment. Also the effectiveness of a logistic tracer as a parameterisation of phytoplankton population dynamics will be assessed.

Tracer dispersal in a two-dimensional turbulent flow will now be considered to test how well the previously derived formula (equation 2.7/3.9, depending on whether nutrient availability is represented) predicts the minimum (equilibrium) width of inert and logistic tracer distributions in a more complex physical field. The propriety of using a logistic growth term to parameterise phytoplankton population dynamics will be tested by comparison of logistic tracer dynamics with a simple ecosystem model. Note that actual width, defined previously within this work as the distance between the tracer isopleths corresponding to 0.01% of the maximum over the entire tracer patch, is the only measure of cross-sectional extent used hereafter. Results from chapters 2 and 3 show that we can expect different shapes to the cross-sectional profiles. Therefore spatial variance is no longer a consistently reliable measure of spatial extent. In chapter 4 the different threshold used for detection of the filament is discussed (section 4.2.3(a)), this does not alter the

definition of width and all fitted curves are solved to the threshold of 0.01% of the maximum tracer concentration.

6.2 Methods

The model details and an in-depth account of the analysis techniques are described in chapter 4. For quick reference: a tracer patch is initialised in a small (6kmx6km) patch within a two-dimensional turbulence model. The model is evolved for 6000 iterations.

Two investigations are carried out: a tracer release experiment investigating inert and logistic tracers, and a fertilization experiment using tracers from a four compartment ecosystem model (NPZD). As previously described, a different biological time scale is used for the tracer studies and for the ecosystem model. It should be stressed that this does not alter the dynamics of the flow. The scaling does mean differing peak velocities: ~40cm s^{-1} for the tracer investigation compared to ~100 cm s^{-1} for ecosystem model investigations. The same flow field is used for all experiments to ensure results are directly comparable. Any changes in observed structure between experiments are solely due to the tracer, or phytoplankton, dynamics. The lower biological time scaling for ecosystem investigations is to ensure that phytoplankton concentrations remain within "observationally detectable" levels within the time taken for the patch to be drawn into suitable filamental structure. The run time corresponds to approximately 30 days for the tracer release experiments and roughly 10 days for the NPZD fertilisation experiment.

The tracer patch is analysed at approximately 3 day intervals, daily for the NPZD model. The width is measured, in a series of across patch cuts perpendicular to the direction of greatest concentration gradient, and a value for effective diffusivity is calculated from this using the appropriate local measure of strain rate according to the formula derived in one-dimensional studies (equation 2.7/3.9). The calculated value is then

compared with the value explicitly applied throughout the run. From this the applicability of the one-dimensional theory for predicting minimum length-scale of both inert and reactive tracers can be evaluated in a more realistic setting. In chapter 5 the period over which inert tracer structure was dominated by straining processes was identified. This is the period for which the formula is likely to be most accurate in predicting the minimum equilibrium width of tracer (and phytoplankton) distributions. However, in this chapter times where rotational processes are significantly affecting tracer dispersal are also considered. To identify periods of strain dominated dispersal we require prior knowledge of how the flow will evolve which is impossible outside of numerical modelling investigations. Without knowledge of the dispersal of the virtual floats the strain dominated period could not have been identified. Visual inspection of the tracer field suggested a far longer period of strain dominated dispersal (characterised by filamental structure of tracer distributions) than indicated by the drifters. It is also useful to investigate the errors resulting from application of the formula for predicting tracer patch widths in a pure strain flow in regions/periods when tracer dispersal is significantly affected by eddying processes.

Inert and logistic tracer studies

The dispersal of an inert tracer was considered in chapter 5 to enable identification of the "best" estimate of effective strain (a representation of the cumulative effects of a temporally and spatially varying strain rate). It is now considered once again for comparison with reactive tracer dynamics. Prior to considering the dispersal of the reactive tracers (one with logistic growth and those from the NPZD ecosystem model) and any modifications to our results from one-dimensional uniform strain investigations we consider modifications due only to the effect of a temporally and spatially varying strain by analysing dispersal of an tracer. The logistic growth tracer is then considered to test the

formula for predicting minimum equilibrium filament widths (equation 2.7) in a two-dimensional turbulent flow. Having previously considered inert tracer dispersal we can highlight modification of the one-dimensional formula due to interaction of the reactive dynamics (the propagating fronts typical of logistic growth tracer dynamics) with the more complex flow conditions.

Three different maximum growth rates are used, μ=0.1, 0.5 and 1.0 day^{-1}, to investigate low, moderate and high growth rate solutions. The population limit remains constant at 1 mMol m^{-3}. The population limit was shown to not affect the width in chapters 2 and 3 and so does not need to be varied in our two-dimensional studies.

Fertilisation experiment

As a progression from the tracer release experiments, and to further the investigation of the suitability of a logistic tracer as a parameterisation to oceanic phytoplankton dynamics, a fertilisation experiment is also considered. A highly simplified phytoplankton model (NPZD) is used embedded in the same two-dimensional turbulence model as for the individual tracer investigations, both as described in chapter 4. All compartments are initially homogeneous at their (non-zero) equilibrium values. However there is a small 'spike' in nutrient concentration at the deep value with the same initial spatial distribution used for initialisation of the individual tracer release experiments. Four biological regimes are investigated: high and low deep nutrient, N_0=15 (mMol m^{-3}) and N_0=2 (mMol m^{-3}); and high and low predator capture rate, ε=1 d^{-1}, and ε=0.2 d^{-1}. This results in the following 4 biological regimes:

B.R.(i): N_0=15 mMol N m^{-3}, ε=1 (mMol N m^{-3})$^{-2}$ d^{-1}, ($0 < \mu^* < 5\text{x}10^{-2}$ day^{-1})

B.R.(ii): N_0=2 mMol N m^{-3}, ε=0.2 (mMol N m^{-3})$^{-2}$ d^{-1}, ($3\text{x}10^{-8} < \mu^* < 5\text{x}10^{-4}$ day^{-1})

B.R.(iii): N_0=15 mMol N m^{-3}, ε=0.2 (mMol N m^{-3})$^{-2}$ d^{-1}, ($3\text{x}10^{-5} < \mu^* < 7\text{x}10^{-3}$ day^{-1})

B.R.(iv): N_0=2 mMol N m^{-3}, ε=1 (mMol N m^{-3})$^{-2}$ d^{-1}, ($2x10^{-6} < \mu^* < 5x10^{-3}$ day^{-1})

The different balance of nutrient availability and grazing pressure result in differing effective growth rates, μ^*. In chapter 3, when considering a nutrient-phytoplankton model, it was shown that the necessary measure of growth rate for use in equation 3.9 is the nutrient dependent apparent or effective growth rate, $\mu^*=\mu N^*/(N^*+K)$ where μ is the maximum (applied) phytoplankton growth rate, N^* is the mean nutrient concentration across the filament width and K is the nutrient half-saturation coefficient. This is the definition of effective growth rate to be used hereafter. This will change throughout the run (the maximum phytoplankton growth rate is constant at 1 day^{-1}) as nutrient distributions alter. As a rough guidance, the range of phytoplankton growth rates experienced throughout the NPZD runs is given above with each biological regime.

6.3 Results

6.3.1 Tracer release experiment

(i) Inert tracer

The width of inert tracer distributions for the applied range of diffusivities is shown in figure 6.3.1. Widths generally increase with effective diffusivity. For a diffusivity of around 30 $m^2 s^{-1}$ widths are within the range 35-45km. For a diffusivity of around 90 m^2 s^{-1} widths are in the range 55-80 km. Not only does the minimum width increase with increased mixing rate but also the range of observed model values does. This is consistent with the tracer occupying a greater spatial extent and thus the width, and shape, being dependent on a greater variety of physical structures influencing the local balance of strain and mixing.

Consider next the regression of calculated to applied effective diffusivity, for the purpose of assessing the accuracy of the formula (equation 2.7/3.9) for predicting

equilibrium width. Figure 6.3.2 shows a plot of calculated vs. applied values of effective diffusivity for an inert tracer. The errors are for the mean plus or minus one standard deviation on data picked within one standard deviation of the modal value. Values are from a single clearly defined filament. The number of measurements of width, from which effective diffusivity is calculated, varies with time but is greater than twenty for the smallest patch (corresponding to the earliest time), and greater than 100 for the longest filaments (latest times). The total numbers of points for each regression are listed in table 4.2. The R^2, root residual mean square (RMS) error and coefficients of the fit are shown in table 6.1. These are plotted in figures 6.3.3(a), 6.3.4(a), 6.3.5(a) and 6.3.6(a) respectively.

The quality of the fit is considered on two criterion: i) the error of the fit to the calculated values, and ii) the deviation of the fit from the 1:1 relationship expected from the one-dimensional uniform strain analysis (chapters 2 and 3). On day 9 both the highest quality of fit (R^2=0.86) and closest reproduction of a 1:1 relationship (gradient=1.9 $\pm$ 0.07) are found. Analysis of the dispersal of virtual floats initialised with the tracer patch, as described in chapters 4 and 5, found an initial period of strain dominated float dispersal (up to day 10) followed by a later longer lasting period of strain dominated dispersal from days 15 to 21 (chapter 5) with rotational effects due to eddies significantly influencing dispersal in the intervening period such that dispersal is less rapid than at strain-dominated times. This is reflected in the deterioration, then subsequent improvement, in quality of the fit throughout the period of analysis after day 9, this is visible in figure 6.3.3(a) and 6.3.4 (b). As the patch experiences strain dominated dispersal again (onwards from day 15) the error of calculated effective diffusivity to the linear regression decreases (lower RMS error) reflecting the improvement in agreement between measured widths and that predicted according to the theory of strain dominated dispersal. This improvement is not to the extent of achieving the 1:1 relationship previously derived. However over days 15 and 18 the coefficients of the regression do not change significantly. The coefficients of the linear

regression (gradient and intercept of the linear fit) reflect the inconsistent stretching experienced by the tracer patch throughout the period. On day 24 the value for R^2 is similar to those calculated over the previous 6 day period, but an increased RMS error is noted. This implies that although a similar percentage of variation in the calculated diffusivity is explained by a linear regression there is an increased scatter in the values. This is explained by the tracer patch being larger, so experiencing a greater variation in the balance of mixing and strain along the filament and resulting in a higher scatter within the data. There is still a linear increase in calculated effective diffusivity with the applied value but the quality is deteriorating (higher RMS error) as the filament length increases (table 6.1 and figure 6.3.4(a)). Eddy features within the flow have diameters in the approximate range 40-80 km. This is approximately the scale over which it is reasonable to expect the velocity field to be de-correlated and for any tracer structure to have significant variation in the balance of physical controls across its extent. Once the filament length significantly exceeds this (~day 18) it can reasonably be expected that the filament is experiencing substantially different balances of local mixing and strain along its extent. This will be much more pronounced than the spatial variation in strain on smaller scales. This is indicated by the highest RMS error being found for the longest considered filament (day 24, RMS error = 77.5 m^2s^{-1}).

With regard to a regression over the entire period a RMS error of 62 m^2s^{-1} is found in a linear regression. The gradient of the fit is approximately 4. Although these are moderate values, compared with those calculated on discrete days throughout the period of analysis, the lowest R^2 value of the analysis is found (0.45). This demonstrates that although a linear relationship can be applied over the period of dispersal and although the regression coefficients are comparable with those found during strain dominated tracer dispersal (day 9, days 15-21) the mean behaviour of the filament is not best described by an average regression in this manner. Throughout the 30 day period the tracer patch experiences different balances of strain and mixing moderating its width. As it increases in size it can

experience a different balance of physical controls throughout its extent. The formula for predicting width is derived from theory of strain dominated tracer dispersal in a situation with uniform strain. Even at times when this is more applicable (day 9, days 15-21) different coefficients of the regression (gradient/intercept), and quality of regression (R^2/RMS error), were calculated. By averaging over a number of distinct times and regions an apparently not unreasonable gradient of the linear regression is found but a deterioration in the relationship is reflected in the lower R^2 value. A lower percentage of observed variability is explained by a single linear regression.

Considering specifically the accuracy of the formula. The gradient of the fit increases generally with prolonged periods of strain dominated dispersal before it as shown in figure 6.3.5(a) (day 9, days 15-21 as indicated by exponential separation of floats in figure 5.2.3). After 21 it should be remembered that the length of the filament is significantly greater than the decorrelation length-scale of the flow as indicated by the size of eddies (40-80 km). The intercept of the fit shows no consistent trend (figure 6.3.6(a)). This suggests that although the general relationship of filament width to effective diffusivity and strain rate is still true the actual numerical scaling coefficient of the formula (shown to be 8.6 in the uniform strain studies, equations 2.7 and 3.9) is greatly modified by the temporally and spatially varying strain rate. Also the magnitude of the intercept, especially with increasing filament length, greatly exceeds the variation in the gradient of the fit (scaling coefficient of the formula) and in application will essentially mask any error in this. Variability in the coefficients of the regression were also found when calculating effective diffusivity using spatial variance of the filament cross-section (table 5.4) rather than our definition of width. The offset from the 1:1 relationship (between calculated and applied effective diffusivity) and the trends in coefficients of the fit are not the same using the different measures of width (actual width and spatial variance). This further complicates quantification of the effect on our formulae derived in a uniform strain flow, and hence the derivation of an

appropriate modification (to equations 2.7 and 3.9), to account for the effects of temporally and spatially varying strain rate.

(ii) Logistic tracer

The variation in the width of the logistic tracer filament as a function of applied effective diffusivity is shown in figure 6.3.7. Displayed on the same subplots the different symbols relate to different maximum growth rates of the tracer. Compared to the inert tracer there is a greater variability in observed filament width. But there is still a general trend for increasing width with diffusivity, and also with increased growth rate. For the lowest growth rate and diffusivity the minimum width is similar to that of an inert tracer, approximately 35 km. However the modal (most frequently occurring) width is increased to approximately 50km compared with 40-45km for the inert tracer. For a diffusivity of around 70 m^2s^{-1} again the minimum width is approximately the same as the inert tracer, 50km, but the modal width is greatly increased to around 80km compared to 50 km for the inert case. Agreement of minimum widths, between inert and logistic growth tracers, is expected for low growth rates. This is because for low growth rates (and an initially low population level) the growth is effectively exponential and it was shown by Martin (2000) that the minimum width of an exponentially growing tracer filament is identical to that of an inert tracer in the same environment (width is independent of growth rate). This result was shown in chapter 2. However the increased range, and modal width, compared to those for an inert tracer suggest that the reactive (logistic growth) tracer filament width is not reaching a satisfactory equilibrium in all cases.

For a higher growth rate of 0.5 d^{-1} again greater widths, and a greater difference between the minimum and modal widths, are observed compared to a lower growth rate and an inert tracer. This difference increases with diffusivity. For the highest growth rate of

1.0 d^{-1} the general trend of increase in widths with diffusivity is difficult to determine except for on day 15. However, observed widths are generally greater than those for lower growth rates. For the longest period of strain dominated dispersal (days 15-21), when it is hoped that the filament width will most likely reach its asymptotic state, for the highest growth rate (μ=1.0 d^{-1}) the patch can only be considered a filament for the start of the period. As is shown in figure 4.3.2(b) the structure is considerably more diffuse and convoluted than filamental. It is therefore not possible to consider later times.

The deterioration in relationship of minimum width with diffusivity and the increasing difference between minimum and modal width may be taken as indicators that the uniform strain theory will not apply straightforwardly in a turbulent context. For a logistic growth tracer the minimum width is based on the reactive front reaching an asymptotic state which requires i) the tracer concentration to reach its limiting value for the fronts to initially form, ii) the fronts to propagate at the analytically determined Fisher speed of $v_{min}=2\sqrt{(\kappa\mu)}$, iii) that a balance is reached between the outward propagation of the front and the opposing advective processes. The difference between minimum and modal widths suggests that for the most part the filament is not in equilibrium. Given the highly variable strain experienced throughout the extent of the patch it is unlikely that fronts will consistently propagate at the minimum speed experienced in a constant strain situation. Reasons why modification of the frontal dynamics prevents further quantitative analysis are presented in the discussion at the end of this chapter.

Even prior to examination of the regression of calculated to applied effective diffusivity, due to the lack of equilibrium found in the width measurements one can expect a deterioration in the quality of fit and for diffusivity calculated via our formula to be in excess of the applied value. The formula for relating width to rates of mixing, strain and growth has been derived for the minimum equilibrium width in a pure strain flow. Error resulting from under quantifying the cumulative effect of strain has already been indicated

in the inert tracer studies: even using the inert tracer the calculated value of effective diffusivity is likely to be in excess of the applied value. For the logistic tracer the consistent difference between minimum and modal widths is an indication that the majority of the filament is not at its equilibrium width. The modal width is the most frequently occurring width measurement. The difference between minimum and modal widths suggests the model logistic growth tracer filament width is not the equilibrium width. A logistic tracer filament can not be narrower than an inert tracer one with the same initial conditions and in the same flow. Yet for the inert tracer, the minimum width roughly matched the equilibrium width.

Plots of calculated versus applied effective diffusivity for the logistic growth tracer are shown in figure 6.3.8(a)-(c) for growth rates of (a) 0.1 d^{-1}, (b) 0.5 d^{-1}, (c) 1.0 d^{-1}. Table 6.2 (a)-(c) lists the corresponding regression coefficients, R^2, and RMS error. The values in table 6.2 are also plotted in figures 6.3.3(b) , 6.3.4(b) 6.3.5(b) and 6.3.6(b). There is a significant deterioration in the expected 1:1 relationship compared to that found for an inert tracer. This deterioration is due to reactive effects as the flow is identical for the two model experiments.

For μ=0.1 d^{-1} the highest quality of fit is found towards the end of the period of strain dominated dispersal (day 24). Considering a regression over output days 9-24 approximately 30% of variability in calculated effective diffusivity is explained by a linear fit. Compared with an inert tracer both the gradient of fit and the RMS error are larger.

The quality of the linear fit further deteriorates with increasing growth rate. For μ=0.5 d^{-1} the RMS error is consistently greater, but the R^2 value is higher for individual days and lower for a regression over the entire period. This is a somewhat deceptive result, the relationship between calculated and applied effective diffusivity is apparently more linear but there are less points over which the regression is carried out (1349 as opposed to

2487, as listed in table 4.2). Although the number of points means that the regression is still significant it should be held in mind that there are fewer points involved in the regression than for the lower growth rate. There is apparently more linearity in the relationship but as indicated by the RMS error (and evident from the overlay of the linear fit on the modal value and standard deviation of the data, figure 6.3.8(b)) there is an increased error of the calculated diffusivity compared to the linear fit. As suggested by a consideration of width plots (figure 6.3.7) the width is not generally reaching equilibrium, and the width (hence effective diffusivity too) is no longer accurately predicted from equation 2.7 which is based on the assumption of constant frontal propagation at the minimum speed achieving a balance with the advecting flow.

For a growth rate of 1 d^{-1} the least squares linear fit explains less than 1% of the observed variation in calculated diffusivity, for a regression over days 9-24: the whole period of consideration. The RMS error is of the same order of magnitude as for $\mu=0.5$ d^{-1}. There is considerable variability in the R^2 during the period of study. Again there are times when the relationship is deceptively good, $R^2 \sim 0.8$. Again this is suggested to be due to the smaller number of points involved in the regression rather than a good linear relationship.

In general, for the linear regressions including a logistic tracer (all growth rates) there is a general increase in the gradient of the regression with maximum applied growth rate (figure 6.3.4(b)) but there is no consistency to this. Considering the intercept of the fit there is no relationship between the value of the intercept and growth rate (figure 6.3.5(b)). The results of Chapters 2 and 3 were that in a uniform strain environment the filament width is strongly dependent on the effective diffusivity and rates of strain and maximum growth, and that the coefficients of proportionality depend upon the measure of width used (actual width, as defined for our uses, or spatial variance). This no longer appears to be consistent when the effects of temporally and spatially varying strain rate are considered.

As for the inert tracer, the intercept of the linear regression is generally large enough to dwarf any error in the gradient of the linear fit.

In summary, the relationship between calculated and applied effective diffusivity is worse for the logistic growth tracer than for the inert tracer. Temporally and spatially varying strain is further obscuring the previously derived relationship. This is not just a physical aspect due to badly estimating the effective strain. The further deterioration from that of an inert tracer means that the turbulent flow is also significantly disrupting the behaviour of the reactive dynamics from that found in the uniform strain flow. The lack of consistent trends with maximum growth rate (hence speed of frontal propagation) or strain period preclude simple quantification of the modification from the uniform strain results.

6.3.2 Fertilisation experiment

Having considered the morphology of inert and logistic growth (reactive) tracers in the two-dimensional turbulence, results relating to an NPZD model in the same flow are now investigated. The filamental morphology in this case is also analysed to assess the propriety of a logistic tracer as a parameterisation of phytoplankton population dynamics.

Results are presented specifically relating to the phytoplankton compartment of the model (P_{NPZD}). However the other compartments have also been analysed. To spare tedious repetition they are mentioned only if of significant difference or interest, as generally very similar features are observed in each compartment. Results are no more clearly defined for the other ecosystem components.

The general evolution of the phytoplankton patch is depicted in figure 6.3.9. An example case for B.R.(i), and κ=107 m^2s^{-1}, is shown. Changing any biological or physical parameters obviously alters observed concentrations but from a visual perspective structure is not significantly changed between the 4 scenarios investigated. The biological effects are

sufficiently repressed in all cases that it is physical dynamics controlling observed structure as far as the eye can see, to this extent there is marked similarity between the structure observed for the inert and P_{NPZD} tracers. Alteration of the effective diffusivity results in a more or less diffuse tracer profile due to increased small scale mixing, as would be expected for any inert or reactive tracer.

The width of the P_{NPZD} filament produced through nutrient spiking is shown in figure 6.3.10. Within this physical regime with strain rates of order 10^{-5} s^{-1} and velocities of up to 1 ms^{-1} (as may be observed typically within open ocean frontal regions) the minimum equilibrium length-scale of phytoplankton filaments is 30-50 km. There is a general increase in minimum and modal width with diffusivity. This is most clearly seen on days 3 and 5 (~days 9 and 15 for comparison with previous tracer dynamics due to the different biological time scaling). Unlike the inert and logistic tracer distributions there is no consistent dependence of the difference between minimum and modal width on diffusivity. As the physical environment has purposely been kept the same as that used for the individual tracer experiments, the only reason for the difference is due to the increased complexity of the biological representation. Although different widths (for the same time and effective diffusivity) are observed between different biological regimes the difference is not consistent between nutrient level, predator adaptation rate, diffusivity, or time. Perhaps unsurprisingly the width of phytoplankton filaments is not the simple function of biological or physical dynamics suggested by logistic tracer investigations.

Similar trends are observed in the nutrient, zooplankton and detritus compartments of the model. The only consistent trend to be deciphered is an increase of width with increased mixing being more evident for most days. The minimum length-scale of these filaments, in the modelled flow, is again 30-50 km.

Considering a regression of calculated to applied effective diffusivity there is a generally poor result (figure 6.3.3(b), table 6.3). The values for the linear regression and

error of the regression for each of the biological regimes are listed in table 6.3 a-d. Plots of the mean and standard deviation for calculated effective diffusivity for data with overlaid 1:1 fit and least squares linear regression against applied diffusivity are shown in figure 6.3.11

For the P_{NPZD} there is some correlation between lower maximum effective growth rate and quality of solution. The 'best' R^2 for a regression over the entire period are achieved for the three biological models with lower maximum effective growth rates, B.R.(ii), (iii), and (iv) (figure 6.3.3(c)). Considering single days, at best the regression is better even than that found for the inert tracer (day 8 for P_{NPZD}, day 24 for the inert tracer), but there are also times when it is worse (prior to day 6/18 and for the regression over all times). The only consistency in this is with prey capture rate (a reflection of grazing pressure on the phytoplankton). The relationship between calculated and applied effective diffusivity is better for B.R.(ii) and (iii) but this consistency in grazing pressure does not directly relate to the general range in effective P_{NPZD} growth rate (effective growth rate is the nutrient dependent growth rate, see methods section on the fertilization experiment for the numbers relating to this). The "best" calculation of effective diffusivity from the width of P_{NPZD} filaments is not necessarily for those which are slowest or fastest growing, nor is there any consistency between biological regimes. The highest RMS error is found for B.R.(i) but again this is not a consistent trend repeated at all times.

The coefficients of the regression (gradient and intercept), as illustrated in figure 6.3.6(c) and 6.3.7(c) respectively, show a similar lack of consistency in trends with period of investigation or biological regime, although a general increase (decrease) is seen in the gradient (intercept) over the period of prolonged strain domination (days 5-8).

The lack of consistency in the relationship between calculated and applied effective diffusivity suggests that even though at certain times the relationship is linear the formula used for calculating effective diffusivity is not appropriate. Our results show that the widths

of the filaments of the P_{NPZD} compartment of the NPZD ecosystem model are not well described by our previously described formula (equation 3.9) relating filament width to rates of effective diffusivity, strain and growth. Logistic growth is not a sufficient representation of the dynamics of phytoplankton. Effective growth rates (nutrient dependent) for P_{NPZD} ($5x10^{-4} < \mu^*_{max} < 0.05\ d^{-1}$) are approximately one or two orders of magnitude smaller than the minimum modelled growth rate of the logistic tracer ($0.1day^{-1}$). Similar gradients, in the linear regression of calculated to applied effective diffusivity, are observed despite the magnitude of the differences in growth rate between the logistic growth and NPZD systems. Under the scope of this investigation the logistic tracer does not predict the minimum equilibrium width of the P_{NPZD} filaments any more accurately than the inert tracer predicts the width of P_{NPZD} filaments. However, the flatter table top shape exhibited by a logistic tracer in its propagating front form does better describe the shape, of the P_{NPZD} filament cross-section, than the Gaussian profile of an inert tracer in some cases. To further comment on the dynamics of a logistic tracer versus phytoplankton tracer runs must be conducted with comparable effective growth rates for both. However, given the similarity in gradients of the linear regressions and yet the differing relationships in quality of the regression further results may not be any more informative than those already provided: A logistic tracer is clearly not a sufficient parameterisation of phytoplankton growth when considering mesoscale dynamics.

The lack of consistent trends between calculated and applied effective diffusivity using widths of the P_{NPZD} compartment is also found for the other compartments of the NPZD model (figure 6.3.12). Aside from an increase in R^2 over days 5-8 (strain dominated dispersal) there is no consistent variation in R^2 or RMS error with the altered variable of deep nutrient value or prey capture rate. Within the context investigated our formula (equation 3.9) relating filament width to rates of effective diffusivity, strain and growth is no more reliable for the N_{NPZD}, Z_{NPZD} or D_{NPZD} tracers than for the phytoplankton tracer.

Effective diffusivity can not reliably be calculated from the width of filaments of any components of the NPZD ecosystem model.

Finally it is worth commenting on our use of the nutrient dependent effective growth rate. When considering an N-P system in chapter 3 we found that the formula derived in chapter 2, using a single tracer, still applied with the proviso that rather than using the maximum applied growth rate as in equation 2.7 we use the nutrient dependent effective growth rate resulting in our slight modification to equation 3.9. None of the dynamics of the system are altered but we now consider growth rate as $\mu^* = \mu N^*/(k_N + N^*)$, where N^* is the mean nutrient concentration across the tracer patch, k_N is the nutrient half saturation coefficient and μ is the maximum applied growth rate specified in the model setup (and used in equation 2.7). Nutrient dependent effective growth rate is not necessarily an obvious definition to consider, therefore runs were also conducted using the rate of change of phytoplankton biomass as an approximation of effective growth rate. A much poorer regression between calculated and applied effective diffusivity was found to the extent that there was no discernible relationship (figure 6.3.13). As found for other tracers and the other definition of growth rate, there are times where the R^2 value suggests the relationship between calculated and applied effective diffusivity is linear. This is contradicted however by a large RMS error and a very large variation in the gradient and intercept of the linear fit. Although our use of nutrient dependent effective growth rate yielded poor results, when comparing calculated to applied effective diffusivity they are substantially better than those obtained using rate of change of phytoplankton biomass. Our result from Chapter 3 is supported, the growth rate to use when considering phytoplankton patch widths is the nutrient dependent effective growth rate.

6.4 Discussion

Compared to our previous study in a uniform strain environment (chapter 2 and 3) there is a significant deterioration in the ability of the formula derived there (equation 2.7 and 3.9) to predict the minimum equilibrium length-scale of tracer filaments (whether inert, logistic or ecosystem model) and hence of phytoplankton distributions. This has been assessed through a regression of effective diffusivity calculated via our numerical derived formula with the value applied throughout the run.

For an inert tracer, between 50% and 80% of variability is explained by the linear regression. The remaining variability is suggested to be due to inaccurate measurement of the strain history of the filament as a result of temporally and spatially varying turbulence. Some lengths were gone to in Chapter 5 to determined the most effective measure of quantifying the effects of temporally and spatially varying strain rate on tracer dispersal. Even the best method, derived therein, is evidently not suitably accurate. Use of a more general measure of strain rate (such as RMS strain rate of the field, or a single value pertaining to strain rate of drifters within the tracer patch) will misleadingly reduce the error in our regression of calculated and applied effective diffusivity. As a single value for strain is being used the only remaining source of variability is in width measurements but the uncertainty in the strain estimates may be very large and yet unquantified. Considering the degree of sensitivity of calculated effective diffusivity to small scale variation in the local balance of mixing and strain repeatedly evident in our results we suggest that this approach is unwise.

The gradient of the best linear regression (using minimisation of the least squares error) for calculated to applied effective diffusivity varies with the period according to whether diffusive or straining effects have been dominating dispersal. From these results it is suggested that diffusivity estimated in this way will be approximately 4 times the actual value (table 6.1). Again this is explained by an overestimate of strain rate due to under

resolved transient turbulent effects. Essentially spatially and temporally varying strain rate is resulting in an over estimate of the effective strain rate for the entire patch (Chapter 4 contains a more comprehensive discussion of errors resulting from incorrect measurement of parameters).

For the logistic tracer there can be a large increase in the RMS error (difference between the calculated effective diffusivity and the linear fit) compared to an inert tracer. This implies that, in addition to strain effects, the variation in predicted diffusivity is greater than in the actual diffusivity to an extent exceeding that expected from the inability to accurately quantify effective strain. The quality of the fit decreases with increasing maximum growth rate. For the lowest considered growth rate, 0.1 d^{-1}, between 20% and 40 % of observed variability in calculated effective diffusivity is explained by the linear regression. Calculated values are approximately 5 times the applied value for a regression over the entire period of consideration (table 6.2). The relationship deteriorates severely for increased growth rate. Less than 10% of variability at best is explained for μ=0.5 d^{-1} with less than 1% for μ=1.0 d^{-1}. It is suggested that this deterioration is due to modification of the behaviour of the Fisher fronts. In a constant, uniform strain environment the speed of frontal propagation was suggested to depend upon the frontal gradient, agreeing with previously derived theory (Murray, 1993). If the frontal profile is constantly being modified due to spatially and temporally varying physical processes (strain) a constant speed of propagation is unlikely. Due to the nature of the tracer dispersal it is also difficult to measure the speed of propagation in the turbulent field as this is observed as a rate of change of width. Consecutive width measurements, necessary for calculating speed of frontal propagation, must be representative of the same section of the tracer patch. This simple statement disguises the complexities of ensuring that width measurements are comparable in this way. Any measurement must be Lagrangian, as we are measuring a tracer which is being advected. The tracer mass as a whole is moving whilst its morphology

is being modified. Measurements averaged along the length of the tracer filament are not sufficient in this case as it is recognised that the spatially inhomogeneous strain rates found in the two-dimensional turbulent field will result in differing local morphology and hence differing local rates of front propagation. For the logistic growth tracer a greater consideration must also be given to how temporally and spatially varying strain rate is best quantified. For the purposes of inert tracer dispersal the maximum finite time Lyapunov exponent with a modification to better resolve small time intervals was found to be the best method (see Chapter 5). When considering a propagating front solution this may not necessarily be the best choice. However without an understanding of how one may expect the fronts to propagate (the reasons precluding this are explained above) it is not possible to repeat the analysis conducted with the inert tracer in Chapter 5 to deduce the "best" strain for logistic tracer studies. Advection of tracer orthogonally to the direction of frontal propagation must also be quantified as this will further complicate local calculations of the rate of change of width. Provided that all these aspects are considered and that accurate methods are developed for Lagrangian measurement of width, strain rate and tracer advection then it may be possible to improve predictions for the minimum equilibrium length-scale of a logistic tracer in a two-dimensional, turbulent field. Whether this is feasible is a question for the prospective investigator. Within the scope of parameterising phytoplankton dynamics it is suggested that is may not merit the effort as will be explained.

The use of a logistic tracer as a parameterisation of phytoplankton dynamics was considered by comparison of results from the dispersal of a logistic growth tracer with those for the P_{NPZD} compartment of a four compartment (NPZD) ecosystem model. On the basis of this work such a parameterisation is suggested to be inappropriate because of the poor relationship between the results. There are times where a DTANH function (roughly the asymptotic form of a propagating front solution, as used in the logistic tracer study) is a closer description of the across patch morphology of the P_{NPZD} filament than a

Gaussian solution. But this in itself is not sufficient to say that a logistic tracer is a suitable parameterisation of phytoplankton population dynamics. The lack of consistent trends in the variation of the P_{NPZD} tracer filament width with any of the altered parameters (deep nutrient value and prey capture rate) make it difficult to comment further on the relationship. There are more consistent trends in the logistic growth tracer over the straining period (increased gradient and intercept of the fit) than found for the P_{NPZD} tracer. This suggests the controls on width of P_{NPZD} are more complex than for the logistic tracer. It has been shown that although structure similar to the eye may be exhibited, a logistic growth tracer is no more a reliable predictor of the minimum width of P_{NPZD} patch widths than an inert tracer is. Although minimum equilibrium widths of similar magnitude are measured for the logistic tracer and for P_{NPZD} tracer distributions this in not an indication that the width has the same controlling factors, as demonstrated by the varying trends with diffusivity and apparent growth rate. Physical controls will be the same for any tracer in the same environment. Reactive or biological controls are specific to that tracer model. In short, a logistic growth model is a poor parameterisation of the ecosystem dynamics which may influence filament morphology on the mesoscale.

Given the generally poor relationship found for all tracers (inert, logistic and those from the NPZD model) it is more relevant to first improve measurements for relating filament width of an inert tracer to effective strain rate and effective diffusivity in a temporally and spatially varying strain environment. Reactive dynamics represents another unknown and will only complicate matters.

6.5 Conclusions

The dispersal of inert tracers has received widespread use in the calculation of approximate *in-situ* mixing rates (Okubo, 1971; Ledwell *et al.*, 1993; Sundermeyer and Ledwell, 2001). In

the model environment used here, where great care has been taken to ensure minimisation of observational error, estimated mixing rates were calculated to be 2-5 times greater than the applied value. It is reasonable to expect the error to be substantially increased in an *in-situ* study as measurements over a sufficiently large spatial area can no longer be synoptic or as precise as those possible in a numerical study such a this. Okubo's extensive studies allowed for an order of magnitude error on observed mixing rate (Okubo, 1971) due in part to local variation in the scale of straining processes. Straining processes will differ substantially with regional effects and latitude. For example, simply due to latitudinal variation in the Rossby radius ($L_E = C/f$, where C is the speed of propagation of gravity waves and f is the Coriolis parameter) the length scale of eddies can reasonably be expected to be 20km greater at 20°N than 50°N. This has a self evident effect on the variability of local strain rate. It must be remembered throughout that effective diffusivity is simply a parameterisation of mixing due to under-resolved advective processes. In a highly dynamic region turbulent effects result not only in greater mixing but also hinder measurements of strain rate by conventional methods, such as measurements of velocity gradients, due simply to the high degree of temporal and spatial variation in velocity. It has been shown here that even in a modelling environment where this is not an issue it is not possible to quantify strain rate sufficiently accurately to calculate effective diffusivity according to existing theory.

Investigation of a logistic growth tracer resulted in a substantial decrease in the quality of regression between applied diffusivity and that calculated from the formula derived in uniform strain studies. The minimum length-scale of patches is increased with respect to an inert tracer, and this difference increases with increasing maximum growth rate. Effective diffusivity calculated from patch width in this instance can be expected to be up to an order of magnitude greater than the actual value. It is suggested that the previously derived formula (equation 2.7), describing the equilibrium length-scale of logistic tracer

patches, can not be applied to a reactive tracer in a turbulent flow. This is primarily due to the spatially and temporally varying modification to frontal dynamics, by variable strain, altering the speed of frontal propagation.

When considering an NPZD ecosystem model, calculation of mixing rate from minimum length-scale is to be carried out with extreme caution. Although there was found to be a linear relationship between calculated and applied values of diffusivity at certain times, the relationship could not be linked to the physical or biological history of the patch. Observed patch size is not unreasonable (50-80km) but it is not simply related to rates of strain, mixing, or apparent growth. There is therefore no reason to expect the width of an *in-situ* phytoplankton patch to be related to the rates of strain and mixing it has experienced via the simple formula as has previously been assumed (Abraham *et al.*, 2000). This is in addition to questions concerning how strain should be measured (described in full in Chapter 5) which further suggests that the *in-situ* calculation of effective diffusivity should not currently be conducted using the width of any type of tracer patch, reactive or inert.

With regard to the use of a logistic tracer as a proxy for phytoplankton growth, this must be left to the conscience of the modeller and the context in which it is to be used. Within the mesoscale investigation of filament size conducted here a logistic growth tracer is a poor parameterisation of phytoplankton dynamics. For differing growth rates neither the quality of regression nor the gradient of the regression was found to be significantly different between the two cases. But there are large differences in the intercept of the fit to mask any error in the gradient of the linear fit. There is however also 50-60% reduction in the number of cross-sectional profiles being well described by a Gaussian or DTANH function (when fitted to the data extracted across the patch) for the phytoplankton distributions compared to the logistic growth tracer. The logistic growth tracer was found to exhibit significant differences in size and shape due to processes other than purely varying strain, as identified through analysis of inert tracer dispersal. The P_{NPZD} tracer

exhibited an even more convoluted profile on occasion, not linked to strain or effective growth rates. All that can be said with confidence is that filament widths of the phytoplankton tracer were greater than for an inert tracer, to a similar extent as the logistic model, and that a number of cross-sectional profiles are well described by fitting of a simple curve known to well describe the asymptotic shape of a logistic tracer. The relationship derived in Chapters 2 and 3 however is no longer viable as indicated by the lack of consistent trends in any aspects of the regression between calculated and applied effective diffusivity.

The widths of inert, logistic tracers and NPZD model tracers in a two-dimensional turbulent model have been considered. The formula for predicting minimum width derived from uniform strain studies has been tested with variable degrees of success. For an inert tracer it is found to apply well with the caveat that strain rate must be accurately measured, that this is difficult in a turbulent field, and that the relationship between calculated and actual effective diffusivity is no longer 1:1. Whether it is practical during observational studies is contentious. For a logistic tracer the complex flow severely disrupts the propagation of fronts resulting in a very poor prediction of minimum width for high growth rates (greater than 0.1 d^{-1}). For a P_{NPZD} tracer there is no reliable relationship between widths predicted by the formula (equation 3.9) and those which are measured in the model. Furthermore a logistic tracer is suggested to be a poor parameterisation of mesoscale phytoplankton dynamics due to the lack of consistent trends between this and a more sophisticated (yet still simple) NPZD ecosystem model.

The quality of the prediction has been assessed from the relationship between the effective diffusivity calculated from the formula and the value applied throughout the run. The necessity for accurate measurement of all parameters has been highlighted. Severe caution is urged for the calculation of mixing rates from the width of inert tracer distributions. It is suggested that the width of phytoplankton distributions can ***not*** be used

for estimation of mixing rates, unless a more effective, and necessarily more sophisticated, formula for predicting the width of phytoplankton distributions is derived. This should be based upon a suitably descriptive ecosystem model and not an over-simple parameterisation of population dynamics. What constitutes a suitable ecosystem model is another open question.

CHAPTER 7 '*In-situ*' surveying of inert tracer and Phytoplankton fields.

7.1 Introduction

Analysis in all preceding chapters has been carried out from the advantageous perspective of synoptic viewing of a model domain. The concentration at every point of a tracer field is accurately known at all times. Obviously this has at best tenuous links to what may reasonably be observed during an *in-situ* oceanic study. The factor most likely to corrupt observed distributions is the high degree of temporal variability of oceanic distributions juxtaposed with the finite time required to sample at sufficient spatial resolution to capture regional features. This may result in a biased dataset when attempting to reconstruct spatial distributions. Separate to this is spatial bias due to an inappropriate sampling strategy. Neither of these aspects affects the validity of a single data point. It is when attempting to reconstruct distributions' variability from a distorted dataset that errors ensue from a distorted dataset. Within the scope of this chapter it is intended to assess errors resulting from an inappropriate spatial sampling and so choose to sample synoptically and investigate differences in observations solely due to the orientation and spatial resolution of the survey strategy. There is evidence that asynoptic sampling of biological fields improves the representation of biological dynamics underlying observed patchiness (Srokosz *et al.*, 2003). There is a given caveat that this result was found in a situation where biological dynamics are controlling observed structure. This is not so in our investigations where physical processes appear to be dominating spatial structure further adding to our motivation for choosing to sampling synoptically. Sampling of the model domain is to be in a manner typical of mesoscale *in-situ* surveys, but eliminating temporal variations within the duration of the spatial survey. Rather than explicitly comparing observational data with

model output comparison is made between actual model distributions and that which could be reasonably observed by sampling.

Availability of accurate and representative observational data is necessary to test and reduce the error in all numerical models that attempt to explain "reality". Observational data is required to define and to parameterise the processes which constitute the component parts of the model, to initialise and to provide the external forcing for simulations, and also to test and to negate the model performance (Allen, 1997). For effective inter-comparison observational data must be available on comparable temporal and spatial scales to the model output. For ecosystem modelling the data requirements comprises of high resolution data, in all three spatial dimensions plus time, for all biological and physical processes represented. The level of data requirements of a model are dependent upon the complexity of the parameterisations included and of the phenomenon being addressed. For any model optimisation (to "reality") to be viable it is vital that the data which a model attempts to reproduce, explain and/or predict is representative of actual properties. An individual data point will be as accurate as technology allows. Errors however can proliferate through misuse of data via over generalisation or over emphasis of possibly spurious data points. This can be reduced through optimisation of sampling strategies. There is a long history of this. As progress in understanding is made new recommendations and optimal strategies can be devised and set as minimum standards necessary for inter-comparison of results (Franks, 1995; Tortell and Awosika, 1996; Crook and Schofield, 1997). This is an on going process, the rate of advance dictated by improvements in technology and new knowledge gained from novel approaches.

With attention to the models used within this study the ecological model is a good, if simple, parameterisation of the biological dynamics of phytoplankton. Zero spatial dimension studies have shown the models used here to give a reasonable reproduction of population dynamics in the North Atlantic and parameters are initialised at reasonable levels (Fasham, 1995). The physical model is also a reasonable representation of mesoscale

open ocean surface, lateral, currents (Martin *et al.*, 2002). Modelled velocities and strains are in a reasonable range of expected values.

The question remains of what "errors" remain purely due to flaws in the adopted sampling strategy. An effort is now taken to understand how the ideal model fields may be distorted as a result of non-ideal sampling. A comparison between actual distributions and what may reasonably be expected to be observed *in-situ* is made. There are two aspects to this consideration.

i) The surveying of a simple filament such as that considered in the previous chapters. The filament is surveyed following a "standard" mesoscale survey track. The reconstructed field is then considered in terms of the size and orientation of the aforementioned survey. By comparing the range, and minimum, of widths observed from each survey and from "ideal" sampling the errors resulting from a biased survey track can be quantified.

ii) The surveying of a convoluted tracer field. It is acknowledged that phytoplankton distributions are not generally found in a clearly defined filament. Expected distributions are generally more complicated as seen in the majority of images of surface ocean colour, such as the example depicted in figure 1.1. An interference experiment is conducted in which a more tortuous tracer field is generated and the errors resulting from sampling this are quantified.

7.2 Methods

For details of the biological and physical models the reader is referred to Chapter 4- Methods for two-dimensional tracer investigations. The standard sampling strategy, and that used here, is continuous along track sampling in a number of parallel tracks (Crook and Schofield, 1997). This recommended standard is on occasion different to that used by Ledwell *et al.* (1993), our repeated reference for evidence for observational support for inert tracer dispersal theory. Ledwell et a. (1993) conducted four surveys of their tracer

patch over four years, each visit to the area involving both depth profiling and continuous sampling of the filament. See Ledwell *et al.* (1993) figures 7, 11, 12, 18, and 23 for an indication of the different survey strategies used. A common aspect of their survey strategy is repeated crossings of the tracer filament following an initial large scale survey to identify the filament through peak tracer concentrations. This is in accordance with our strategy and justification for starting all surveys from the same position in the spatial grid: it is assumed that a previous survey has been conducted for features identification and the peak concentrations located. As a consequence for investigation of the single filament all surveys are centred on the maximum tracer concentration throughout the domain. Surveys of the convoluted fields are centred on the same position to ensure the same section of the physical domain is sampled, it is only the extra tracer and nutrient initialisations which are resulting in any alteration to previously observed distributions. The same original filament, considered throughout all of the two-dimensional studies, is still present but it is now obscured by additional tracer filaments. Details relating to the two methods of investigation are discussed below.

i) Single Filament- variation of track size/orientation

A single inert tracer distribution is chosen for the '*in-situ*' survey. An inert tracer is investigated as the asymptotic structure (Gaussian) and how the size of this relates to the physical environment is which it has evolved is known theoretically (Garrett, 1983), has been supported observationally (Ledwell *et al.*, 1993), and has been repeatedly shown to agree with this throughout previous investigations (Chapters 5, 6) albeit with the caveat of a re-scaling of the equation to predict minimum equilibrium length-scale (equation 2.7). The field of choice is from mid-way through the model run, approximately day 15. The particular one used is chosen for its properties of being a clearly defined filament, with morphology determined by strain dominated dispersal. The lowest diffusivity of 35.6 m^2s^{-1}

is chosen arbitrarily. It is no longer a particular physical property of tracer dispersal that is being investigated, just the effect of varying survey strategy on the accuracy of the resulting dataset.

The highest tracer concentration in the filament is taken as the centre point for each survey. Three distinct survey track spacings are used: 20 km, again taken to be standard for a mesoscale survey, and two finer scale surveys at 10km and 5km spacing. The number of parallel tracks for each survey are 6, 10 and 12 respectively. The number of parallel legs for each survey is greater than the four necessary for sufficient spatial representation of oceanic features as recommended in the current European standards (Crook and Schofield, 1997). The total survey length remains constant at 700 km, again standard for a survey of this type. This distance will take approximately 1.5 days to cover at a speed of 10 knots. Reducing speed to 5 knots, or allowing for time for the ship to be stationary for depth profiling, this rises to roughly 3 days. A longer survey time allows a greater scope for temporal bias due to evolution of any reactive tracer and also simply due to advection resulting in modification of the underlying distributions that are being mapped, the only concern when considering an inert tracer. Although it is not a consideration for this synoptic virtual survey, as the data is extracted instantaneously, for *in-situ* purposes it must be assumed (usually incorrectly) that the structure and positioning for the tracer will not alter substantially within the time-scale of the survey. This creates a fundamental bias when comparing model output and *in-situ* observations as a synoptic view is seldom observationally possible. Returning to spatial considerations, the virtual surveys conducted here are completed at four different track orientations, taken as two pairs perpendicular to each other- a pair with vertical/horizontal track, and a pair with tracks at 45° to these. The different orientations are used to investigate the effect of not sampling a distributions orthogonally to its maximum gradients as conducted with previous analysis (Chapter 6).

Both the tracer and strain fields are continuously sampled at each point along the cruise track resulting in a 2km resolution as with previous two-dimensional analysis. The sampled tracer field is then re-gridded, using linear interpolation (Watson, 1992), but only for visual comparison of apparent fields. Any interpolation routine fills absent positions with values according to the computing algorithm. Any resulting distributions are therefore strongly influenced by the assumptions underlying the algorithm. Different interpolation algorithms make different assumptions as to how to fill "missing" data points. It is not the aim of this thesis to judge which is the most appropriate therefore quantitative analysis is restricted to along track data which is free from such issues. Maxima and minima of the tracer concentrations are determined, the distribution divided into "peaks" according to this, and a Gaussian curve fitted to each peak by minimisation of least squares error as used in Chapters 5 and 6 and described in Chapter 4. A Gaussian curve is always used as an inert tracer is being investigated, it has been shown theoretically and through the previous one-dimensional and two-dimensional studies of this thesis that this is the asymptotic shape of an inert tracer under the influence of a strain dominated flow. These curves are then solved to find the width of each peak, as defined as the distance between the points of 0.01% of maximum tracer concentration as in all previous chapters. The widths observed in each survey are then compared, with each other and with those obtained as per previous analysis where filaments are optimally sampled assuming full knowledge of the field (Chapters 5 and 6- two-dimensional tracer distributions).

ii) Interference exp.

A 20km survey track spacing is assumed for all analysis in this section, a standard spacing for mesoscale *in-situ* studies. There is the benefit of a greater survey area than possible with a finer scale study. This is a continuing balance of covering a sufficient spatial extent to be representative of the field, within the shortest time-scale on which the field can be expected

to vary, at a resolution sufficient to quantitatively analyse distributions. This is not particular to this numerical study, this just provides the setting to investigate the various payoffs.

The same four track orientations are adopted as in (i). Both an inert tracer and fertilization type experiment with the NPZD model are considered (attention is again restricted only to the Phytoplankton compartment of this, P_{NPZD}). The interference experiment is conducted with two model setups. It is an aim to assess if the original filament investigated throughout can be mapped in a more convoluted field. The 6kmx6km patch known to result in this is used in addition to:

i) *Multiple tracer release*- the inert tracer/ nutrient spikes, are initialised in a number of distinct patches (6x6km) (one of which being the original).

ii) *Release above background*- there is a general, lower, background concentration (half the value within the 6kmx6km patch) for the inert tracer/nutrient spiking in cells from which drifters were known to interfere with the dominant filament.

The areas for the additional tracer releases/nutrient spiking are determined through the backtracking of virtual floats. Those which are within, or in close proximity to, the filament on day 15, are identified, their initial positions identified and these positions used for the interference initialisations.

Again the observed concentrations are re-gridded for visual comparison, but no quantitative measurements taken from this. Along track tracer concentrations are again segmented into individual peaks, fitted with a Gaussian curve and the width calculated. It should be noted that phytoplankton (P_{NPZD}) distributions are fitted with a Gaussian curve. In previous chapters (5 and 6) analysis of width has previously been carried out using whichever of a Gaussian or DTANH function minimises the least squares error of the data to the curve. This forced fitting of a Gaussian curve is chosen to conform with observational convention. Although this was shown to be not always appropriate for the shape of phytoplankton profiles we are testing the accuracy of widely used observational

techniques. Results relating to other components of the NPZD model are not presented as similar structure is observed to that in the P_{NPZD} compartment. The similarity is sufficient that the same sampling errors occur and no further information gained from analysis of the other model components.

Widths from each interference set-up, and each survey orientation, are compared along with the single filament used throughout previous two-dimensional analysis (Chapter 6). It is sought to investigate if a more convoluted field can "mask" the appearance of a supposedly dominant feature and also if this interference can alter the length-scale of observed distributions: are observed length-scales an artefact of the complexity of the tracer (or phytoplankton) distributions or of the physical environment in which the field as a whole evolves?

7.3 Results

i) Track size/ orientation

A simple strain-dictated filament has been surveyed at 3 different track spacings and 4 orientations. The original and observed model fields are shown in figure 7.3.1. The reconstructed field- a linear gridding of observed concentrations- is shown under each respective survey track. The reconstructed fields indicate that apparent features in "observed" distributions are a worrying artefact of sampling strategy. The reconstructed fields can be strikingly different to and unrepresentative of actual tracer distributions. Unless sampled at a sufficiently fine scale the orientation of the survey is vital in ensuring correct reconstruction of distributions. Survey orientation (ii), a zonal progression, is consistent between track spacings in providing the qualitatively most accurate representation of the field. For this particular filament a predominantly zonal progression results in the filament being transected nearly orthogonal to the maximum tracer gradients: the shortest route across the filament is being taken resulting in the closest measurement of

the actual width of the filament. A number of parallel crossings result in the across patch morphology being reasonably represented. For survey orientations (i) and (iv) conducted at 20km track spacing the reconstructed field is apparently of distinct round patches as opposed to the filamental structure from which observations are taken. For increasing resolution (10km, 5km) the reconstructed field is less distorted. This suggests that unless there is prior knowledge of the underlying tracer distribution to allow correct initialisation and orientation of survey tracks, reconstructed distributions can be worryingly unrepresentative of actual distributions. Surveys at an increased track spacing results in the unfortunate downside of covering a smaller spatial extent, there must be a balance to ensure that a reasonable area is surveyed but at sufficient track resolution as to minimise misrepresentation of the tracer field.

All surveys are centred upon the point of highest concentration and actual concentrations between surveys are not substantially different. Individual data points are a reliable and accurate measurement of actual concentrations. It is when attempting to reconstruct general distributions that errors ensue.

Comparison of the length-scales of "observed" distributions, with those measured from knowledge of the full modelled field, further emphasises the importance of survey orientation. Mean, minimum and standard deviation of the length-scale, measured as the length of peaks within the along track concentration profiles, of "observed" tracer distributions are shown in figure 7.3.2. The corresponding numbers are listed in table 7.3.1. Provided that the filament is crossed in an appropriate orientation- primarily orthogonal to the filament- a minimum width of approximately 40km is observed. This can be up to 75km for other orientations. The mean and standard deviation of the widths do not vary substantially between survey track spacings, again on the condition that the filament is correctly sampled. Comparing length-scale from the "observed" distributions with the analysis of the full model field a lower minimum width is observed, ~30km. It is not unreasonable that the two differ when one remembers that a greater extent of the filament

is being measured when analysing the full model field hence encompassing a greater variation in local strain rate. The mean width is similar for both the full and observed model fields and the range of survey-measured widths fall within the range of the full model measured widths. When crossed at an inappropriate angle (in this case tracks i and iv) the minimum, mean and standard deviation of widths are all greatly increased. Without prior knowledge of the tracer distribution the majority of surveys, and measured widths, could be incorrectly accepted as reasonable.

ii) Interference.

The reconstructed fields for an inert tracer and for P_{NPZD} are shown in figure 7.3.3 and 7.3.4 respectively. Again the perils of an inappropriately devised sampling strategy, reflected in the apparently observed distributions, are striking.

With the interference experiment we are trying to see first what effect multiple patches, and their interference, have upon observed mean and minimum length scales, and second if a known structure can be identified amongst a convoluted field. For visual identification of patch structure survey orientation is again vital. For the considered scenarios a zonal track, (ii), again most advantageously samples the embedded filament. This is not unexpected as the orientation of the original filament has not changed between initialisation scenarios, just that it is now embedded in a generally more convoluted tracer distribution. Considering the multiple releases each distinct patch or filament is best identified if transected at an appropriate orientation, which is clearly not possible with a single gridiron survey due to the parallel survey tracks. Concerning the detection of a patch above a general background concentration the more diffuse boundaries are reasonably depicted with all track orientations (Figure 7.3.3(c) i-iv for inert, figure 7.3.4(c) i-iv for P_{NPZD}). This suggests that although the detection and reconstruction of finer spatial scale aspects of the inert and P_{NZPD} tracer fields are dependent upon the correct survey

orientation larger scale features are less sensitive to the way in which they are surveyed., with the typical 20km track spacing.

Mean and minimum widths are depicted in figure 7.3.5 with corresponding values listed in table 7.3.2a,b. For the single filament investigations a "true" value is given. This is the mean, standard deviation and minimum widths measured during the in-depth investigations carried out in chapter 6. This analysis was not carried out for the interference experiments due to the convoluted nature of the tracer field. The purpose of the interference experiment is to investigate the possibility of identifying a specific feature against a non-zero background field. Widths relating to surveying of a single filament should be taken as "truth", hence the single filament is shown for reference. For the multiple release experiment there is a greater dependence of observed width on survey orientation, compared to the single patch as indicated by the greater range of variability in measured widths for the convoluted fields. Minimum width varies but less so than the mean and variance of widths. Perhaps oddly, the width of an inert tracer can exceed those for a phytoplankton-like tracer. Although the difference between the width of the inert and phytoplankton filaments is generally of order 5km, provided the filament is traversed orthogonally, it can be up to an order of magnitude greater than this when survey tracks are orientated along structure of interest.

For a release above a general background concentration mean, standard deviation and minimum widths are generally greater than for discrete multiple releases. This applies to both the inert tracer and to P_{NPZD}. The variation in inert tracer widths exceeds that for phytoplankton patch widths in this particular model scenario.

Discussion

Completion of a survey track with a random orientation is likely to result in a gross misrepresentation of actual field distributions unless the features of interest are surveyed

orthogonally to maximum tracer, or phytoplankton, gradients or unless concentrations change on scales significantly greater than the track spacing. The likelihood of poorly sampling a filamentous field increases as the spacing of survey track legs is increased. Furthermore, completion of two surveys at right angles to each other by no means guarantees that either survey will be representative as there is no guarantee that either survey will correctly traverse the "small" scale structure of interest. This is especially true when there is no prior survey of the field such as that used here to provide another "best case scenario". When crossed at an inappropriate angle the observed minimum, mean and standard deviation of width are generally all increased with respect to actual widths. This in itself can not be taken as an indication of poor sampling. First there are exceptions to poor sampling meaning a greater range of width measurements simply due to variation in the number of achieved solutions (when fitting curves to "observed" data). Secondly for a more convoluted field a greater variance of widths can be expected, and a greater range will correctly represent the variation in scale of actual structures within the tracer distribution. Lastly, and above all, actual values for widths are not generally unreasonable when compared to typical widths measured throughout the model analysis.

Prior knowledge of the field is ideally required for optimal surveying. This may be available though prior surveying. Due to the level of knowledge required however, satellite imagery or a suitable good local ocean forecast from an appropriate bio-physical model will be of more assistance in devising a survey strategy. It is acknowledged that a suitable model for providing sufficiently high quality ocean/phytoplankton forecasts may not exist at this time. However real-time forecasting of bio-physical distributions, combined with optimisation of sampling strategy, has been used to good effect during sampling of the Iceland-Faeroes front (Popova *et al.*, 2002; Rixen *et al.*, 2003). The findings of the investigations of sampling strategy reported here provide further evidence of the necessity for ocean forecasting for devising sampling strategies which will hopefully provoke further model development and implementation.

Returning to currently available options for the mitigation of surveying errors, consideration of velocity fields may provide an underway indication of the preferred survey orientation, although it must remain in mind that the velocity field can change significantly within the time-scale of the survey.

In a convoluted tracer or phytoplankton field, such as may be anticipated in an oceanic survey, it has been shown that the mean and variance of widths of both an inert tracer and phytoplankton are greater than those observed for any of the single filaments making up the convoluted field. It should be noted that in the investigations reported here the same filament is present, although embedded in a more complicated distribution, and that the same spatial extent is purposely surveyed to exclude the possibility of contamination from previously un-sampled strain regions.

When considering multiple, generally distinct, inert tracer filaments the minimum observed width of these fields is similar to that of a single filament. When considering structure above a general background level this is not so, nor should it be expected to be. The minimum length scale of strain dominated dispersal has been investigated and shown to depend upon local physical controls. With the case of multiple release, although a generally more convoluted field is observed, the controls upon equilibrium width are similar. The spatial scales of the release and therefore those of the associated rates of strain and mixing are similar. Therefore filaments will tend to roughly the same width. If a single filament is imposed upon a general background level then due to the larger length-scale, associated with the lager background patch, tracer dispersal is now dependent on larger-scale advective processes and is more analogous to homogenisation of the tracer field, the third dispersal regime described by Garrett (Garrett, 1983). This results in much larger observed length-scales.

For P_{NPZD} although similar trends are exhibited, with increased mean and variance of width for a convoluted field, controls on width are more complex as biological controls must also be considered. It has been demonstrated how biological dynamics can modify

distributions resulting in different length-scales to those expected from physical considerations (Chapter 2 onwards). When considering the spatially varying effective growth rate of P_{NPZD}, due to spatially varying nutrient availability and the time lag of the responses of the interrelated compartments of nutrients, zooplankton and detritus, due to the finite time taken for compartments to react to variability in the others, it is not surprising that smaller scale structure is created as a result of biological dynamics. Transient events in the biological model can reasonably be expected to result in short lived responses observed as small-length-scale structure associated with gradients in the field. This is evident in the smaller widths observed in P_{NPZD} distributions, compared with those for the inert tracer, for a release above a locally non-zero background level. This is an excellent example of how the morphology of a biologically reactive entity can differ from those expected when considering local, physical, dynamics alone. It may be obvious to expect a reactive tracer, one which is growing in time, to exceed the length-scales of an inert tracer, in the same flow, as biological effects overcome constraining physical processes, but it must be remembered that the opposing case also applies. It remains true that biological length-scales, such as those relating to phytoplankton, may be both larger or smaller than those observed in an inert tracer in the same physical environment. This is more apparent in a scenario allowing for a greater extent of biological activity. Despite different length-scales between inert and reactive tracers such as phytoplankton, elongating patches of both will still tend towards an orientation determined by the local strain rate.

Conclusions

Conducting a number of different sized and orientated survey tracks, over common underlying fields, has highlighted the necessity of an effective sampling strategy when conducting mesoscale studies of tracer and phytoplankton distributions. Unless the survey is correctly orientated a strikingly different field can be "observed" in comparison to the

field from which it is sampled. A finer scale survey (closer spacing of survey tracks) results in a more representative reconstruction of underlying fields, but at the expense of loss of regional coverage. Quantitative bias of widths results from along as opposed to across patch sampling is independent of resolution. If the filament (or tracer field) is not crossed orthogonally to its maximum tracer gradients the measured minimum width is higher than its "true" value. There is an additional issue when considering three-dimensional investigations in that along track resolution is also limited by that of the equipment used, for example SeaSoar a combination package capable of acquiring bio-physical information such as is suitable for mapping the upper ocean has an along track resolution of 4km (Srokosz *Pers. Comm*). Two-dimensional continuous sampling may have a higher spatial resolution but these measurements are limited solely to the ocean surface.

Considering a convoluted tracer field in the interference experiment has shown again how the minimum length-scale is dependent on both biological and physical dynamics. It has been shown how the minimum length-scale of a phytoplankton patch can be both larger and smaller than that of an inert tracer in the same physical environment, and initial location. For visual comparison this may not be striking, it is at scale of less than tens of kilometres that reactive processes are of increased effect.

When conducting an *in-situ* mesoscale survey of tracer and phytoplankton distributions it is helpful to have some prior knowledge of field properties in order to correctly orientate survey tracks. From this an appropriate, and hence more representative, survey strategy may be devised. If this is not possible then a reduction in spacing of survey tracks aids with reconstructing observed distributions but the higher local resolution is at the peril of the regional extent of survey.

It should be noted that these results relate to variations resulting from spatial bias in survey strategy. Temporal effects resulting from evolution and modification of the surveyed field within the time-scale of an investigation have not been considered here but are likely only to increase the magnitude of error.

CHAPTER 8: General Conclusions and Future Directions.

The aim of the thesis has been to investigate the minimum equilibrium length-scale of phytoplankton distributions at the mesoscale. It was wished to improve understanding of the bio-physical interactions responsible for the size and shape of phytoplankton patchiness in a strain dominated region, and to relate the minimum equilibrium length-scale of this patchiness to the controls under which it is formed. This has been done using a hierarchy of simple models.

The first stage was to investigate the behaviour of a logistic tracer in a one-dimensional purely straining flow. The motivation for this was to further the studies of Martin (2000) who found that the minimum predicted width of an exponentially growing reactive tracer, taken as a crude proxy for phytoplankton, was the same as that of an inert tracer. The across patch morphology in that case is a Gaussian profile with a spatial variance simply determined by the ratio of the rates of small-scale mixing to strain:

$$\sigma^2 = \frac{\kappa}{\lambda} \qquad 8.1$$

where σ^2 is the across filament spatial variance, κ is the effective diffusivity, and λ is the strain rate. The width is seen to be independent of growth rate, μ, which only impacts on the magnitude of the distribution (if μ is greater than the strain rate, λ, the concentration increases exponentially with time, if less than the strain rate then it will tend exponentially to zero).

A logistic growth tracer is the logical progression from this model and was taken as the starting point of this thesis. By inclusion of a population limit effects such as resource limitation are implicitly represented. The logistic growth model is no more complex than

the exponential growth one and computational demands are not significantly increased but another step is taken towards 'reality'.

For initially low population levels the logistic growth tracer will grow exponentially. As levels tend towards the population limit the death rate is increased, eventually exceeding the growth rate until a balance is achieved and the tracer will tend towards its population limit.

The inclusion of a population limit was found to result in an additional behavioural regime. For low growth rates the tracer behaves as found for exponentially growing tracer investigations. The distribution tends towards a Gaussian profile of variance as described by equation 8.1. A qualification is now that, for a suitable ratio of growth to strain rate, a steady state Gaussian solution can now be achieved, without the need for the practically impossible balance of $\mu=\lambda$. The most interesting new behaviour occurs for higher growth rates. In the event of the population achieving its imposed limit two reactive (Fisher) fronts are formed propagating outwards in each direction from the tracer source at a speed (in the absence of advection) dependent upon the rates of mixing (parameterised by the effective diffusivity) and growth, $v_{\min} = \sqrt{\kappa\mu}$. These fronts stop where the opposing straining velocity is of equal magnitude to the frontal speed. Hence width is now dependent upon a balance of rates of mixing, strain and growth in this regime. Taking account of the two regimes the behavioural dynamics of the system have been summarised in a new formula for describing the minimum length-scale of phytoplankton distributions:

$$W = 8.6\sqrt{\frac{\kappa}{\lambda}}\max\left(1, \sqrt{\frac{\mu}{\lambda}} - 1.6 + 1\right) \qquad 8.2$$

where W is now the actual width of the filament, defined as the distance between isopleths of 0.01% of maximum tracer concentration. Width is now used because spatial variance is no longer a reliable measure of filament width due to the two different asymptotic filament profiles. The formula predicts that if the growth rate is less than two and a half times

(roughly the square of 1.6) greater than the strain rate then a Gaussian solution is achieved for the filament width as previously described. For a sufficiently high growth rate however a propagating front solution is formed and the width has an increased dependence on the strain rate (width now varies as λ^2) and is additionally dependent on the growth rate.

Continuing the investigation of a logistically growing tracer filament in a uniform strain environment the effect of explicit nutrient representation was considered. This was found to have the potential to dramatically alter the cross-sectional profile of the logistic tracer distributions. Nutrients were supplied as a boundary condition ensuring a plentiful supply at the edges of the tracer patch. This represents a case in which ambient waters are rich in nutrients. However, in the case of high growth rate there is still potential for nutrient depletion at the patch centre. This can result in a decrease in population at the centre of the domain whilst that at the sides continues to grow unhindered, resulting in doubled-peaked cross-sectional profile. Although a striking visual feature this phenomenon was not found to affect the actual predicted width of tracer distributions. The small caveat is that rather than the maximum growth rate, μ, the growth rate that should be used for predicting width is now the nutrient dependent effective growth rate ($\mu^* = \mu N^*/(k+N^*)$, where N^* is the mean nutrient concentration across the tracer patch and k is the nutrient half-saturation coefficient).

The one-dimensional investigations resulted in the derivation of a formula (equation 8.2) giving a very good prediction of the minimum equilibrium width in the case of constant uniform strain, growth and effective diffusivity. It was then sought to test the derived formula in a more complex physical environment chosen here to be two-dimensional, horizontal, quasi-geostrophic turbulence. This is a reasonably realistic representation of the flow at the mesoscale. With progression to a more complex physical environment arose the opportunity, and necessity, for a number of extra lines of investigation. The primary goal, however, remained the need to test the formula for

predicting minimum length-scales derived in a uniform constant strain environment in a more realistic flow. With the progression to a two-dimensional field we are considering a temporally and spatially varying strain field, combined with rotational effects. Prior to any runs it was foreseen that observed structure would be more convoluted than that observed in the one-dimensional studies. It was also expected that greater care must be taken in quantifying the strain rate. We would no longer be considering a constant, homogeneous, strain rate. This requires consideration of how best to represent the cumulative effects of varying strain rate on the tracer patch dispersal.

An aside taken to this was consideration of effective strain rate and how best to quantify its cumulative effects. Previous comparable investigations of oceanic tracer, and phytoplankton, dispersal use a number of differing methods for quantifying strain rate ranging, from the crude to the mathematically precise (Haidvogel and Keffer, 1984; Ledwell *et al.*, 1993; Pierrehumbert and Yang, 1993; Abraham, 1998; Sundermeyer and Price, 1998; Neufeld *et al.*, 1999). It was found that for the purposes of studying tracer dispersal the most effective measure of the effect of strain history on tracer morphology is provided by the finite time Lyapunov exponents modified to better resolve short period temporal effects. Although possible in a numerical modelling setting, where velocities are known at all points in space and time, this is near impossible for *in-situ* studies. Hence the numerically precise exponents lack practical application. Analysis, however, showed that a reasonable measure of strain can be calculated from the separation of floats initially 400-2000m apart. These floats should be deployed simultaneous to the tracer under investigation. In short a strong practical message from this study is that for any future tracer release or fertilization experiment the only reliable *in-situ* method of calculating strain rate on the spatial range required is from high resolution float deployments. Commenting in particular on the use of rate of change of patch length for calculating strain rate, as used by (Ledwell *et al.*, 1993; Abraham *et al.*, 2000; Sundermeyer and Ledwell, 2001), it has been shown to be highly subjective and the value calculated for strain rate very dependent upon

the method used for finding the patch length, the local rate of mixing (effective diffusivity) and the nature of the tracer (inert or reactive).

To test the formula derived for uniform strain in a more realistic setting it was decided to use it to estimate effective diffusivity. This was done using the measured width of a filament and rates of effective strain and growth in the model. This estimate of the effective diffusivity was then compared with the applied value.

An inert tracer provided a "clean" way of testing the effect of spatial and temporal changes in the strain rate on tracer dispersal before investigating the influence of the more complex physical model on reactive tracers' dispersal. In the case of an inert tracer a passable relationship between applied and effective diffusivity is found provided that the filament is analysed only at times of strain dominated dispersal. The region of strain domination varies with location, patch size and time. It is important to note that what was visually identified to be a period of strain dominated dispersal from the tracer contour evolution was found not to be so when the separation of seeded floats was considered. This inadvertent misclassification of the dispersal regime is also evident in the deterioration in the relationship between calculated and applied diffusivity outside of the period of strain domination as indicated by the drifter trajectories. However the relationship found was good enough to encourage further investigations with reactive tracers.

With the progression to a logistic growth tracer in the turbulent environment a number of new effects become apparent. The constant modification of the tracer, by inhomogeneous straining, means that in the event of a frontal solution being formed its speed of propagation is not that found in a pure strain flow, nor is it simple to calculate. The tracer patch, or filament, was also not found to be reaching an equilibrium width over its entire length resulting in misleading transients, which there is no way of diagnosing *in-situ*. With these points held in mind it was not surprising to find a substantial decrease in quality of relationship between calculated and applied values of effective diffusivity when calculating effective diffusivity from the width of logistic tracer patches using the one-

dimensional formula. This relationship further deteriorates with increasing maximum tracer growth rate, when one expects a greater likelihood of a propagating front solution being formed.

With the progression to a two-dimensional environment it was now also felt appropriate to assess the propriety of a logistic growth tracer as a proxy for phytoplankton. This was done by comparing the dispersal of a logistic growth tracer with that of the "phytoplankton" tracers of an NPZD ecosystem model. Though far from the complexities of reality this NPZD model provided an important test of the effectiveness of a logistically growing tracer in representing the dynamics of an ecosystem model that has been shown to provide a reasonable reproduction of observed phytoplankton ecosystem dynamics (Fasham, 1993). The results were disappointingly poor. Although visually similar to those observed for the inert and low growth rate logistic tracers the phytoplankton filament generated (and those of the corresponding compartments) had a width which was not well described by the previously described formula linking rates of mixing, strain and growth. There were no discernible trends with rates of growth or mixing (the user defined variables). This lack of consistency in behaviour hindered any statements as to why the formula is not well describing the width of phytoplankton filament. This provides a stark message for investigations such a SOIREE where the width of a phytoplankton filament generated through iron fertilisation was used to estimate a value for effective strain rate and hence estimate effective diffusivity (Abraham *et al.*, 2000; Boyd and Law, 2001a).

A plausible reason for the poor result is that the logistic tracer does not adequately parameterise phytoplankton dynamics. Although the high rate of growth, and acceleration, of population levels occurs when conditions become favourable (we provide an extra input of nutrients to seed the patch) the longevity of this was not sufficient for prolonged "bloom" behaviour with this particular ecosystem model configuration. Excess nutrient consumption quickly extinguishes the imposed perturbation leading to dynamics which are not well described by logistic growth. That said, the rapid increase in populations levels

before reaching a limit is well described by a logistic growth model and the modification of the shape of filament profiles from a Gaussian one to the flatter table top distributions observed on occasion in the NPZD system suggests that the logistic growth model may still be appropriate for some of the time. Generally, however, although certain aspects are reasonably mimicked by a logistic growth tracer it is not a sufficiently sophisticated model for quantitative purposes (at the mesoscale). Another possibility is that we are not properly capturing the dynamics of the ecosystem with our measurement of effective growth rate. A better theoretical measure may be the chemical Lyapunov exponent but this is impossible to estimate without perfect knowledge of the ecosystem.

The use of ecosystem models for the purpose of predicting length-scales needs to be considered further, although the appropriate physical environment for testing must be carefully considered. Although simple individual reactive tracers are reproducing certain dynamics observed in phytoplankton populations it appears that vital aspects are being overlooked. The phytoplankton ecosystem must be more accurately represented. With increased biological complexity the physical context in which it is embedded must also be considered. Within our two-dimensional model certain aspects are excluded. Vertical processes such upwelling of nutrients, variable light and temperature distributions, will impact upon phytoplankton growth rates. These can be represented as temporally and spatially heterogeneous fluxes, and forcing terms within a biological model. This is often taken as sufficient by many other modelling studies. Given the sensitivity of results demonstrated here (particularly at the mesoscale and below) on the biological model used, the context of application must be carefully considered prior to application. Too often models are used without consideration of how their characteristic behaviour may influence the results.

With regard to investigation of phytoplankton patch length-scales there remain equally pertinent problems as the over simplification of population dynamics. As for the logistically growing tracer, a lower proportion of the "phytoplankton" tracer filament was

reaching an equilibrium than found for inert tracer studies. This creates a fundamental flaw in attempts to test a formula for predicting the minimum expected equilibrium width. It is not a fault of the model or parameterisations that equilibrium is not being achieved. This is a simple and unavoidable fact of life when considering the interaction of variable physical and biological processes. Although knowledge of expected minimum length-scales may have implications with regards model resolution necessary for estimation of the minimum magnitude of export fluxes from the surface ocean (Waite and Johnson, 2003)it may be necessary to consider a description of modal, rather than minimum, width for application in mesoscale studies. Given the highly variable nature of surface ocean dynamics it is unlikely that many distributions can be expected to achieve (and/or maintain) a minimum, equilibrium length-scale. An approximation of the width at which the majority of phytoplankton distributions may be found, in relation to the local rates of mixing, strain and population growth, may be more widely applicable.

Although it may be seen as disappointing not to receive affirmation of the previously derived theory, it is nevertheless instructive. Important points should be noted and suggestions for future directions can be made. It appears to be a popular activity when investigating oceanic tracer dispersal or fertilisation to calculate effective diffusivity (a parameterisation of mixing assumed due to the effect of under resolved straining processes) from observed tracer or phytoplankton dispersal. On the basis of these results it is strongly urged to pursue this activity carefully. Inherently flawed measurements of strain rate, under resolved widths, and subjectivity in depiction of the ecosystem make it a task fraught with error. What purpose does an estimate of mixing rate with a (conservative) estimate of an order of magnitude error serve? If this is carried out by studying the dispersal of a reactive tracer the errors increase further. These are considerations for the practical application of predictive formulae for minimum length-scale. It is suggested that our current formula is not yet suitable for description of the equilibrium width of

phytoplankton distributions. The results of these studies suggest that it is unlikely that a general formula ever will suffice.

The application of any formula should be held in mind throughout any theoretical investigation. The formula derived here relates the minimum equilibrium length scale of phytoplankton distributions to the local rate of effective strain, effective diffusivity, and effective population growth rate. The two applications of the formula are to predict the minimum length scale of phytoplankton patches or to estimate the value of the processes on which the length-scale is dependent, having quantified the other relevant components. Mesoscale phytoplankton distributions have been suggested to reach a minimum equilibrium length scale as small as 1km (Martin, 2000), with an upper limit (for strain dominated dispersal) being on the order of 40 km. This is a very reasonable estimate that conforms with observational estimates (although it is recognised that the scale of phytoplankton heterogeneity is dependent upon the scale of sampling). Issues with estimates of effective diffusivity have been dealt with above. It is suggested that a more promising path for further investigation is perhaps the quantification of effective strain rate. Results were found here to be dependent upon the particular method used to calculate the effective strain rate. The most appropriate method for this study was derived. To make general recommendations, enabling a direct comparison between numerical studies with different physical dynamics, an ensemble of studies is required investigating tracer dispersal and corresponding strain rate in a variety of physical conditions: different dynamics, regional effects and size, strength, and number of eddy features. When performing such numerical studies it would be useful if observational constraints were kept in mind such that recommendations could be made for both computational and *in-situ* studies.

Summary of Tracer investigation results:

- One-dimensional investigations provided a formula to accurately describe the width of a logistic growth tracer, with or without explicit representation of resource depletion, (equation 8.2).
- When considering tracer dispersal in a turbulent flow the spatially and temporally varying strain rate significantly obscures the relationship between size of an inert tracer patch and the rate of mixing it has experienced.
    - The most effective method of measuring the strain history of a tracer patch was found to be finite time Lyapunov exponents modified for small time intervals (Pierrehumbert and Yang, 1993).
    - When considering methods for *in-situ* measurement of strain rate the rate of change of patch length was shown to be highly subjective and dependant upon the methods used for finding patch length, the local mixing rate, and the reactive nature of the tracer.
    - Separation of high resolution drifters deployed simultaneously to the tracer release is suggested to be the most reliable method for *in-situ* measurement of the strain history of a tracer patch.
- The relationship between patch width and mixing rate deteriorates further when considering a logistic growth tracer. The spatially and temporally varying strain rate is further obscuring the relationship due to modification of the behaviour of the propagating fronts associated with logistic growth tracers.
- The logistic growth tracer is not a sufficient representation of phytoplankton growth when considering mesoscale dynamics.
- The width of phytoplankton distributions can ***not*** be used for estimation of mixing rates.

Suggestions for further directions:

- A more effective formula for predicting the width of phytoplankton distributions is required. This should be based on:
    - A suitable representation of the effects of a temporally and spatially varying strain history of a tracer patch.
    - A suitably descriptive ecosystem model and not an over-simple parameterisation of population dynamics. What this constitutes in the context of investigation of mesoscale phytoplankton heterogeneity could provide ample scope for investigation of ecosystem models.

  - A more representative length-scale than the minimum equilibrium length-scale which appeared not to be consistently achieved within our investigations.
- A more thorough investigation of methods for measuring the variable strain history of a tracer patch. This should have application in the context of both numerical and observational studies and enable comparison between the two.
- A more structured approach to investigation of tracer dispersal may provide the link between the one-dimensional pure-strain investigations and those in a two-dimensional turbulent flow. Simpler representation of two-dimensional flows, and approaches to turbulent representation (e.g. blinking vortices) may prove a worthwhile avenue of investigation.

The second section of investigation (chapter 7) provided a further connection has been made between the theoretical work described here and *in-situ* studies by consideration of mesoscale sampling strategies. This was achieved by investigating "observed" fields derived from the model in a manner similar to typical mesoscale surveys, sampling using a number of different track orientations and spacings. Observed fields were found to be concerningly dependent on the survey track used. Without some prior knowledge of observed distributions, a very different field can be reconstructed from observations to that from which they were sampled. This error decreases as the spacing between survey tracks is decreased, although this necessitates a smaller spatial extent of the sampled area for the same duration of survey. This is not suggested as a recommendation for ship based surveying of mesoscale fields, but to further highlight the necessity for multidisciplinary studies in this area. For understanding mesoscale plankton patchiness concurrent biological and physical fields must be known, and effective sampling of these can be achieved through the collaboration of numerical and observational studies. A local forecast of bio-physical distributions of sufficient resolution is required to correctly determine orientation of survey tracks. In turn suitable high resolution data is required for model initialisation, tuning, testing and improvement. This somewhat circular problem suggests that there is

ample scope for further collaboration between numerical and observational studies (Popova *et al.*, 2002; Rixen *et al.*, 2003) in improving understanding of the exact nature of the controls on observed length-scales of phytoplankton distributions, and that neither of these approaches is likely to decipher the answer alone. Consideration of the controls on phytoplankton patchiness from a single discipline or methodology appears likely to result in a solution which, though seemingly plausible, may be somewhat removed from reality.

Summary of sampling investigations:

- Observed distributions are very dependant upon the resolution of the survey tracks and their orientation with respect to the structure of interest.
    - This dependence is reduced by conducting a higher resolution survey, although at the peril of the spatial extent which can be surveyed.
- Without prior knowledge of the field to be investigated it will be very difficult to construct a survey strategy which will enable reconstruction of spatial distributions, whilst maintaining a resolution which will enable coverage of a sufficient spatial area within a sufficiently short time scale to eliminate temporal variations.
    - An area of approximately 50km x50km takes 3 days to survey at are solution sufficient that orientation of the survey track has minimal effect on reconstructed distributions.

Suggestion for further directions:

- There is ample evidence for the necessity to further the work of e.g. Popova *et al.* (2002) and Rixen *et al.* (2003) in collaboration between observational and numerical investigations.
    - There is evidence that real-time ocean forecasting and optimisation of survey strategies is of huge benefit with regards accurate sampling of spatial distributions and this improved data will in turn improve the ability of regional models in representing small scale local variations.

Although an initially bleak picture can be taken from these results it is in turn suggested that these should be taken as an indication of the necessity for increased collaboration between approaches, disciplines and platforms.

We have investigated the minimum-equilibrium length-scale of oceanic phytoplankton distributions. Great care has been taken throughout to investigate the "best case scenario". Hence all results presented throughout can be taken as "a best case". Associated errors will only increase if studies are less diligent or do not have the accuracy and/or synopticity afforded to numerical investigations. With regards to this, efforts have been made to provide practical suggestions for minimisation of errors in comparable studies. Although the work in this thesis is theoretical it has provided strong practical suggestions for future observational studies of tracer (and phytoplankton) dispersal.

It has been shown that the width of phytoplankton patches can not be used for estimating effective diffusivity. The importance of biology, and its representation, in determining phytoplankton patch size has also been shown and the difficulties of quantifying it illustrated. It has been demonstrated that a simple single tracer representation of phytoplankton population dynamics is not sufficient for investigations of the morphology of phytoplankton patches. The subtle dynamics of an ecosystem must be represented with sufficient accuracy for the scale of the problem. At mesoscales and below a simple individual reactive tracer does not sufficiently parameterise phytoplankton population dynamics for meaningful quantification of expected length-scales.

The representation of growth, stirring and mixing in the context investigated within this thesis provides the simplest case of their interaction. The considerable complexities, and practical difficulties, unearthed within these investigations raise questions about studies of more complex systems: if the simplest case can not be understood, what meaningful understanding can be obtained in more complex systems? The sensitivity of model output to the complexity of the representation within the model, and the method of observation and analysis, should not be underestimated.

References

Abraham, E. R. (1998). "The Generation of Plankton Patchiness by Turbulent Stirring." Nature **391**: 577-580.

Abraham, E. R. and M. M. Bowen (2002). "Chaotic Stirring by a Mesoscale Surface-Ocean Flow." Chaos **12**(2): 373-380.

Abraham, E. R., C. S. Law, P. W. Boyd, *et al.* (2000). "Importance of Stirring in the Development of an Iron-Fertilized Phytoplankton Bloom." Nature **407**: 727-733.

Allen, J. I. (1997). The Importance of High Frequency Data in Ecological Modelling. *Operational Oceanography. The Challenge for European Co-Operation. Proceedings of the First International Conference on EUROGOOS*,. J. H. Stel, H. W. A. Behrens, J. C. Borst, *et al.* Amsterdam, Elsevier Science. **62:** 778.

Bainbridge, R. (1957). "The Size Shape and Density of Marine Phytoplankton Concentrations." Biological Review **32**: 91-115.

Banse, K. (1991). "Rates of Phytoplankton Cell Division in the Field and in Iron Enrichment Experiments." Limnology and Oceanography **36**(8): 1886-1898.

Batchelor, G. K. (1967). Section 3.6. *An Introduction to Fluid Dynamics*. London and New York, Cambridge University Press.

Bennett, A. F. and K. L. Denman (1985). "Phytoplankton Patchiness: Inferences from Particle Statistics." Journal of Marine Research **43**: 307-335.

Boyd, P. W. and C. S. Law (2001a). "The Southern Ocean Iron Release Experiment (Soiree)- Introduction and Summary." Deep Sea Research Part II: Topical Studies in Oceanography **48**: 2425-2438.

Boyd, P. W. and C. S. Law (2001b). "The Southern Ocean Iron Release Experiment (Soiree)--Introduction and Summary." Deep Sea Research Part II: Topical Studies in Oceanography **48**(11-12): 2425-2438.

Boyd, P. W., A. J. Watson, C. S. Law, *et al.* (2000). "A Mesoscale Phytoplankton Bloom in the Polar Southern Ocean Stimulated by Iron Fertilization." Nature **407**: 695-702.

Brentnall, S. J., K. J. Richards, J. Brindley, *et al.* (2003). "Plankton Patchiness and Its Effect On larger-Scale Productivity." Journal of Plankton Research **25**(2): 121-140.

Cassie, R. M. (1963). Micro-distribution of Plankton. *Oceanography and Marine Biology, an Annual Review.* B. H. London, George Allen and Unwin LTD. **1:** 223-252.

Crook, J. and C. Schofield (1997). Sampling Strategies for Oceanographic Features. *Operational Oceanography. The Challenge for European Co-Operation. Proceedings of the First International Conference on EUROGOOS.* J. H. Stel, H. W. A. Behrens, J. C. Borst, *et al.* Amsterdam, Elsevier Science. **62:** 778.

Damköhler, R. and T. Heumann (1982). "Experimental Studies to Clarify the Diffusion Behavior of Copper-Nickel-Alloys with a High Copper Content." Physica Status Solidi A-Applied Research **73**(1): 117-127.

Denman, K. L. (1976). "Co-variability of Chlorophyll and Temperature in the Sea." Deep Sea Research Part I: Oceanographic Research Papers **23**: 539-550.

Denman, K. L. and T. Platt (1976). "The Variance Spectrum of Phytoplankton in a Turbulent Ocean." Journal of Marine Research **34**(4): 593-601.

Fasham, M. J. R. (1978). The Application of Some Stochastic Processes to the Study of Plankton Patchiness. *Spatial Patterns in Plankton Communities.* J. H. Steele. New York, Plenum Press: 131-156.

Fasham, M. J. R. (1993). Modelling the Marine Biota. *The Global Carbon Cycle.* M. Heinmann, Springer-Verlag Berlin Heidelberg. **I 15:** 457-500.

Fasham, M. J. R. (1995). "Variations in the Seasonal Cycle of Biological Production in Subarctic Oceans: A Model Sensitivity Analysis." Deep Sea Research Part I: Oceanographic Research Papers **42**(7): 1111-1149.

Fisher, R. A. (1937). "The Wave Advance of Advantageous Genes." Annals of Eugenics 7: 355-369.

Flament, P. and L. Armi (2000). "The Shear, Convergence, and Thermohaline Structure of a Front." Journal of physical oceanography 30: 51-66.

Franks, P. J. S., Ed. (1995). "Sampling Techniques and Strategies for Coastal Phytoplankton Blooms". *Intergovernmental Oceanographic Commission Manuals and Guides.*

Garrett, C. (1983). "On the Initial Streakiness of a Dispersing Tracer in Two- and Three-Dimensional Turbulence." Dynamics of Atmospheres and Oceans 7: 265-277.

Griffa, A., K. Owens, L. Piterbarg, *et al.* (1995). "Estimates of Turbulence Parameters from Lagrangian Data Using Stochastic Particle Model." Journal of Marine Research 53: 371-401.

Haidvogel, D. B. and T. Keffer (1984). "Tracer Dispersal by Mid-Ocean Mesoscale Eddies. Part I. Ensemble Statistics." Dynamics of Atmospheres and Oceans 8: 1-40.

Hassel, M. P., H. N. Comins and R. M. May (1991). "Spatial Structure and Chaos in Insect Population Dynamics." Nature 353: 255-258.

Haury, L. R., J. A. McGowan and P. H. Weibe (1978). Patterns and Processes in the Time-Space Scales of Plankton. *Spatial Patterns in Plankton Communities.* J. H. Steele. New York, Plenum Press: 277-327.

Jackson, G. A. and A. B. Burd (1998). "Aggregation in the Marine Environment." Environmental Science and Technology 32(19): 2805-2814.

Jackson, G. A. and A. B. Burd (2002). "A Model for the Distribution of Particle Flux in the Mid-Water Column Controlled by Subsurface Biotic Interactions." Deep Sea Research Part II-Topical Studies in Oceanography 49: 193-217.

Jeffrey, S. W. and R. F. C. Mantoura (1997). Development of Pigment Methods for Oceanography: Scor-Supported Working Groups and Objectives. *Phytoplankton Pigments in Oceanography: Guidelines to Modern Methods.* S. W. Jeffrey, R. F. C. Mantoura and S. W. Wright. Paris, UNESCO. 10: 19-36.

Kierstead, H. and B. L. Slobodkin (1953). "The Size of Water Masses Containing Plankton Blooms." Journal of Marine Research **12**: 141-147.

LaCasce, J. H. and C. Ohlmann (2003). "Relative Dispersion at the Surface of the Gulf of Mexico." Journal of marine research **61**: 285-312.

Ledwell, J. R., A. J. Watson and C. S. Law (1993). "Evidence for Slow Mixing across the Pycnocline from an Open-Ocean Tracer-Release Experiment." Nature **364**: 701-703.

Ledwell, J. R., A. J. Watson and C. S. Law (1998). "Mixing of a Tracer in the Pycnocline." Journal of Geophysical Research **103**(C10): 21499-21529.

Lindley, D. V. and W. F. Scott (1996). "New Cambridge Statistical Tables", Cambridge university press.

Lumpkin, R. (2003). "Decomposition of Surface Drifter Observations on the Atlantic Ocean." Geophysical Research Letters **30**(14): 1753.

Mackas, D. L., K. L. Denman and M. R. Abbott (1985). "Plankton Patchiness: Biology in the Physical Vernacular." Bulletin of Marine Science **37**(2): 652-674.

Martin, A. P. (2000). "On Filament Widths in Oceanic Plankton Distributions." Journal of Plankton Research **22**(3): 597-602.

Martin, A. P. (2003). "Phytoplankton Patchiness: The Role of Lateral Stirring and Mixing." Progress in Oceanography **57**: 125-174.

Martin, A. P., K. J. Richards, A. Bracco, *et al.* (2002). "Patchy Productivity in the Open Ocean." Global Biogeochemical Cycles **16**(2): 9.1-9.9.

Martin, A. P., K. J. Richards and M. J. R. Fasham (2001a). "Phytoplankton Production and Community Structure in an Unstable Frontal Region." Journal of Marine systems **28**: 65-89.

Martin, A. P., K. J. Richards, C. S. Law, *et al.* (2001b). "Horizontal Dispersion within an Anticyclonic Mesoscale Eddy." Deep Sea Research Part II: Topical Studies in Oceanography **48**: 739-755.

Martin, A. P., I. P. Wade, K. J. Richards, *et al.* (1998). "The PRIME Eddy." Journal of Marine Research **56**: 439-462.

Matthews, L. and J. Brindley (1997). "Patchiness in Plankton Populations." Dynamics and Stability of Systems **12**(1): 39-59.

McGillicuddy, D. J., A. R. Robinson, D. A. Siegel, *et al.* (1998). "Influence of Mesoscale Eddies on New Production in the Sargasso Sea." Nature **394**: 263-266.

Murray, J. D. (1993). Biological Waves: Single Species Models. *Mathematical Biology.* New York, Springer-Verlag: 274-310.

Neufeld, Z. (2001). "Excitable Media in a Chaotic Flow." Physical Review Letters **87**: 108301.

Neufeld, Z., C. Lopez, E. Hernandez-Garcia, *et al.* (2000). "Multifractal Structure of Chaotically Advected Chemical Fields." Physical Review E **61**(4): 3857-3866.

Neufeld, Z., C. Lopez and P. H. Hsynes (1999). "Smooth-Filamental Transition of Active Tracer Fields Stirred by Chaotic Advection." Physical review letters **82**(12): 2606-2609.

Neufeld, Z. and T. Tel (1998). "Advection in Chaotically Time-Dependent Open Flows." Physical Review E **57**(3): 2832-2842.

Okubo, A. (1970). "Horizontal Dispersion of Floatable Particles in the Vicinity of Velocity Singularities Such as Convergences." Deep Sea Research Part I: Oceanographic Research Papers **17**: 445-454.

Okubo, A. (1971). "Oceanic Diffusion Diagrams." Deep Sea Research Part I: Oceanographic Research Papers **18**: 789-802.

Okubo, A. (1978). Horizontal Dispersion and Critical Scales for Phytoplankton Patches. *Spatial Pattern in Plankton Communities*. J. H. Steele, Plenum Press. **4:** 21-42.

Oschlies, A. and V. Garcon (1998). "Eddy-Induced Enhancement of Primary Production in a Model of the North Atlantic Ocean." Nature **394**: 266-269.

Oschlies, A., W. Koeve and V. Garcon (2000). "An Eddy-Permitting Coupled Physical-Biological Model of the North Atlantic. 2. Ecosystem Dynamics and Comparison with Satellite and JGOFS Local Studies Data." Global Biogeochemical Cycles **14**(1): 499-523.

Ottino, J. M. (1989). "The Kinematics of Mixing: Stretching, Chaos and Transport", Cambridge university press.

Parsons, T. R., M. Takahashi and B. Hargrave (1984). "Biological Oceanography", Pergamon Press.

Petrovskii, S. V. (1999a). "On the Diffusion of a Plankton Patch in a Turbulent Ocean." Oceanology **39**(6): 737-742.

Petrovskii, S. V. (1999b). "On the Plankton Front Waves Accelerated by Marine Turbulence." Journal of Marine Systems **21**: 179-188.

Pierrehumbert, R. T. and H. Yang (1993). "Global Chaotic Mixing on Isentropic Surfaces." Journal of the Atmospheric Sciences. **50**(15): 2462-2480.

Platt, T. and K. L. Denman (1975). "A General Equation for the Mesoscale Distribution of Phytoplankton in the Sea." Memoires de la Societe Royale des Sciences de Liege **6**(7): 31-42.

Popova, E. E., M. A. Srokosz and D. A. Smeed (2002). "Real-Time Forecasting of Biological and Physical Dynamics at the Iceland-Faeroes Front in June 2001." Geophysical Research Letters **29**(4): 14.1-14.4.

Rixen, M., J. T. Allen, R. T. Pollard, *et al.* (2003). "Along or across Front Ocean Survey Strategy? The Estimation of Quasi-Geostrophic Vertical Velocities and Temperature Fluxes." Geophysical Research Letters **30**(5): 68.1-68.4.

Rood, R. B. (1987). "Numerical Advection Algorithms and Their Role in Atmospheric Transport and Chemistry Models." Reviews of geophysics. **25**(1): 71-100.

Seuront, L., F. Schmitt, Y. Lagadeuc, *et al.* (1999). "Universal Multifractal Analysis as a Tool to Characterize Multiscale Intermittent Patterns: Examples of Phytoplankton Distribution in Turbulent Coastal Waters." Journal of Plankton Research **21**(5): 877-922.

Siegel, D. A., D. J. McGillicuddy and E. A. Fields (1999). "Mesoscale Eddies, Satellite Altimetry, and New Production in the Sargasso Sea." Journal of Geophysical Research **104**(C6): 13359-13379.

Simberloff, D. S. and E. O. Wilson (1969). "Experimental Zoogeography of Islands: The Colonization of Empty Islands." Ecology **50**: 278-296.

Skellam, J. G. (1951). "Random Dispersal in Theoretical Populations." Biometrika **38**: 196-218.

Smith, C. L., K. J. Richards and M. J. R. Fasham (1996). "The Impact of Mesoscale Eddies on Plankton Dynamics in the Upper Ocean." Deep Sea Research Part I: Oceanographic Research Papers **43**(11-12): 1807-1832.

Smolarkiewicz, P. K. (1984). "A Fully Multidimensional Positive Definite Advection Transport Algorithm with Small Implicit Diffusion." Journal of Computational Physics **54**: 325-362.

Smolarkiewicz, P. K. and W. W. Grabowski (1989). "The Multidimensional Positive Definite Advection Transport Algorithm: Non-oscillatory Option." Journal of Computational Physics **86**: 355-375.

Smolarkiewicz, P. K. and L. G. Margolin (1998). "MPDATA: A Finite-Difference Solver for Geophysical Flows." Journal of Computational Physics **140**(2): 459-480.

Srokosz, M. A., A. P. Martin and M. J. R. Fasham (2003). "On the Role of Biological Dynamics in Plankton Patchiness at the Mesoscale: An Example from the Eastern North Atlantic Ocean." Journal of Marine Research **61**: 517-537.

Stammer, D. (1997). "Global Characteristics of Ocean Variability Estimated from Regional TOPEX/POSEIDON Altimeter Measurements." Journal of Physical Oceanography **27**(August): 1743-1769.

Steele, J. H. (1974). "Spatial Heterogeneity and Population Stability." Nature **248**: 83.

Steele, J. H. (1978). "Spatial Pattern in Plankton Communities". New York, Plenum Press.

Strass, V. H. (1991). "Chlorophyll Patchiness Caused by Mesoscale Upwelling at Fronts." Deep Sea Research Part I: Oceanographic Research Papers **39**(A): 75-96.

Strogatz, S. H. (1994). Population Growth. *Nonlinear Dynamics and Chaos*. Reading, Massachusetts, Perseus Books: 21-24.

Sundermeyer, M. A. and J. R. Ledwell (2001). "Lateral Dispersion over the Continental Shelf: Analysis of Dye Release Experiments." Journal of Geophysical Research **106**(C5): 9603-9621.

Sundermeyer, M. A. and J. F. Price (1998). "Lateral Mixing and the North Atlantic Tracer Release Experiment: Observations and Numerical Simulations of Lagrangian Particles and a Passive Tracer." Journal of Geophysical Research **103**(C10): 21481-21497.

Tortell, P. and L. Awosika, Eds. (1996). "Oceanographic Survey Techniques and Living Resource Assessment Methods". *Intergovernmental Oceanographic Commission Manuals and Guides*.

Waite, A. M. and D. Johnson (2003). "Critical Scales for Aggregation-Mediated Carbon Export From Ocean Fertilization." Geophysical Research Letters **30**(13): 1690.

Watson, D. F. (1992). "Contouring: A Guide to the Analysis and Display of Spatial Data", Pergamon Press.

Weiss, J. (1991). "The Dynamics of Enstrophy Transfer in Two-Dimensional Hydrodynamics." Physica D **48**: 273-294.

Wiggins, S. (1988). "Fluid Dynamics- Stirred Not Mixed." Nature **333**: 395-396.

Wroblewski, J. S. and J. J. O'Brien (1976). "A Spatial Model of Phytoplankton Patchiness." Marine Biology **35**: 161-175.

Wroblewski, J. S., J. J. O'Brien and T. Platt (1975). On the Physical and Biological Scales of Phytoplankton Patchiness in the Ocean. *Memoires De La Societe Royale Des Sciences De Liege.* J. C. J. Nihoul. **7**: 43-58.

Tables

Chapter 4

Parameter		Value		Units
SC	Biological time scaling	5.5	Individual Tracers*	d^{-1}
		1.83	NPZD	
s	Nitrate vertical transport rate.	0.00648		d^{-1}
V_P	maximum phytoplankton growth rate.	1.0		d^{-1}
k_N	nitrate half saturation value.	0.5		mMol N m^{-3}
g	Maximum grazing rate	2.0		d^{-1}
γ_1	Percentage grazing assimilation (messy eating)	0.75		
γ_2	Zooplankton excretion	0.03		d^{-1}
μ_D	Remineralisation rate	0.05		d^{-1}
μ_P	Phytoplankton mortality rate	0.03		d^{-1}
μ_Z	Zooplankton mortality rate	0.05		(mMol N m^{-3})$^{-2}$ d^{-1}
N_0	Nitrate subsurface value	2.0	Low	mMol N m^{-3}
		15.0	High	
w_s	Detrital sinking rate	5.0		m d^{-1}
h	Detrital length scale	25.0		m
ε	Prey capture rate	1	fast (big**)	(mMol N m^{-3})$^{-2}$ d^{-1}
		0.2	slow (little**)	
V_p	Maximum phytoplankton growth rate	1.0		d^{-1}

* inert and logistic, ** sizes refer to Zooplankton

Table 4.1: Listing of parameter values used for the 4 compartment ecosystem model.

(a)

Passive	cuts	solutions	κ_{calc}
Day 9	219	219	176
12	253	253	227
15	612	612	470
18	669	669	632
21	624	624	546
24	499	499	342
Total	2906	2906	2393

(b)

Logistic μ=0.1 d^{-1}	cuts	solutions	κ_{calc}
Day 9	191	191	165
12	200	200	177
15	460	460	444
18	665	665	618
21	712	712	618
24	617	617	465
Total	2845	2845	2487

(c)

Logistic μ=0.5 d^{-1}	cuts	solutions	κ_{calc}
Day 9	196	196	163
12	225	225	205
15	465	465	389
18	312	312	202
21	335	335	171
24	233	233	219
Total	1766	1766	1349

(d)

Logistic μ=1.0 d^{-1}	cuts	solutions	κ_{calc}
Day 9	205	205	167
12	181	181	170
15	113	113	77
18	37	37	16
21	36	36	26
24	0	0	0
Total	572	572	456

(e)

P_{NPZD} B.R.(i)	cuts	solutions	κ_{calc}
Day 3	188	73	73
4	249	59	59
5	502	171	166
6	579	323	322
7	557	219	219
8	474	96	93
Total	2549	941	932

(f)

P_{NPZD} B.R.(ii)	cuts	solutions	κ_{calc}
Day 3	192	83	83
4	250	39	39
5	635	211	210
6	680	334	334
7	714	297	296
8	488	108	108
Total	2959	1072	1070

(g)

P_{NPZD} B.R.(iii)	cuts	solutions	κ_{calc}
Day 3	175	78	78
4	233	40	40
5	531	150	147
6	641	296	296
7	633	255	255
8	489	122	188
Total	2702	941	934

(h)

P_{NPZD} B.R.(iv)	cuts	solutions	κ_{calc}
Day 3	165	68	68
4	233	36	36
5	582	206	206
6	653	315	315
7	611	261	259
8	480	108	108
Total	2724	994	992

Table 4.2: Numbers of total cuts, cuts for which a solution of width is achieved, widths for which a satisfactory effective diffusivity (κ_{calc}) is calculated. (a) inert tracer, (b)-(d) logistic tracer, (e)-(h) Phytoplankton tracer of NPZD model.

λ_N	Method	Description	Example
1	Eigenvalues of whole flow (considering positive value only)	$\lambda_1 = \sqrt{u_x^{\,2} + u_y v_x}$	
2	Eigenvalue of strain component of flow (positive only)	$\lambda_2 = \sqrt{u_x^{\,2} + \frac{(u_y + v_x)^2}{4}}$	(Haidvogel and Keffer, 1984)
3	Gradient of Velocity Field	$\lambda_3 = \sqrt{u_x^{\,2} + v_y^{\,2}}$	(Garrett, 1983)
4,5	Instantaneous Lyapunov Exponents (ILE's) due to whole flow (pair)	$\lambda_{4,5} = \frac{1}{dt}\log(X_t)$, X_t is the magnitude of stretching experienced by the unit vector pairs **x**, **y**, as described above in one time step. Due to flow tensor.	
6	ILE's anti-symmetric flow	λ_6, stretching due to rotational effects.	
7,8	ILE's symmetric flow (pair)	$\lambda_{7,8}$, stretching due to pure strain.	
9,10	FTLE's (pair)	$\lambda_{9,10} = \frac{1}{t}\log(X_t)$, cumulative measure of stretching experienced by unit vectors due to flow tensor.	(Neufeld and Tel, 1998; Neufeld *et al.*, 1999; Neufeld *et al.*, 2000; Neufeld, 2001)
11,12	MFTLE's (pair)	$\lambda_{11,12} = \frac{1}{t}\log(\theta)$, θ is the eigenvalue of the matrix as described in the text.	(Pierrehumbert and Yang, 1993; Abraham and Bowen, 2002)
13	Rate of change of length (crude approximation to LE's)	$\lambda_{13} = \frac{1}{t}\log(L_t)$, L_t is the length of the filament at time t.	Tracer Release Experiments: (Ledwell *et al.*, 1993, 1998; Abraham *et al.*, 2000)
14	Separation of drifters	$\lambda_{14} = \left\langle \frac{1}{t}\log(D_t) \right\rangle$, D_t is the distance (averaged over all drifters) between drifters at time t.	(Flament and Armi, 2000; LaCasce and Ohlmann, 2003; Lumpkin, 2003)

Table 5.1: Summary of methods used for calculating effective strain rate/strain history.

Strain		Strain rate (s^{-1})					
		(i) All times, all domain			(ii) Days 15-21, strain within filament.		
		Mean	±	σ	Mean	±	σ
Eigenvalue (whole flow)	1	4.6e-6		4.6e-6	3.0e-6		1.4e-6
Eigenvalue (pure strain)	2	4.5e-6		3.2e-6	3.8e-6		1.9e-6
Velocity Gradient	3	4.0e-6		3.7e-6	3.2e-6		2.1e-6
ILE's (whole flow)	4	5.6e-8		3.9e-6	0.1e-6		2.6e-6
	5	-4.1e-8		3.9e-6	-0.1e-6		2.6e-6
ILE (rotation)	6	7.7e-9		2.8e-8	0.00		0.00
ILE's (pure strain)	7	4.9e-8		3.9e-6	0.1e-6		2.5e-6
	8	-4.9e-8		3.9e-6	0.1e-6		2.6e-6
FTLE's	9	2.0e-6		2.6e-6	1.7e-6		1.1e-6
	10	1.8e-6		2.7e-6	1.6e-6		1.1e-6
MFTLE's	11	-6.0e-7		1.1e-5	-0.1e-6		1.8e-6
	12	-1.3e-6		1.2e-5	0.1e-6		1.8e-6
Rate of change of length	13				1.5e-6		2.1e-7 *
Separation of drifters	14				2.6e-6		2.0e-8

* Only method where value varies with effective diffusivity. Lower diffusivity, higher apparent strain.

Table 5.2: Each method of strain, the mean and standard deviation of strain over the run. (i) averaged over all points in domain and times, (ii) averaged over positions within filament, averaged over days 15 and 21.

(a)

Strain	Max	Min	Mean	Median	Max(abs)	Min(abs)	Mean(abs)	Median(abs)	'Best'
1	0.6217	0.0040	0.4624	0.1027	0.6217	0.0040	0.4624	0.1027	**0.62**
2	0.6412	0.0031	0.5168	0.1025	0.6412	0.0031	0.5168	0.1025	**0.64**
3	0.5603	0.0074	0.3963	0.0664	0.5603	0.0074	0.3963	0.0664	**0.56**
4	0.2584	0.5815	0.1375	0.0002	0.5612	0.0067	0.3893	0.0380	**0.58**
5	0.5810	0.2577	0.1391	0.0002	0.5605	0.0068	0.3894	0.0382	**0.58**
6	0.4105	0.0001	0.3330	0.0000	0.4105	0.0001	0.3330	0.0000	**0.41**
7	0.2584	0.5815	0.1374	0.0002	0.5612	0.0067	0.3892	0.0381	**0.58**
8	0.5815	0.2580	0.1377	0.0002	0.5605	0.0068	0.3892	0.0382	**0.58**
9	0.6786	0.3179	0.4126	0.0098	0.6786	0.0038	0.4265	0.0177	**0.68**
10	0.6977	0.1721	0.5521	0.0193	0.6977	0.0043	0.5449	0.0239	**0.70**
11	0.5666	0.6553	0.1583	0.0143	0.6871	0.0039	0.4880	0.0089	**0.69**
12	0.6553	0.5666	0.1583	0.0143	0.6871	0.0039	0.4880	0.0089	**0.69**
13									**0.69**
14									**0.69**

(b)

Strain	Max	Min	Mean	Median	Max(abs)	Min(abs)	Mean(abs)	Median(abs)	'Best'
1	0.7807	-	0.6734	0.1779	0.7807	-	0.6734	0.1779	**0.78**
2	0.7648	-	0.6767	0.1256	0.7648	-	0.6767	0.1256	**0.77**
3	0.7641	-	0.6267	0.1159	0.7641	-	0.6267	0.1159	**0.76**
4	0.5792	0.6938	0.0643	0.0396	0.7641	-	0.6229	0.0849	**0.76**
5	0.6936	0.5774	0.0664	0.0398	0.7631	-	0.6230	0.0845	**0.76**
6	0.6747	-	0.6465	0.0226	0.6747	-	0.6365	0.0226	**0.68**
7	0.5794	0.6938	0.0642	0.0395	0.7642	-	0.6231	0.0852	**0.76**
8	0.6938	0.5787	0.0646	0.0396	0.7638	-	0.6230	0.0853	**0.76**
9	0.7470	0.2299	0.6133	0.0985	0.7470	-	0.6209	0.1182	**0.75**
10	0.8130	0.1970	0.6883	0.0435	0.8130	-	0.6943	0.0555	**0.81**
11	0.7187	0.7525	0.1192	0.0016	0.7759	-	0.6447	0.0727	**0.78**
12	0.7525	0.7187	0.1192	0.0016	0.7759	-	0.6447	0.0727	**0.78**
13									**0.79**
14									**0.79**

(c)

Strain	Mean over days		
	15-18	15-21	9-24
1-14	0.78	0.78	0.69

Table 5.3: Regression coefficients for calculated diffusivity, $\sigma^2\lambda$, with applied diffusivity for each method of effective strain ($\lambda_{1\text{-}14}$) considering maximum, minimum, mean, median, of each effective strain along a cut and of the magnitude of strain. (a) regression over days 9-24. (b) regression over days 15-21. (c) days 15-24 using mean strain within filament. N.B.: Strains 13 and 14 are single value as they always provide an average of strain rate over space and time.

Strain Method λ_N	Days 9-21			Days 15-18			Days 15-21 using mean values		
	m	±ε	c	m	±ε	c	m	±ε	c
1	3.85	0.16	-10.73	4.98	0.22	-47.69	1.71	0.07	10.12
2	3.91	0.16	9.13	5.10	0.23	-34.75	2.18	0.09	12.90
3	3.81	0.18	13.26	4.96	0.23	-31.98	1.81	0.08	10.68
4	2.70	0.13	9.09	3.51	0.16	-22.65	0.04	0.00	0.25
5	2.69	0.13	9.15	3.50	0.16	-22.49	0.04	0.00	0.22
6	0.01	0.00	-0.03	0.01	0.00	-0.21	0.00	0.00	0.01
7	2.70	0.13	9.10	3.51	0.16	-22.65	0.04	0.00	0.25
8	2.70	0.13	9.18	3.50	0.16	-22.51	0.04	0.00	0.25
9	2.22	0.08	7.42	2.47	0.12	-1.86	0.98	0.04	5.77
10	2.51	0.09	-5.31	2.91	0.12	-20.90	0.94	0.04	5.54
11	2.46	0.09	-0.85	2.71	0.12	-9.69	0.16	0.01	0.93
12	2.46	0.09	-0.85	2.71	0.12	-9.69	0.16	0.01	0.93
13	0.80	0.03	7.28	0.87	0.04	5.13	0.87	0.04	5.13
14	1.37	0.05	12.55	1.50	0.06	8.84	1.50	0.06	8.85

Table 5.4: Coefficient from regression of calculated with applied effective diffusivity. m is the gradient of the linear regression, ε the error variability in the gradient, and c the intercept of the fit.

Day	Gradient of fit		Intercept	R^2	RMS error
		± error			
9	1.9	0.07	-9.8	0.86	13.0
12	4.1	0.32	-49.9	0.47	63.1
15	3.2	0.15	-31.8	0.55	44.4
18	3.1	0.10	-22.0	0.62	36.8
21	5.1	0.22	-135.6	0.56	64.7
24	6.8	0.38	-184.4	0.62	77.5
Time Average	3.7	0.09	-55.6	0.45	62.1

Table 6.1: Coefficients of a linear regression of calculated to applied effective diffusivity for an inert tracer on discrete days, plus the time mean average over this period. The standard error in the gradient is also shown. Two measures of error are also listed- the R^2 and root residual mean square (RMS) error.

(a) μ=0.1 d^{-1}

Day	Gradient of fit		Intercept	R^2	RMS error
		± error			
9	1.5	0.54	85.9	0.06	73.8
12	2.7	0.73	114.4	0.08	113.6
15	3.3	0.29	17.7	0.28	59.4
18	6.0	0.32	-95.1	0.41	79.5
21	7.0	0.45	-160.1	0.34	104.4
24	7.8	0.29	-178.2	0.66	62.6
Time average	5.4	0.18	-71.5	0.32	88.7

(b) μ=0.5 d^{-1}

Day	Gradient of fit		Intercept	R^2	RMS error
		± error			
9	3.1	0.64	32.3	0.15	94.1
12	5.9	0.74	-62.6	0.28	111.7
15	6.1	0.55	19.28	0.28	107.0
18	13.5	0.98	-294.30	0.54	119.6
21	27.6	1.82	-744.70	0.68	237.8
24	28.8	1.40	-756.38	0.78	189.5
Time average	10.9	0.68	-179.78	0.20	252.2

(c) μ=1.0 d^{-1}

Day	Gradient of fit		Intercept	R^2	RMS error
		± error			
9	5.4	0.70	50.6	0.33	105.5
12	5.1	1.10	168.9	0.21	138.3
15	3.3	2.14	-662.5	0.82	167.7
18	5.7	19.43	-1282.6	0.42	285.5
21	10.5	15.54	-3006.8	0.84	165.4
24	n/a	n/a	n/a	n/a	n/a
Time average	3.7	1.46	311.6	0.01	315.7

Table 6.2: Coefficients of a linear regression of calculated to applied effective diffusivity on discrete days, plus the time mean average over this period for a logistic tracer with maximum growth rate (a) 0.1 d^{-1}, (b) 0.5 d^{-1}, and (c) 1.0 d^{-1}. Two measures of error are also listed- the R^2 and the residual mean square (RMS) error.

(a) B.R.(i)

Day	Gradient of fit		Inter.	R^2	RMS error
		± error			
3	1.2	0.23	117.11	0.33	62.9
4	0.1	0.70	568.37	0.04	139.4
5	2.8	0.29	-12.93	0.48	99.9
6	3.4	0.39	-49.43	0.23	171.8
7	3.9	0.87	62.59	0.10	385.5
8	5.1	0.71	-90.99	0.41	174.5
T	2.8	0.31	90.06	0.11	262.4

(b) B.R.(ii)

Day	Gradient of fit		Inter.	R^2	RMS error
		± error			
3	1.51	0.26	62.09	0.37	71.5
4	0.58	0.88	511.69	0.02	159.4
5	2.37	0.32	76.19	0.28	119.4
6	3.47	0.26	-68.02	0.43	109.0
7	4.75	0.34	-267.66	0.52	115.9
8	9.39	0.52	-734.05	0.82	131.9
T	3.62	0.18	-89.54	0.33	151.5

(c) B.R.(iii)

Day	Gradient of fit		Inter.	R^2	RMS error
		± error			
3	1.37	0.27	126.10	0.29	82.7
4	0.79	0.97	512.75	0.03	161.67
5	3.55	0.48	71.54	0.23	129.90
6	3.55	0.23	-75.75	0.52	105.46
7	4.55	0.34	-205.13	0.49	156.44
8	9.51	0.43	-718.33	0.86	133.76
T	4.07	0.19	-129.94	0.39	167.35

(d) B.R.(iv)

Day	Gradient of fit		Inter.	R^2	RMS error
		± error			
3	0.81	0.28	193.06	0.16	71.47
4	-0.65	0.84	707.59	0.03	142.56
5	1.88	0.35	145.65	0.17	117.16
6	3.76	0.25	-96.02	0.50	108.76
7	4.95	0.24	-292.95	0.73	191.70
8	7.97	0.77	-607.87	0.64	191.70
T	3.74	0.18	-97.92	0.39	149.19

Table 6.3: Coefficients for a regression of applied diffusivity to that calculated from the width of Phytoplankton patches. Four biological regimes (a)-(d) corresponding to different combinations for Nitrate saturation value and Zooplankton capture rate. Columns as described for previous tables.

B.R.(i): N_0=15 mMol m^{-3}, ε=1 (mMol N m^{-3})$^{-2}$ d^{-1}, ($0 < \mu^* < 5x10^{-2}$ day^{-1})

B.R.(ii): N_0=2 mMol m^{-3}, ε=0.2 (mMol N m^{-3})$^{-2}$ d^{-1}, ($3x10^{-8} < \mu^* < 5x10^{-4}$ day^{-1})

B.R.(iii): N_0=15 mMol m^{-3}, ε=0.2 (mMol N m^{-3})$^{-2}$ d^{-1}, ($3x10^{-5} < \mu^* < 7x10^{-3}$ day^{-1})

B.R.(iv): N_0=2 mMol m^{-3}, ε=1 (mMol N m^{-3})$^{-2}$ d^{-1}, ($2x10^{-6} < \mu^* < 5x10^{-3}$ day^{-1})

Survey		Width (km)		
Orientation	Size	Mean	STD	Minimum
Model "Truth"		47.4	18.6	31.5
i	20km	96.1	27.5	56.4
	10km	105.5	22.3	74.4
	5km	110.4	50.8	46.5
ii	20km	49.8	9.81	39.7
	10km	49.2	7.2	39.9
	5km	49.5	7.5	39.2
iii	20km	50.9	14.5	39.3
	10km	49.7	11.5	41.9
	5km	55.2	11.5	41.8
iv	20km	70.9	22.6	51.8
	10km	81.8	12.1	67.2
	5km	94.6	25.0	72.5

Table 7.3.1: Mean, standard deviation (STD) and minimum width for different size (20, 10 and 5km) and orientation (i-iv) of survey track. Widths measured from model analysis (Chapters 5&6) included for comparison.

(a) Inert tracer

		Width (km)		
Survey	IP	Mean	STD	Minimum
i	S	96.1	27.5	56.4
	I1	101.1	50.4	52.3
	I2	167.0	68.9	54.9
ii	S	49.9	9.8	39.7
	I1	90.6	30.9	39.0
	I2	150.5	51.6	90.2
iii	S	50.9	14.5	39.3
	I1	100.1	58.1	47.4
	I2	136.6	38.0	92.2
iv	S	70.9	22.6	51.9
	I1	113.3	56.8	50.8
	I2	175.8	74.1	77.4

(b) Phytoplankton

		Width (km)		
Survey	IP	Mean	STD	Minimum
i	S	97.1	29.4	57.2
	I1	112.9	38.0	55.0
	I2	167.6	54.6	78.8
ii	S	51.0	8.3	40.1
	I1	82.9	20.9	38.6
	I2	173.7	63.7	85.4
iii	S	51.0	14.8	40.3
	I1	92.9	52.7	42.5
	I2	105.5	57.2	39.6
iv	S	83.8	27.3	56.3
	I1	118.1	68.0	44.9
	I2	146.3	52.7	76.3

Table: 7.3.2: Mean, minimum and standard deviation (STD) of width for (a) inert tracer and (b) phytoplankton interference experiments. Forced Gaussian fit for both. 20km survey track spacing, 4 different orientations (i-iv), three different setups- (S) simple, (I1) multiple release, and (I2) release above a locally non-zero background level.

Figures

Chapter 1

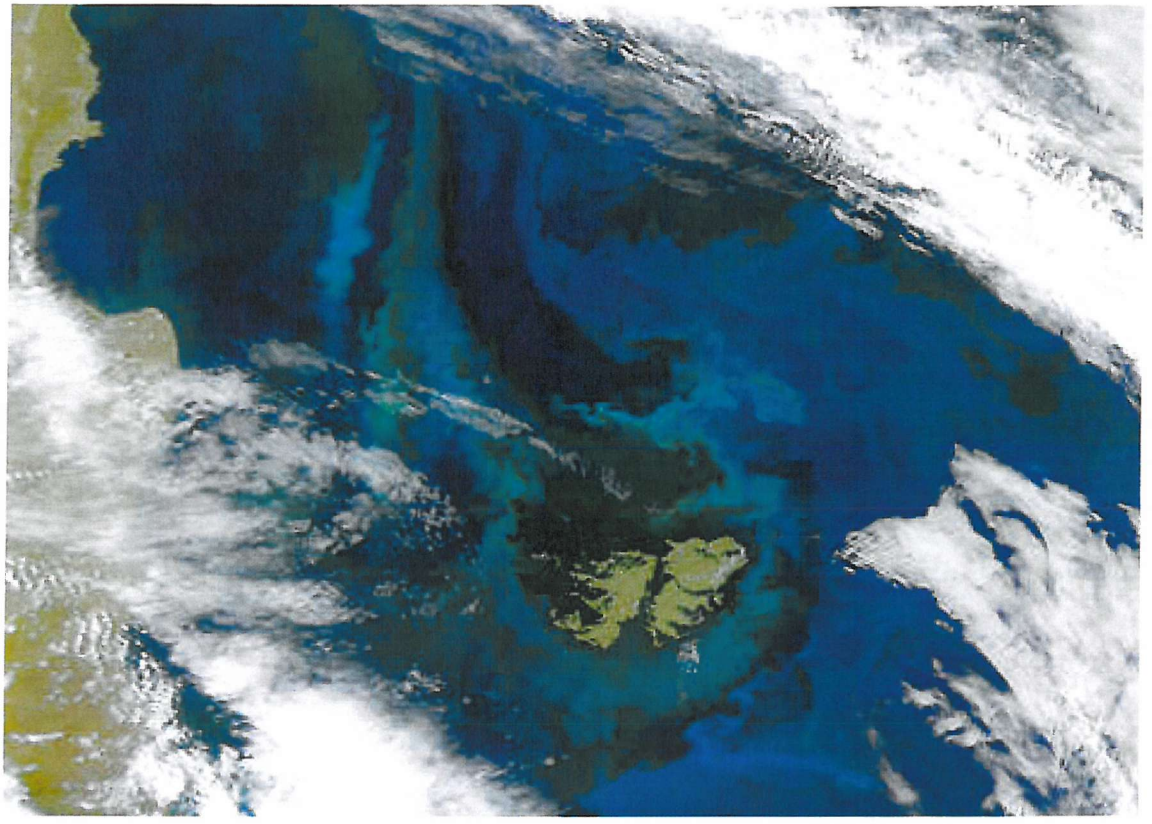

Figure 1.1: A true colour SeaWiFS view of the Falkland Islands, 19th December 1999. A Coccolithophore (plankton) bloom is evident as bright blue patches on the dark blue ocean. The concentrated streaks or filaments are the structure which we are to investigate, and to explain how their size is dependent upon the local balance of physical processes (strain and mixing) and population growth.
The image is provided by the SeaWiFS project, NASA/ Goddard Space Flight Center, and ORBIMAGE.

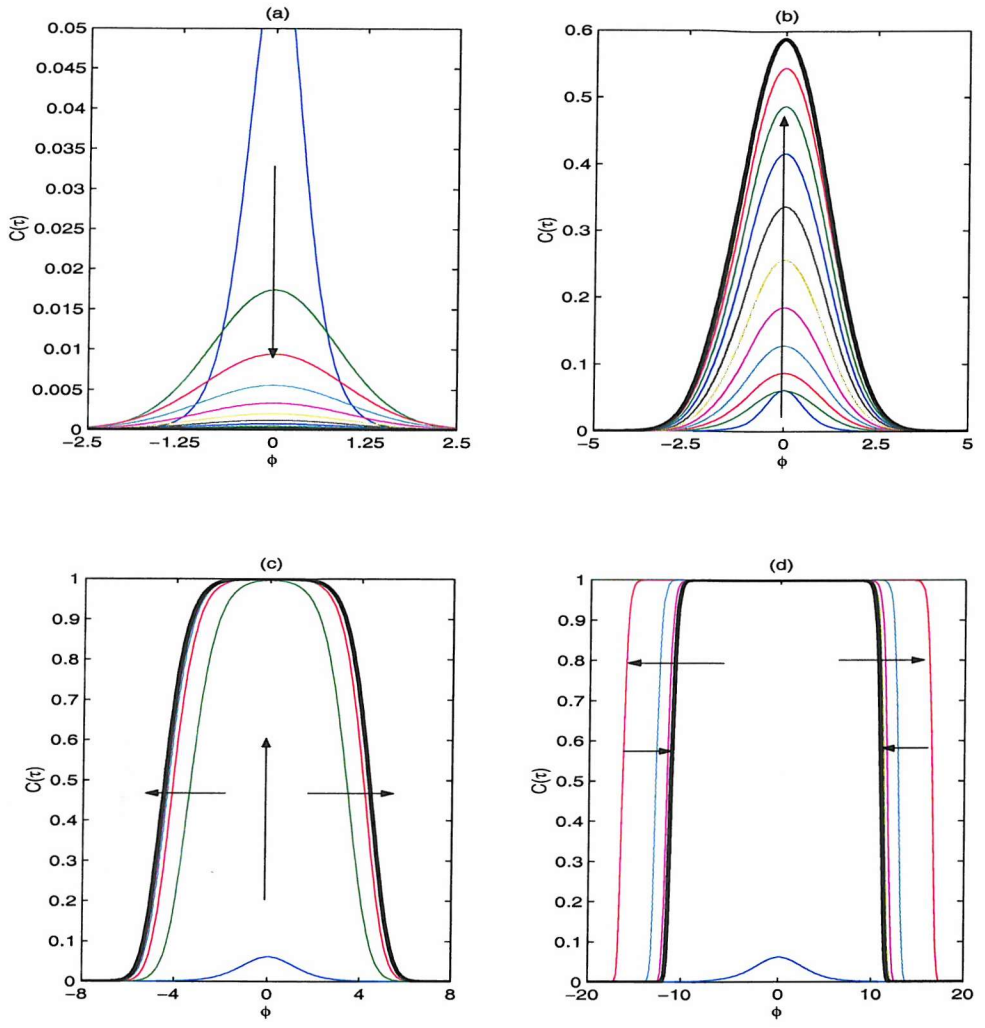

Figure 2.3.1: Evolution of a reactive tracer, in a convergent flow field, from an initial double hyperbolic tangent (DTANH) function. The arrows show direction of movement with time, τ. The asymptotic solution (solution at large time, hereafter denoted by A.S.) is shown in bold. Results for (a) β=0.01, the A.S. is a decaying Gaussian; (b) β=2, the A.S. has a steady state which is neither exactly Gaussian nor a DTANH shape; (c) β=10, a steady state A.S. is achieved with propagating fronts resulting in structure well described by a DTANH function; (d) β=50, again a propagating front solution but now fronts accelerate past their final position before subsequently converging upon A.S. of a DTANH shape.

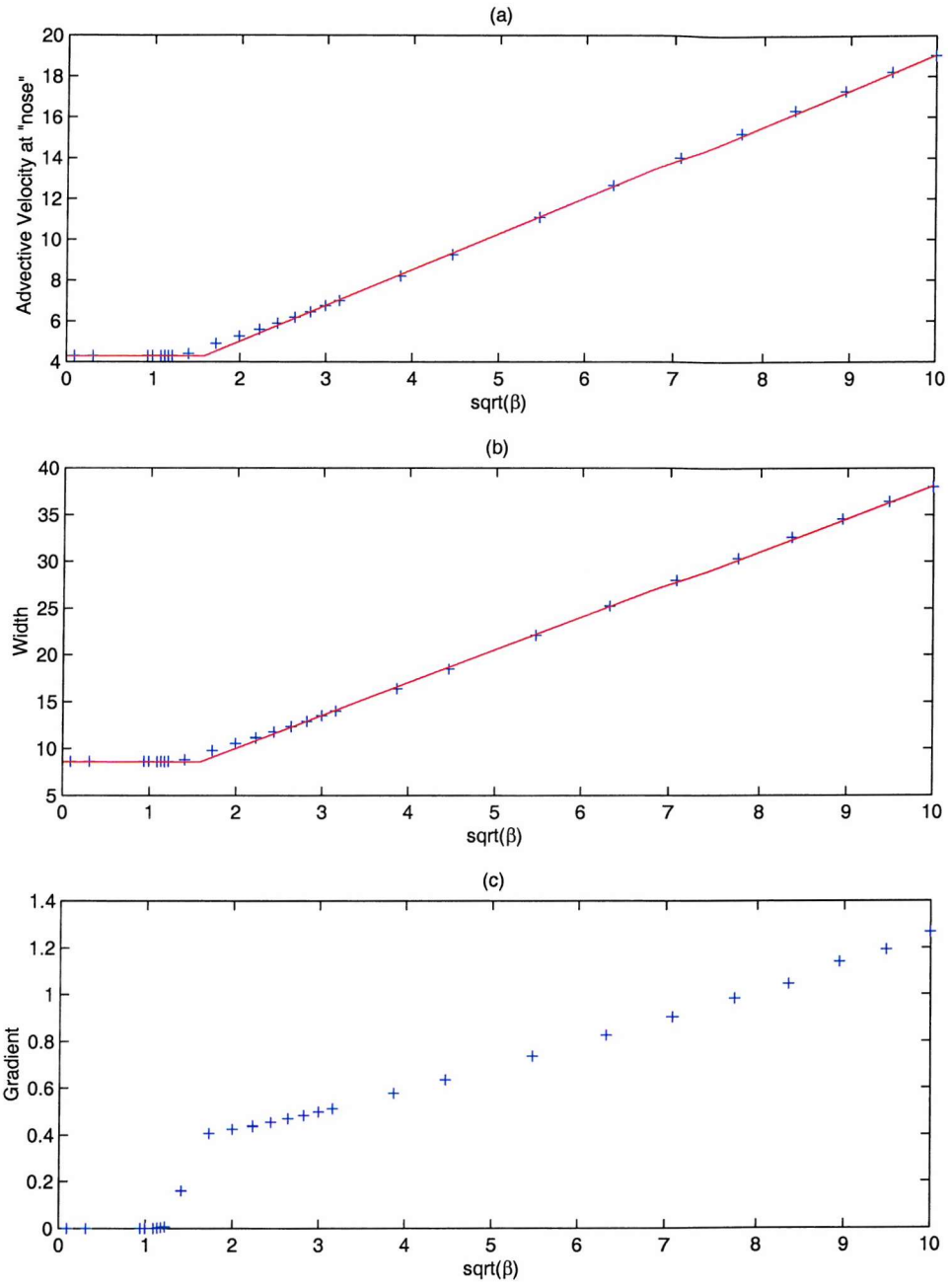

Figure 2.3.2: Asymptotic variation with growth rate of (a) Velocity of fronts, ~4.3*max (1,0.4[√β-1.6]+1), (b) Width, ~8.6*max (1,0.4[√β-1.6]+1), (c) Gradient of fronts. The solid lines indicate the empirically derived relationship describing asymptotic frontal velocity and width.

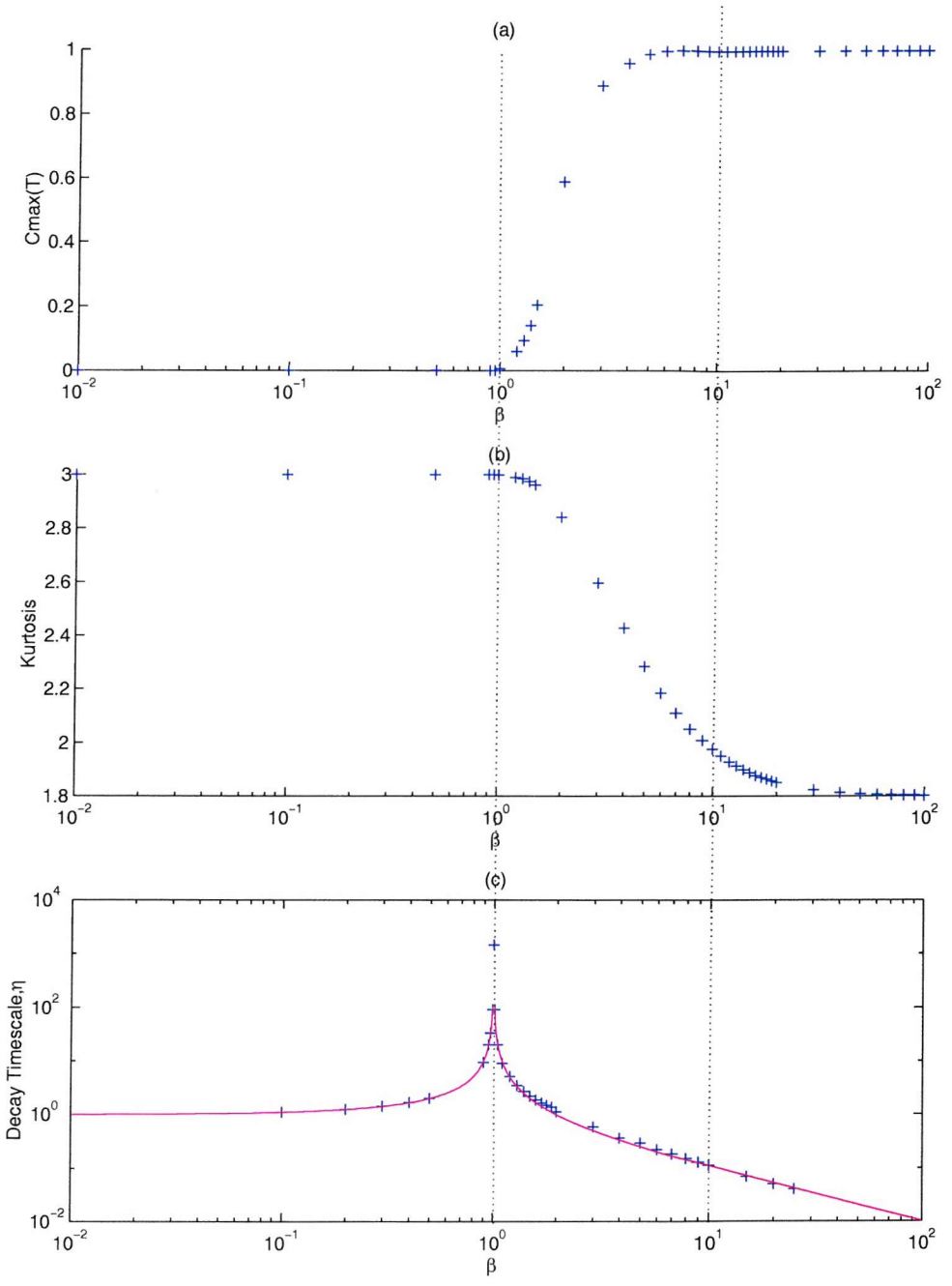

Figure 2.3.3: (a) Variation of maximum asymptotic tracer concentration, Cmax (T), with parameter value, (b) Kurtosis, Gaussian=3, propagating front =1.8, (c) Variation of (concentration at centre of filament) decay timescale, η, with parameter value. Solid line indicates approximation $\eta = \frac{1}{|\beta - 1|}$.

Note log scale. The dotted lines across all plots distinguish between geometric regimes as described in the text.

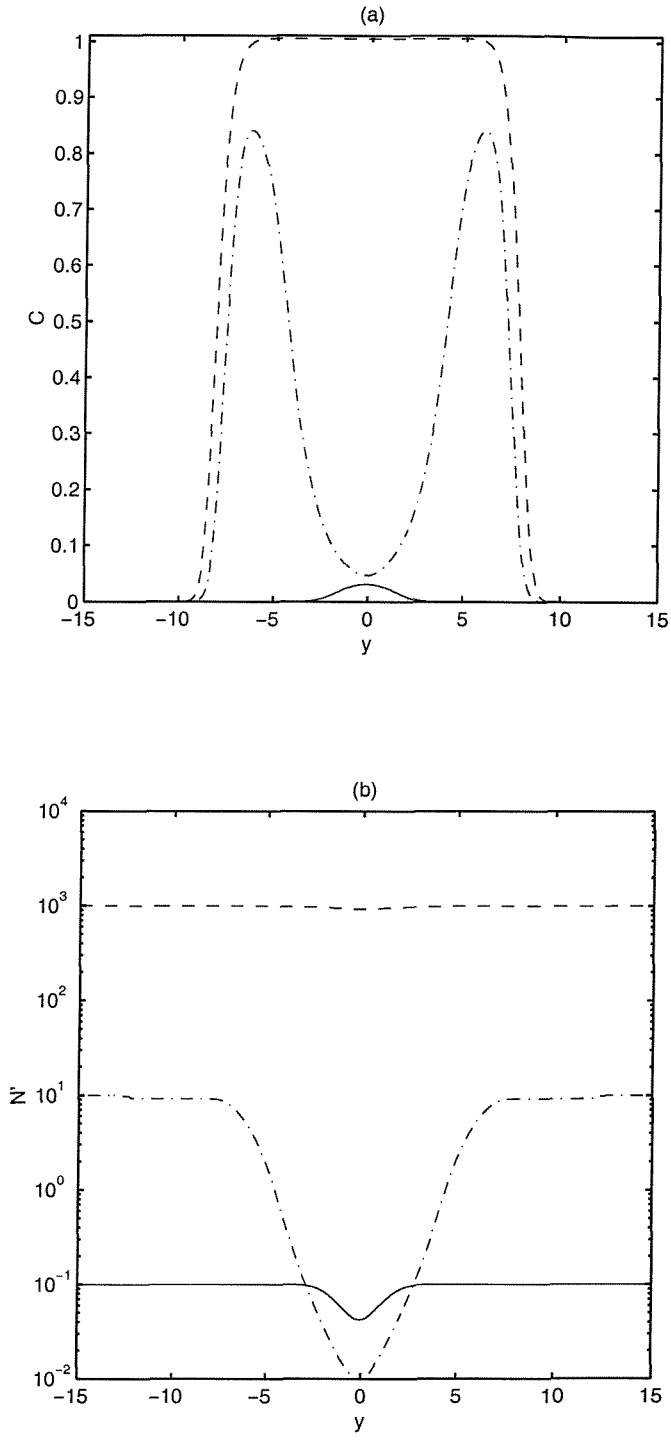

Figure 3.3.1: Asymptotic reactive tracer profile of (a) phytoplankton concentration, P, (b) nutrient concentration, N'. β=30, N_0'=0.1(solid line), 10 (dashed-dot line), 1000 (dashed line). N_s=1. y is the non-dimensional length-scale. Domain centred on ϕ=0.

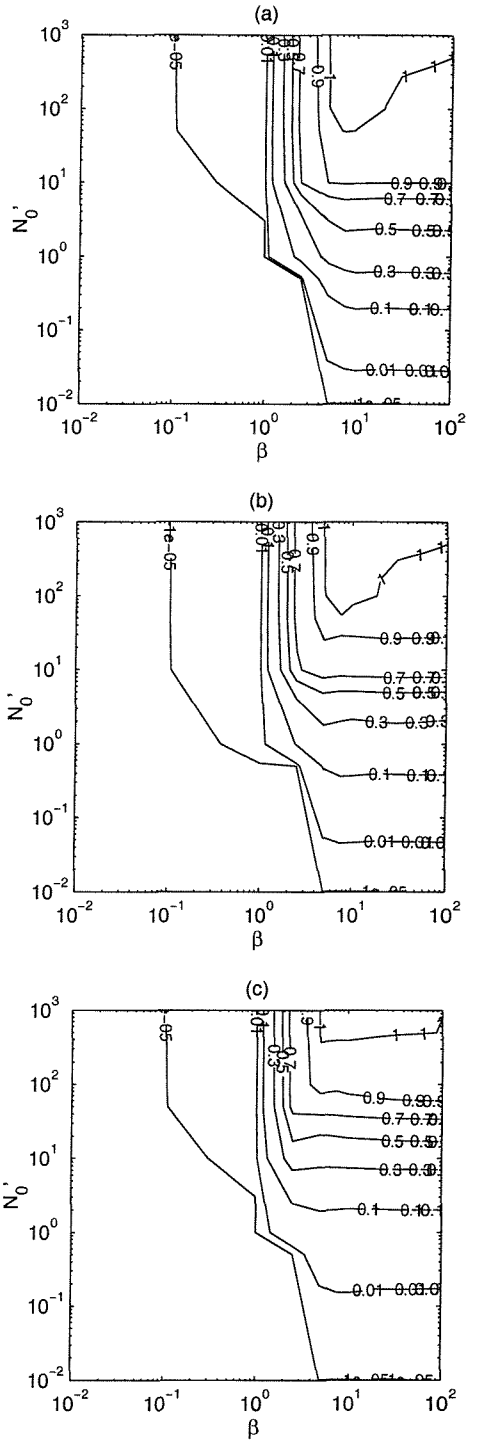

Figure 3.3.2: Variation of asymptotic maximum non-dimensional phytoplankton concentration across filament, C_{max}, as a function of non-dimensional nutrient concentration and maximum growth rate. Note: prescribed population limit is 1. β is the maximum growth rate, N_0' is the boundary nutrient concentration. (a) N_s=0.1, (b) N_s=1, (c) N_s=10.

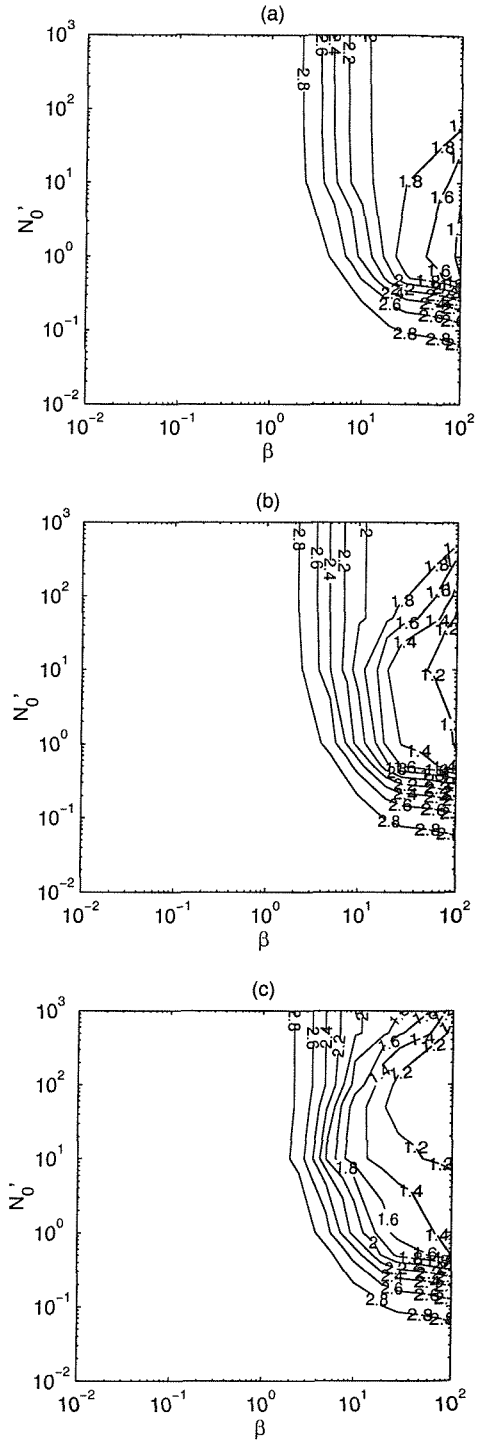

Figure 3.3.3: Variation of asymptotic Kurtosis. Gaussian = 3, Propagating front solution =1.8, double peak can be distinguished by a lower Kurtosis. β is the maximum growth rate, N_0' is the boundary nutrient concentration. (a) N_s=0.1, (b) N_s=1, (c) N_s=10.

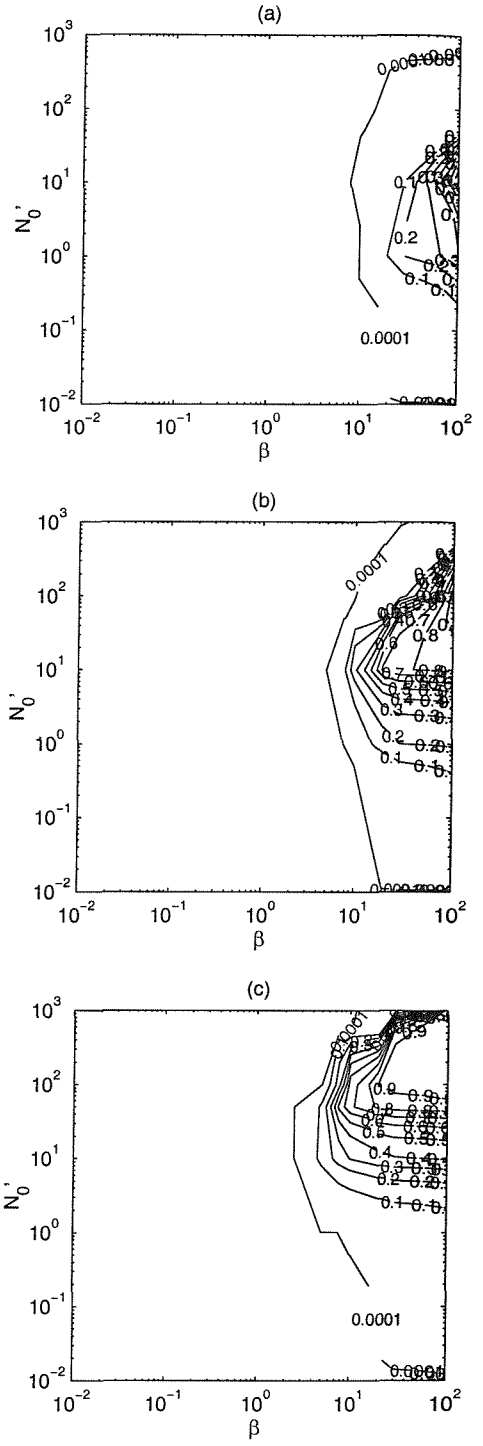

Figure 3.3.4: Height of double peak, measured by the difference between the maximum tracer concentration and that at the centre of the domain, C_{max}-C_{mid}. β is the maximum growth rate, N_0' is the boundary nutrient concentration. (a) N_s=0.1, (b) N_s=1, (c) N_s=10.

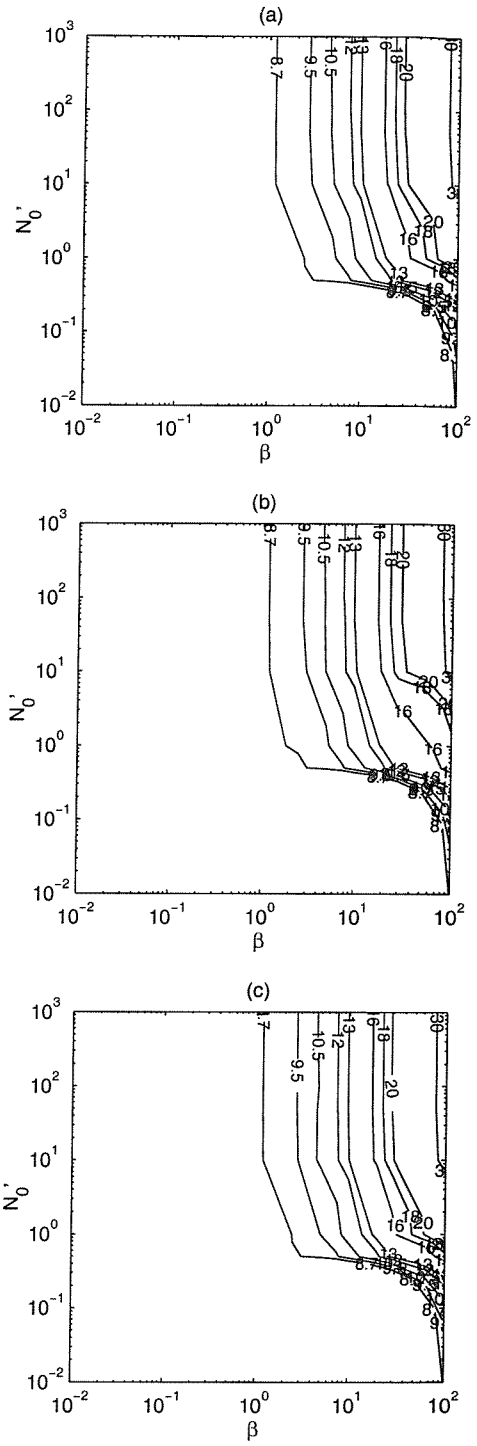

Figure 3.3.5: Variation of asymptotic width (non-dimensional). For comparison a Gaussian filament would have width ~8.6. β is the maximum growth rate, N_0' is the boundary nutrient concentration. (a) N_s=0.1, (b) N_s=1, (c) N_s=10.

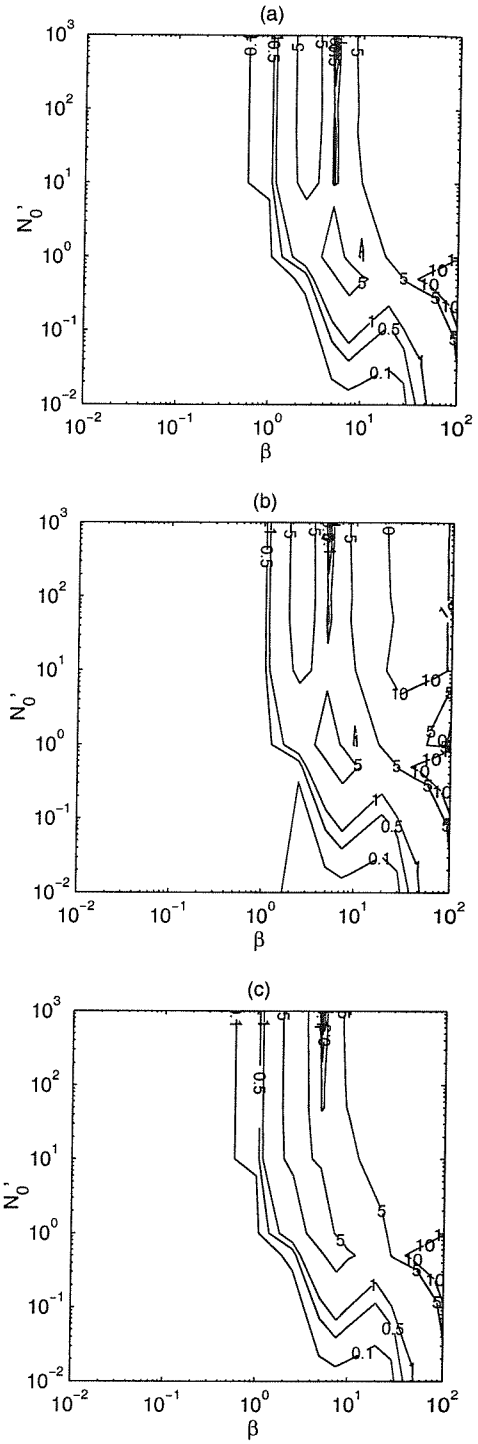

Figure 3.3.6: Percentage difference between actual and predicted (non-dimensional) widths. β is the maximum growth rate, N_0' is the boundary nutrient concentration. (a) N_s=0.1, (b) N_s=1, (c) N_s=10.

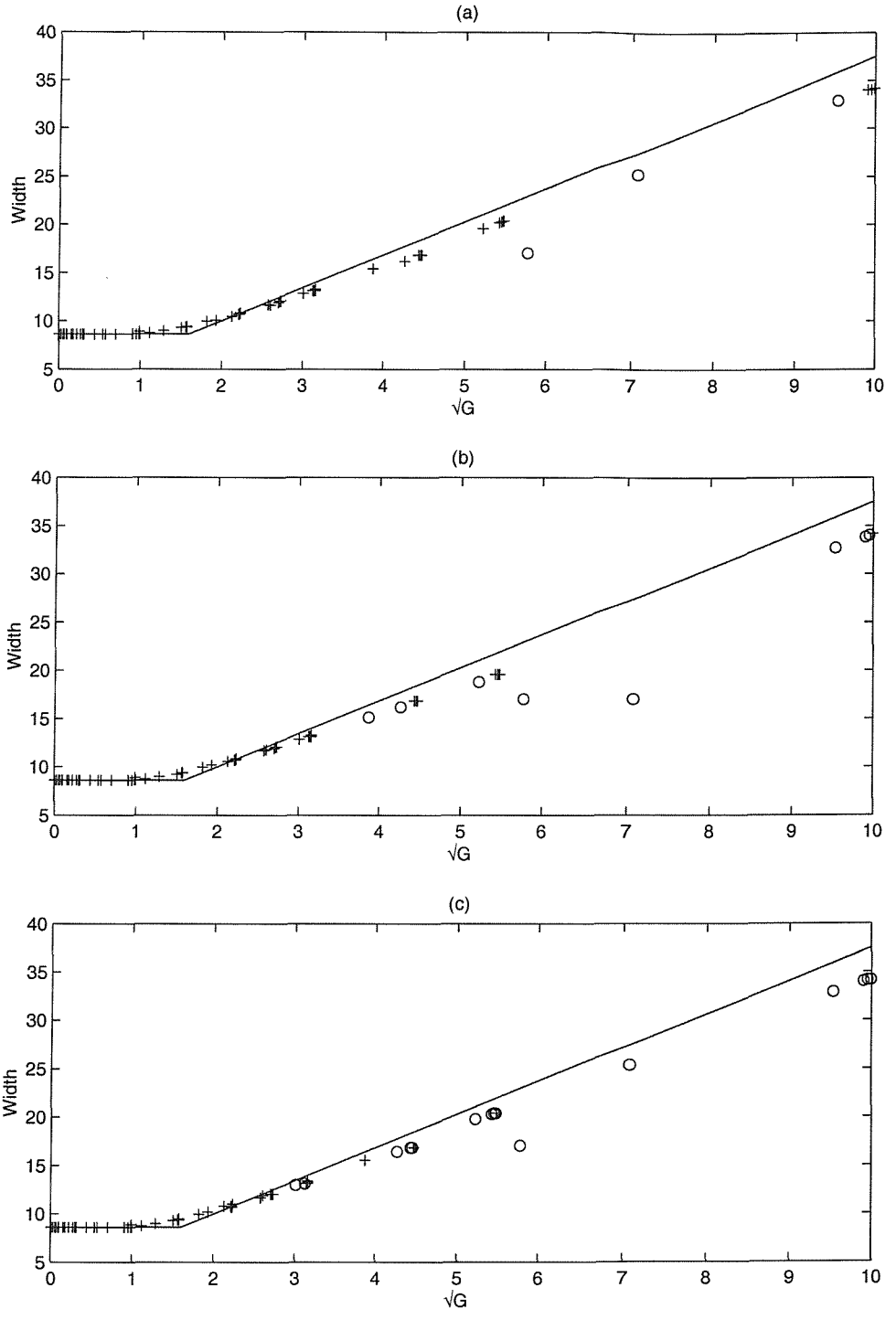

Figure 3.3.7: Variation of asymptotic width with $\sqrt{G}$, where $G=\beta N^*/(N^*+1)$ and N^* is the mean nutrient concentration across the tracer patch width. Solid line indicates the theoretical fit $W=8.6*\max(1,0.4(\sqrt{G}-1.6)+1)$. Results for (a) $N_s=0.1$, (b) $N_s=1$, (c) $N_s=10$. Markers distinguish height of the double peak (d.p.). '+': d.p.<25% of maximum height, 'o': d.p.>25% of maximum height.

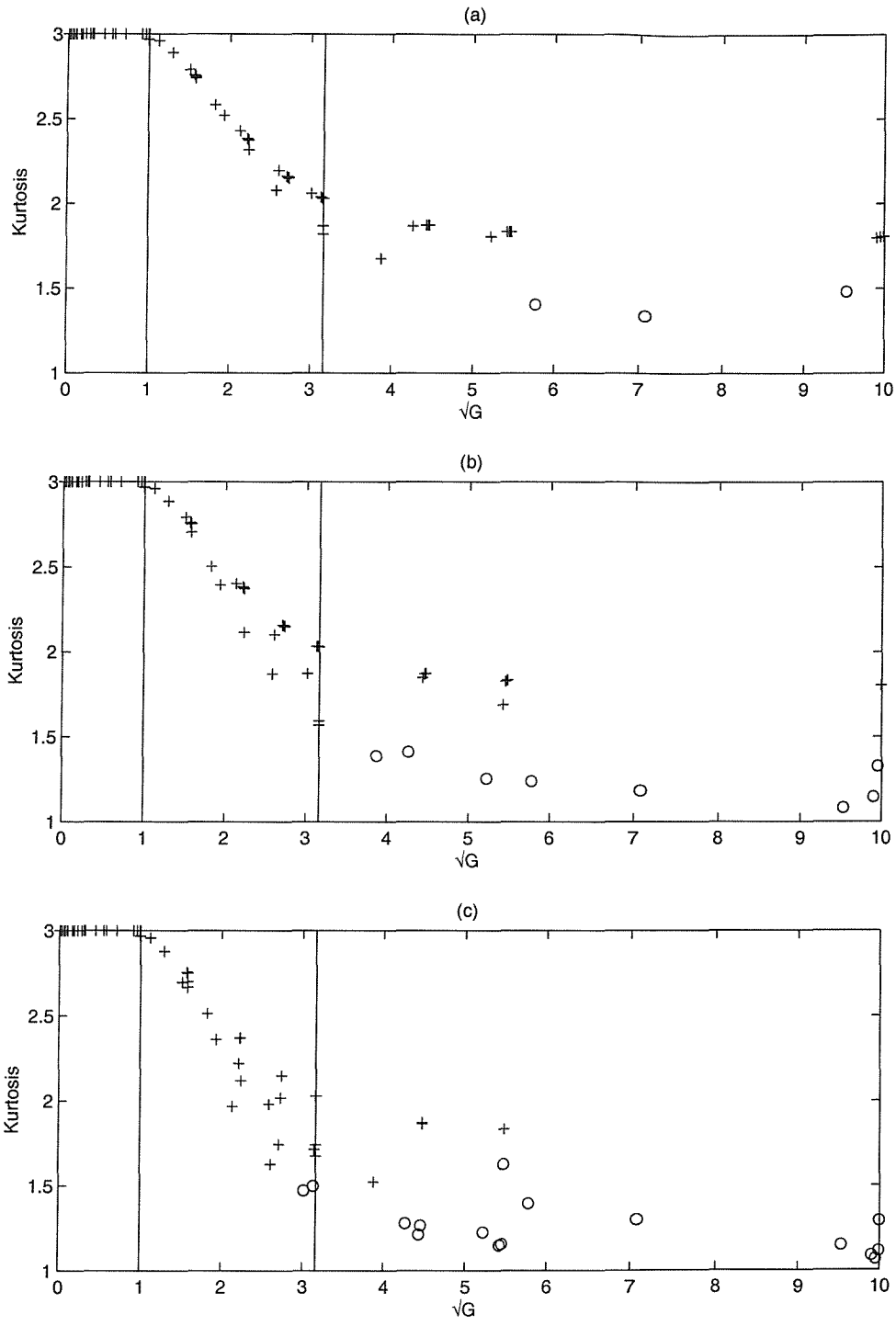

Figure 3.3.8: Variation of asymptotic Kurtosis with $\sqrt{G}$, where $G=\beta N^*/(N^*+1)$ and N^* is the mean nutrient concentration across the tracer patch width. Dotted lines indicate the expected separation between geometric regimes with $\sqrt{G}$. Results for (a) $N_s=0.1$, (b) $N_s=1$, (c) $N_s=10$. Markers distinguish height of the double peak (d.p.). '+': d.p.<25% of maximum height, 'o': d.p.>25% of maximum height.

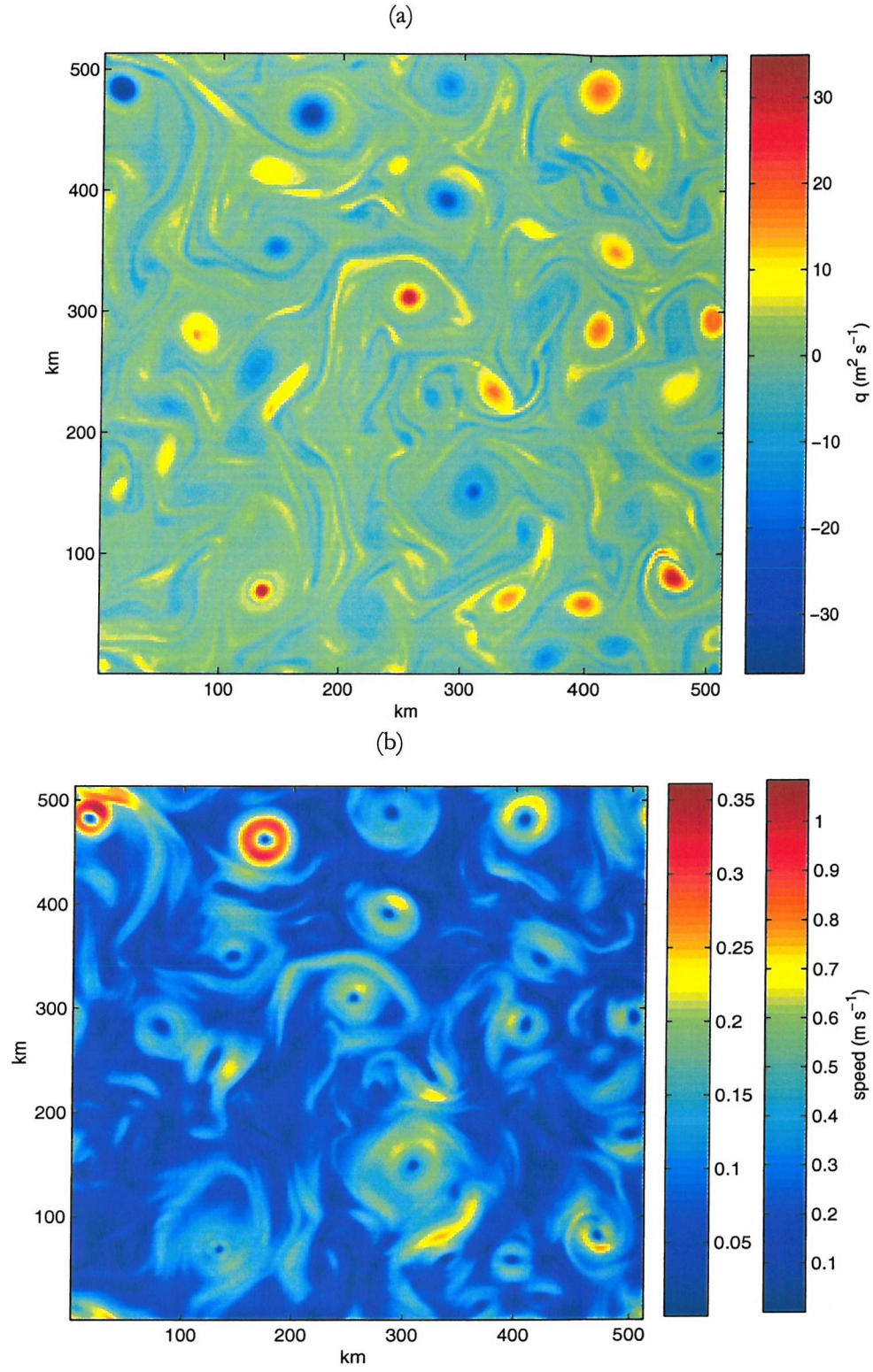

Figure 4.2.1: (a) Initial potential vorticity field. (b) field indicating initial speed of flow. The two scales in (b)relate to the different biological scales used for the tracer and ecological model investigations (see chapter 4, section 4.2). Lower (left-hand) scale is for individual tracer scaling, SC=5.5, higher (right hand)scale for NPZD ecological model, SC=1.83. The axes are marked in kilometres.

A

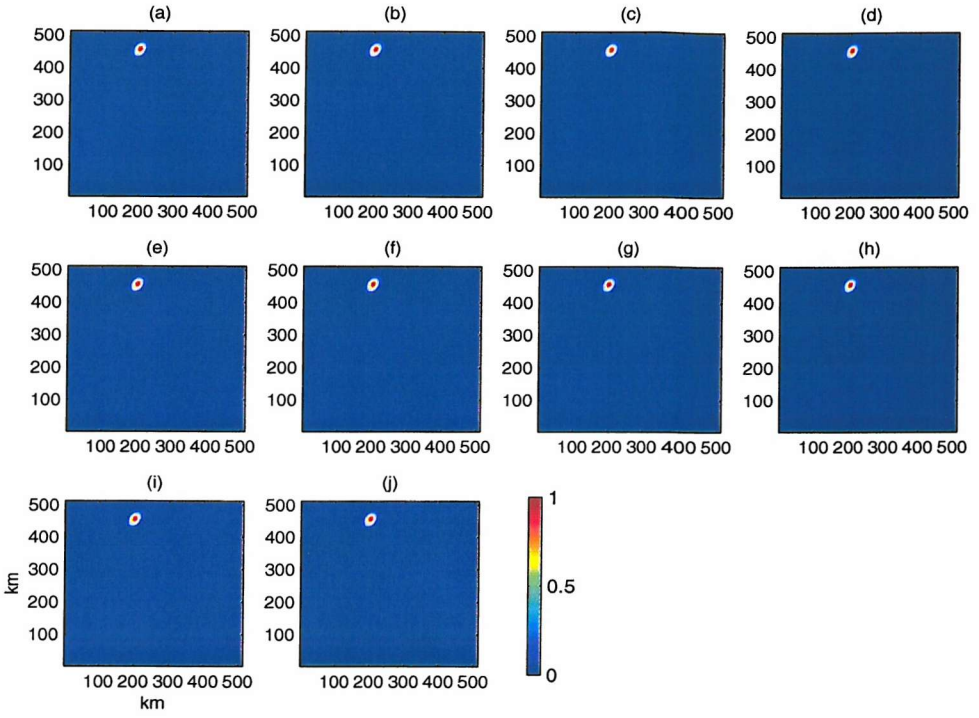

B

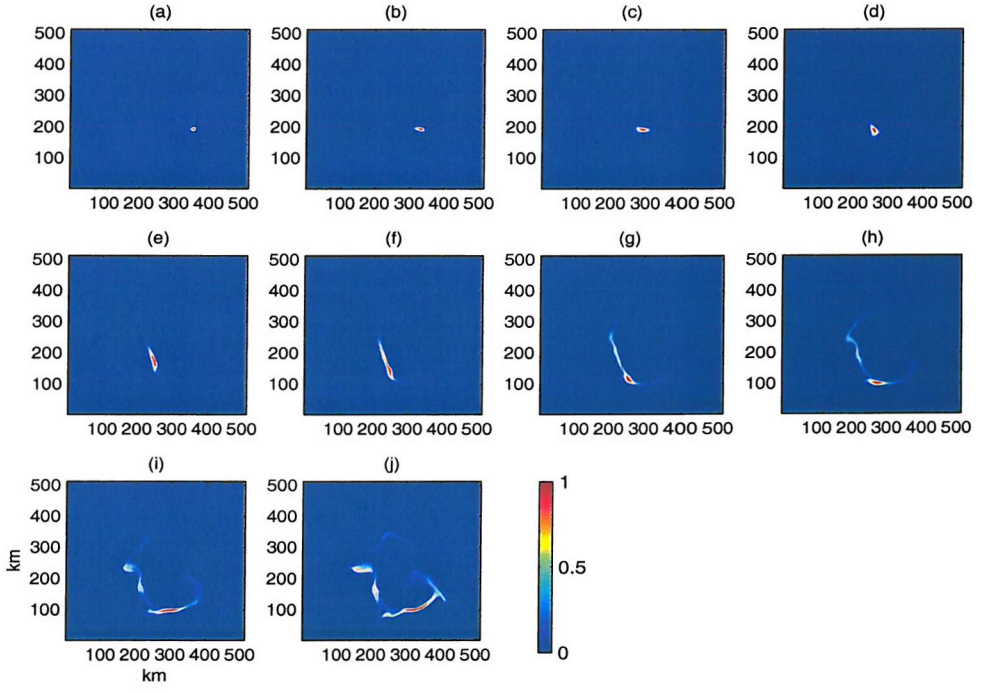

Figure 4.3.1: Instantaneous image of inert tracer field for tracers initialised within an eddy (A), and in a high strain region (B), on days (a) 3,(b) 6, (c) 9, (d) 12, (e) 15, (f) 18, (g) 21, (h) 24, (i) 27, (j) 30. Axes are marked in kilometres. The colour bar refers to normalised (with respect to maximum at that time) tracer concentration.

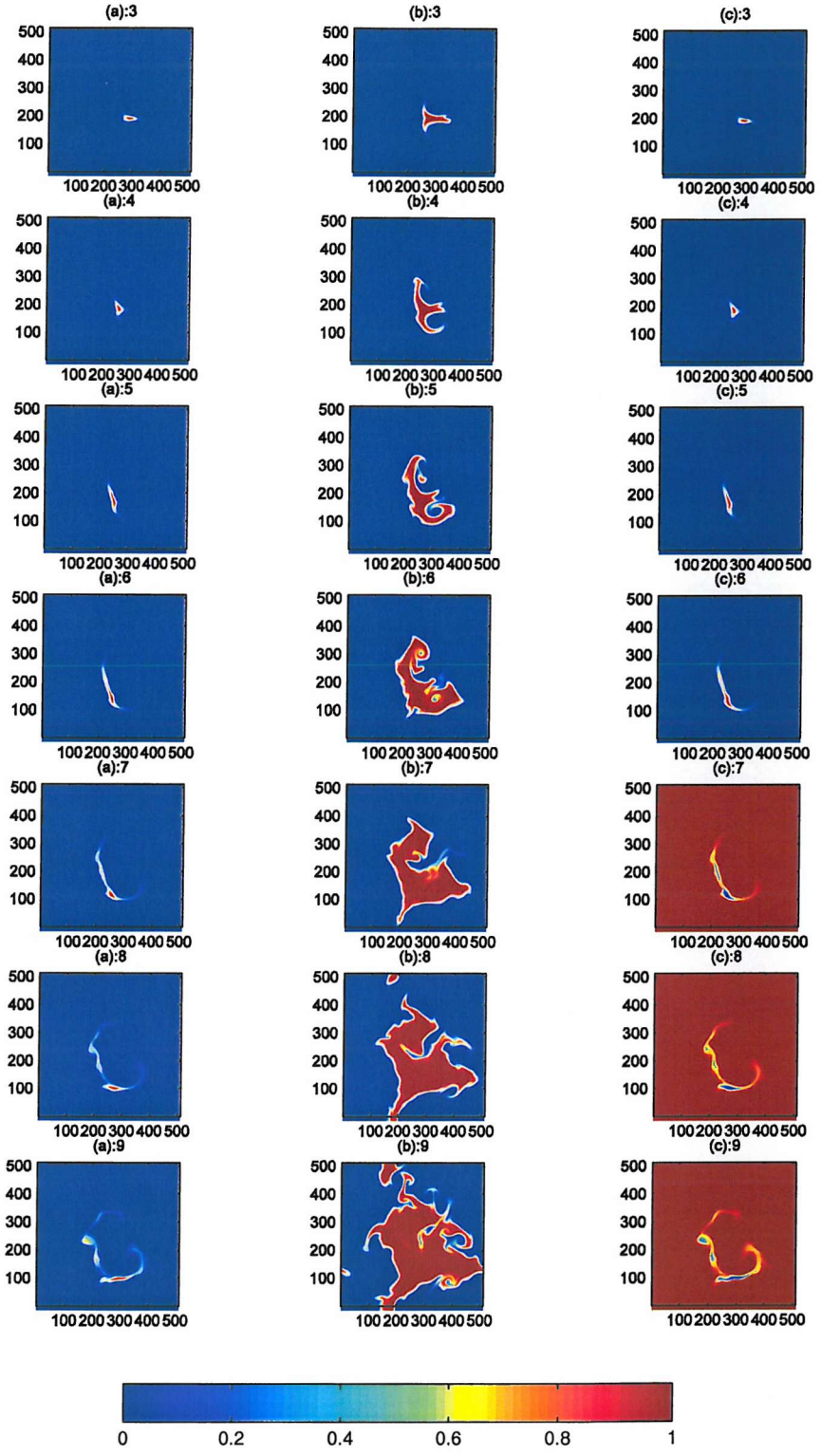

Figure 4.3.2: Images of evolution of (a) passive tracer, (b) logistic tracer μ=1.0 d^{-1}, (c) Phytoplankton compartment of NPZD ecosystem model. The applied diffusivity is 35.4 m^2s^{-1} for the inert and logistic tracers, 107m^2s^{-1} for the NPZD tracers. These are equivalent in non-dimensional model units.

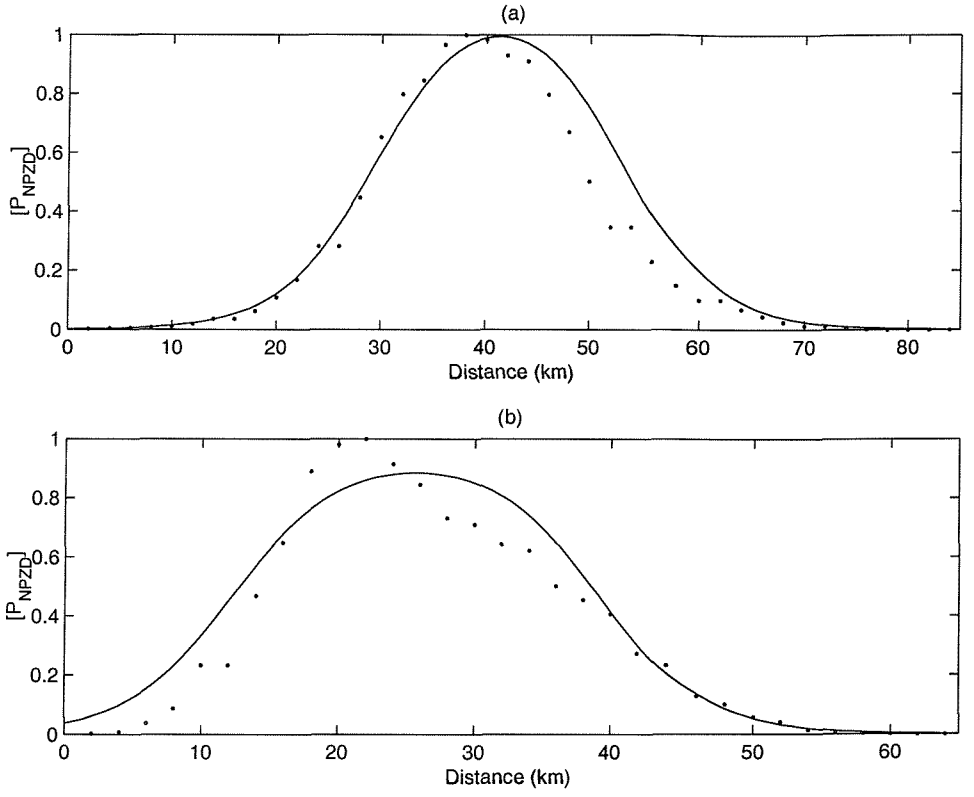

Figure 4.3.3: Example of the concentration from cuts across the phytoplankton filament (dots) and "best" fitted curve (solid line). Concentrations are normalised with respect to maximum across the cut. (a) R^2=0.99, (b) R^2=0.92. Example for Biological regime (ii) (N_0=2 mMol N m^{-3}, ε=0.2 (mMol N m^{-3})$^{-2}$ d^{-1}) on day 8. The criterion for fitted curves to be used for calculation of effective diffusivity is R^2>0.95.

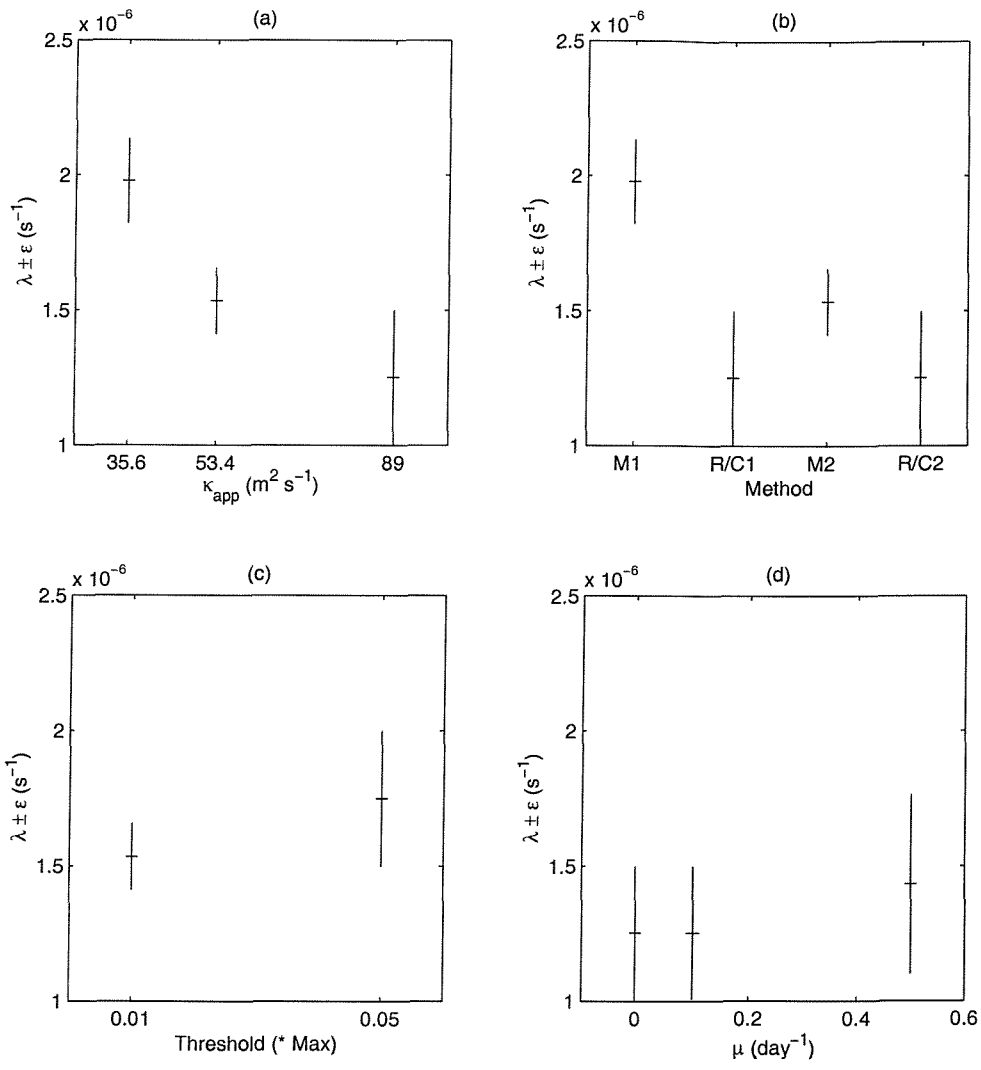

Figure 5.2.1: Strain measured from rate of change of filament length (a) maximum tracking, different applied diffusivity. (b) M=maximum tracking, R/C= rows and column tracking, for 1) κ_{app}=35.6 2) κ_{app}=53.4 ms^{-1}. (c) κ_{app}=53.4 ms^{-1}, maximum tracking, boundary threshold =0.01, 0.05 * maximum tracer concentration. (d) κ_{app}=53.4, row/column tracking, inert (μ=0) and reactive tracer, maximum growth rate = 0, 0.1, 0.5 day $^{-1}$.

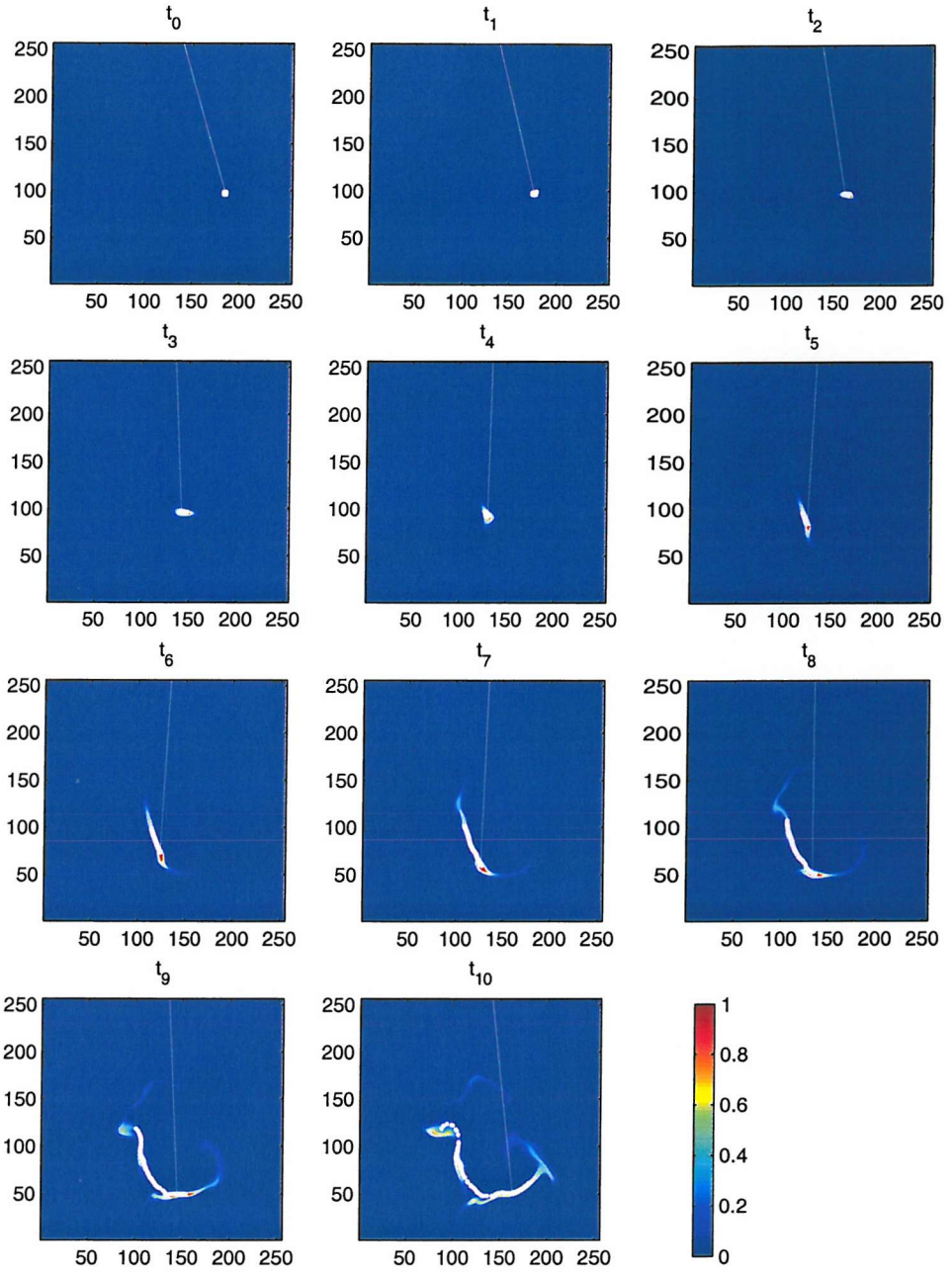

Figure 5.2.2: Tracer distribution overlain with position of drifters initialised within the tracer patch (white dots- they merge to form an apparent line due to their high density). The colour bar refers to normalised tracer concentration. Axes are in grid cells- 1 cell =2x2km, hence 512x512km domain size. Time interval between subplots is 3 days.

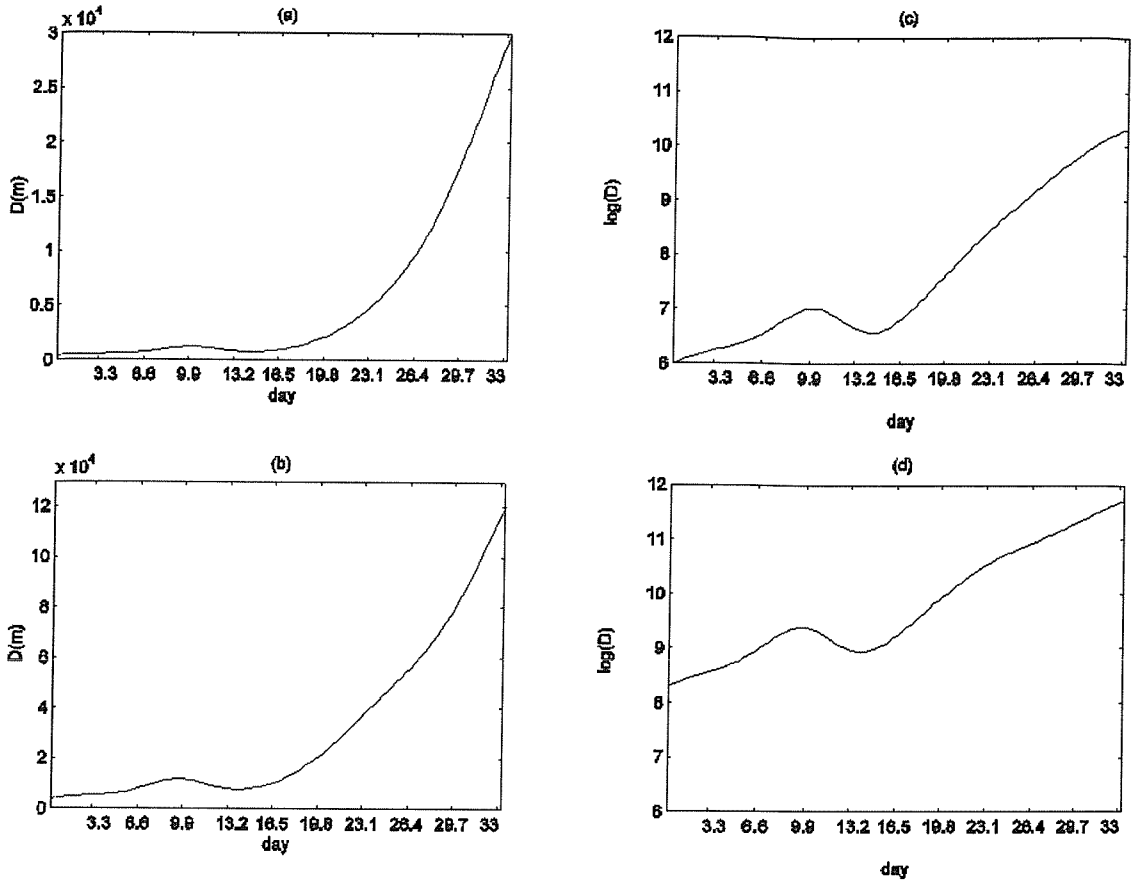

Figure 5.2.3: Mean separation in metres (D) of pairs of drifters initially separated by (a) 400m, (b) 4000m. Log of distance in metres between drifters initially at (c) 400m, (d) 4000m.

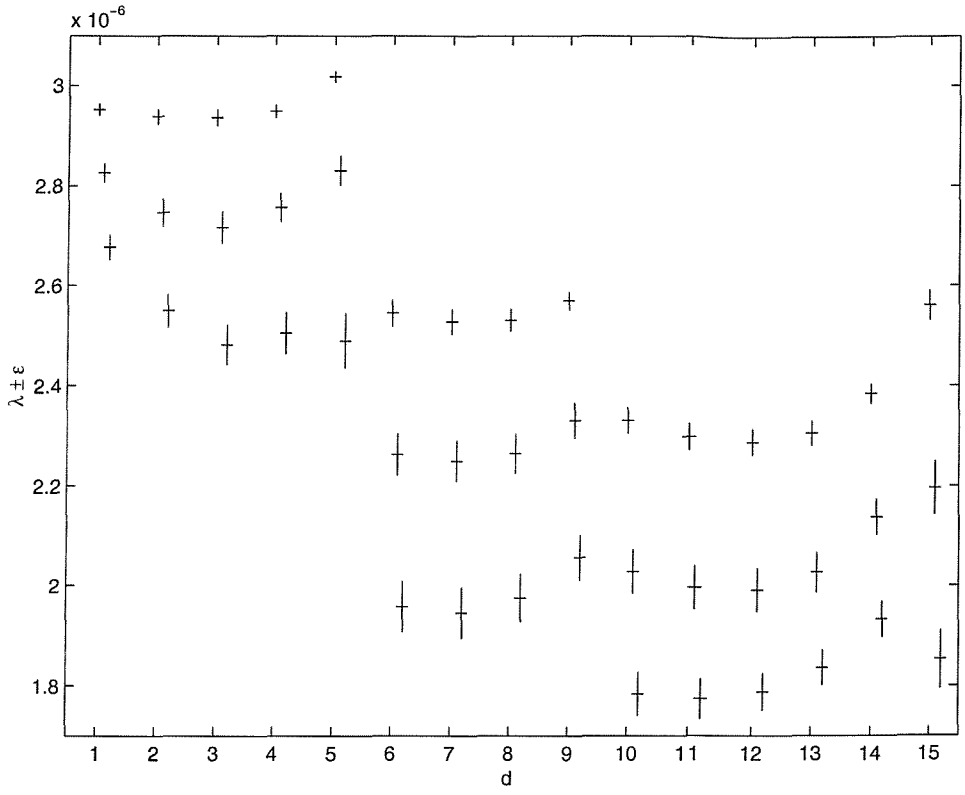

Figure 5.2.4: Mean ± standard deviation of strain rate calculated from rate of separation of drifters initially separated by (d)*400m. For each separation top bar refers to strain calculated over days 15-21, middle to strain over days 15-24, bottom to strain over days 15-27. In addition to the natural decrease in strain rate calculated over an increasing period the points are staggered around the separation to which they refer, (1:15)*400m covers to range of 400m to 6000m in 400m intervals.

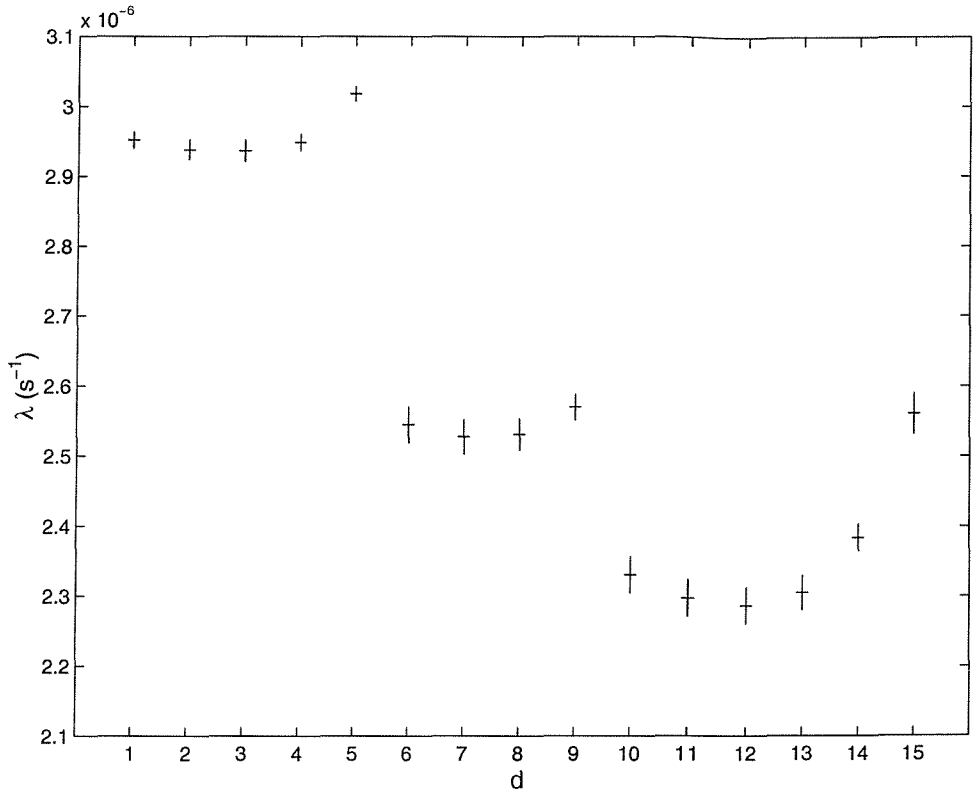

Figure 5.2.5: Mean ± standard deviation of strain rate (s^{-1}) for drifters initially at (d)*400m separation. Calculated over days 15-21. Repeated from previous figure for clarity as this is the period for which we considered the separation of drifters to be most dominated by strain.

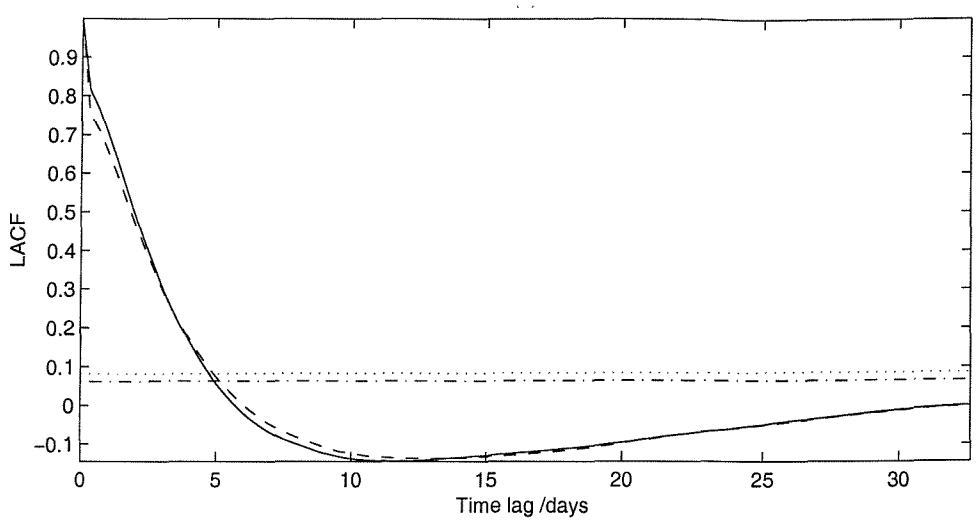

Figure 5.2.6: Lagrangian autocorrelation function/ integral time scale of field. Solid line indicated correlation function for the x component of velocity, dashed line indicates the correlation function for the y component of velocity. Dotted line is the 99% confidence boundary, dashed dot line is the 95% confidence.

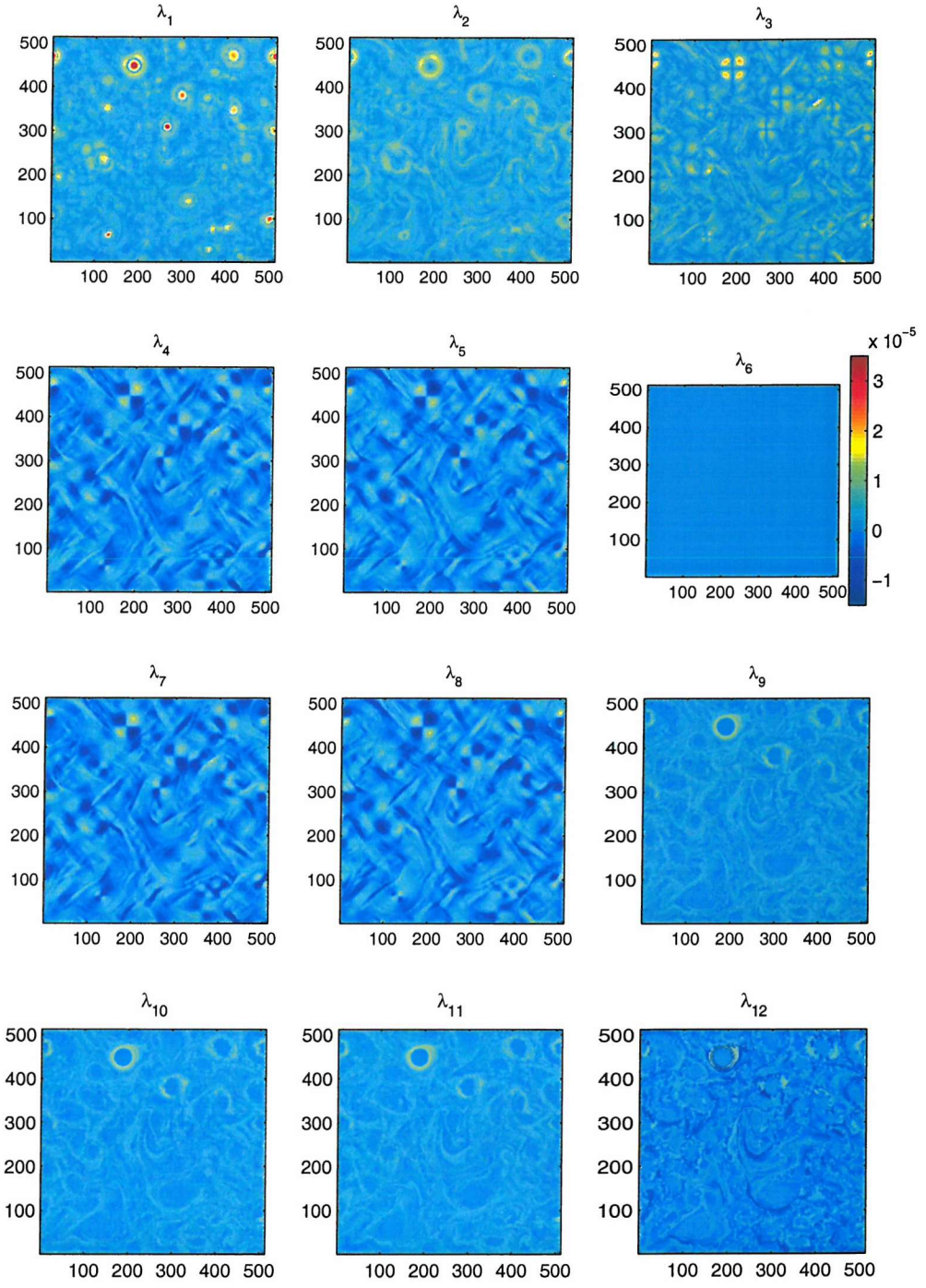

Figure 5.3.1: Image of strain field on day 15 for methods 1-12. See table 5.1 for explanation of methods. Colour bar indicates strain rate (s^{-1}). Axes are marked in kilometres.

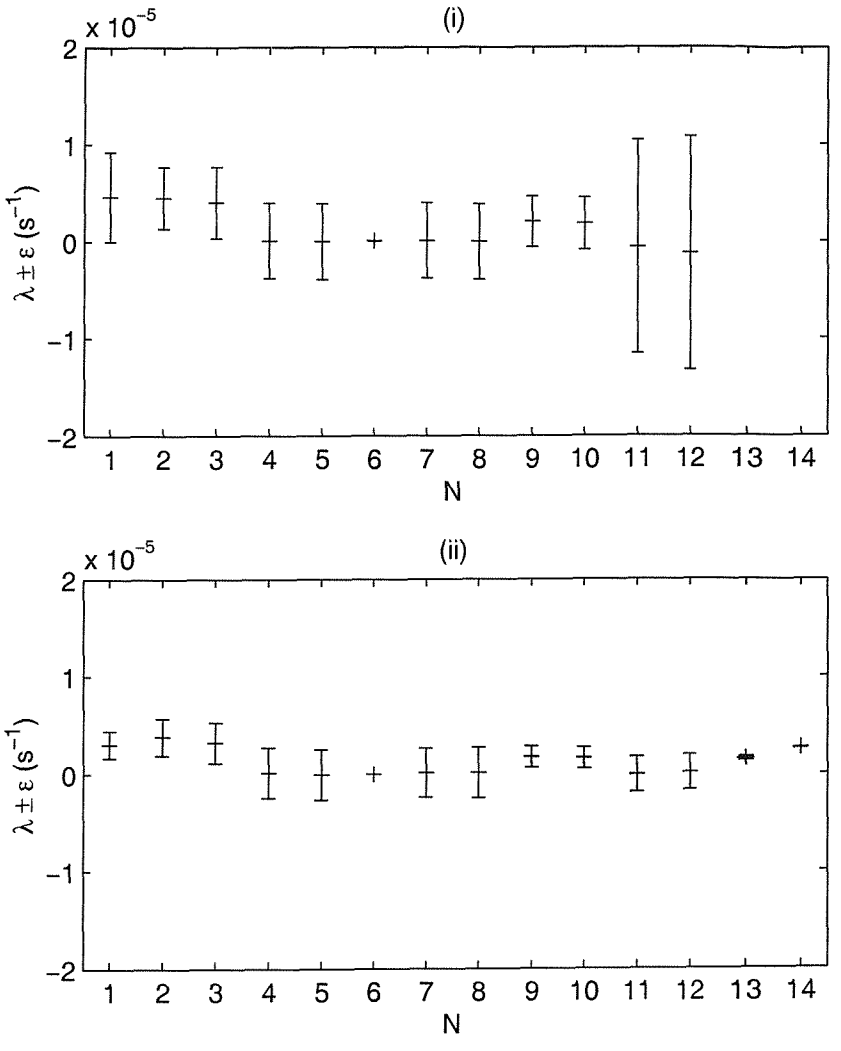

Figure 5.3.2: Mean ± one standard deviation of strain rate (i) over entire field, for days 9-24, for methods λ_N, N=1:12, (ii) within filament over days 15-21 for methods λ_N, N=1:14. See table 5.1 for explanation of methods.

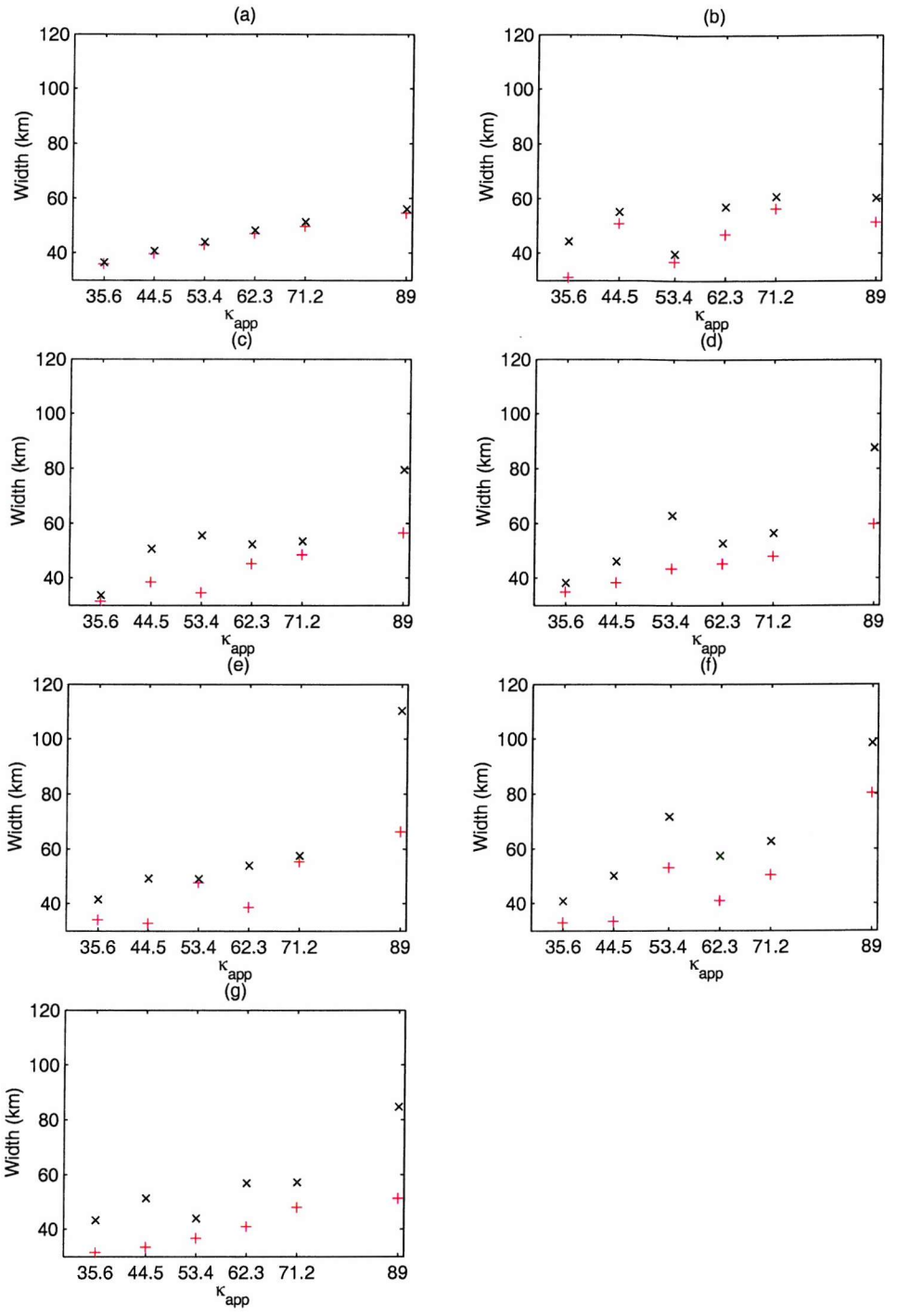

Figure 6.3.1: Variation of minimum (red plus) and modal (black cross) inert tracer filament width with applied effective diffusivity (m^2s^{-1}) on: (a) day 9, (b) day12, (c) day 15, (d) day 18, (e) day 21, (f) day 24, (g) average over all above days.

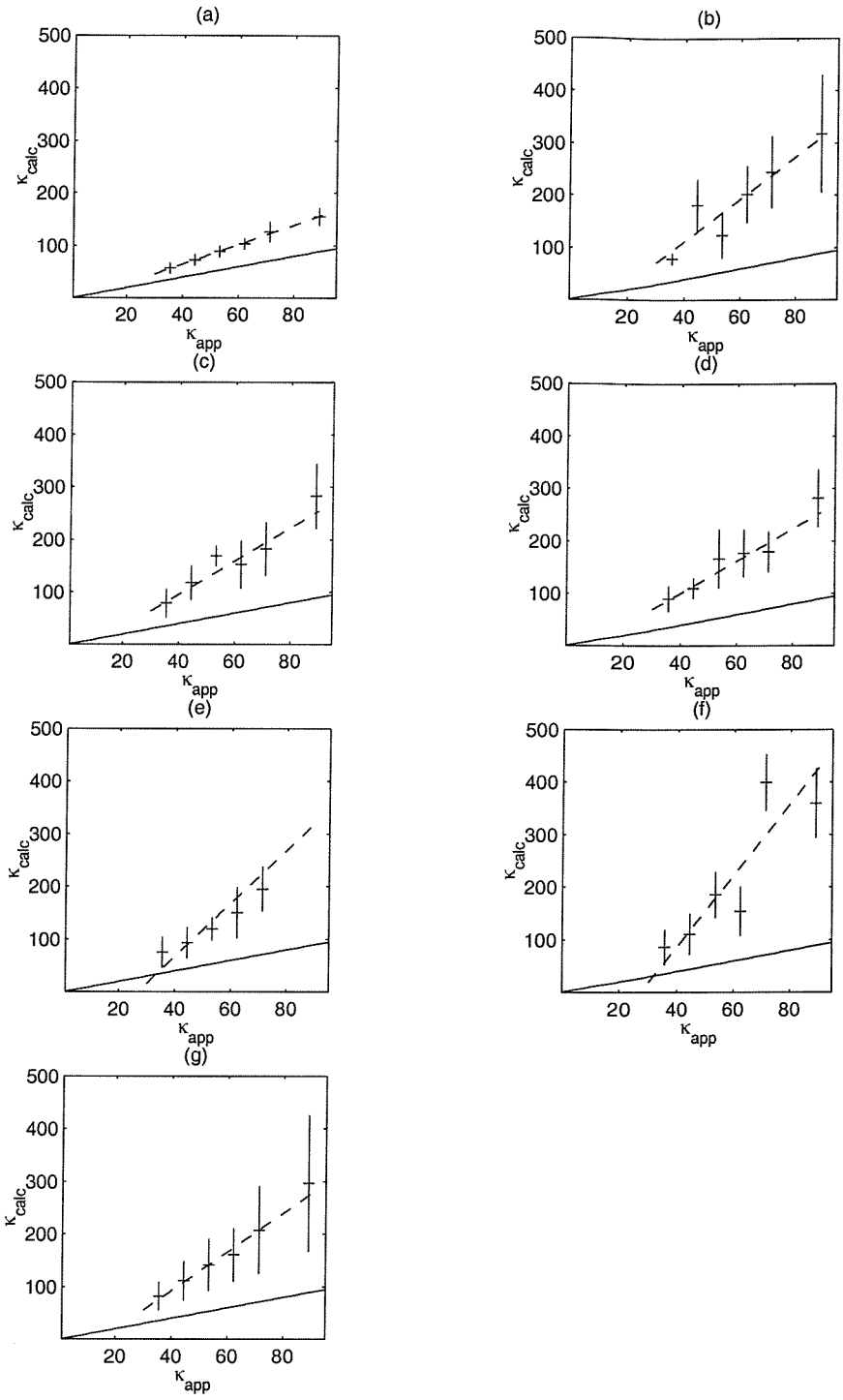

Figure 6.3.2: Plot of calculate versus applied effective diffusivity for inert tracer. Error bars showing mean plus and minus one standard deviation. Solid line indicates a 1:1 fit (expected from theory), dashed line indicates linear regression. Distribution on (a) ~day 9, (b) day12, (c) day 15, (d) day 18, (e) day 21, (f) day 24, (g) average over all above days.

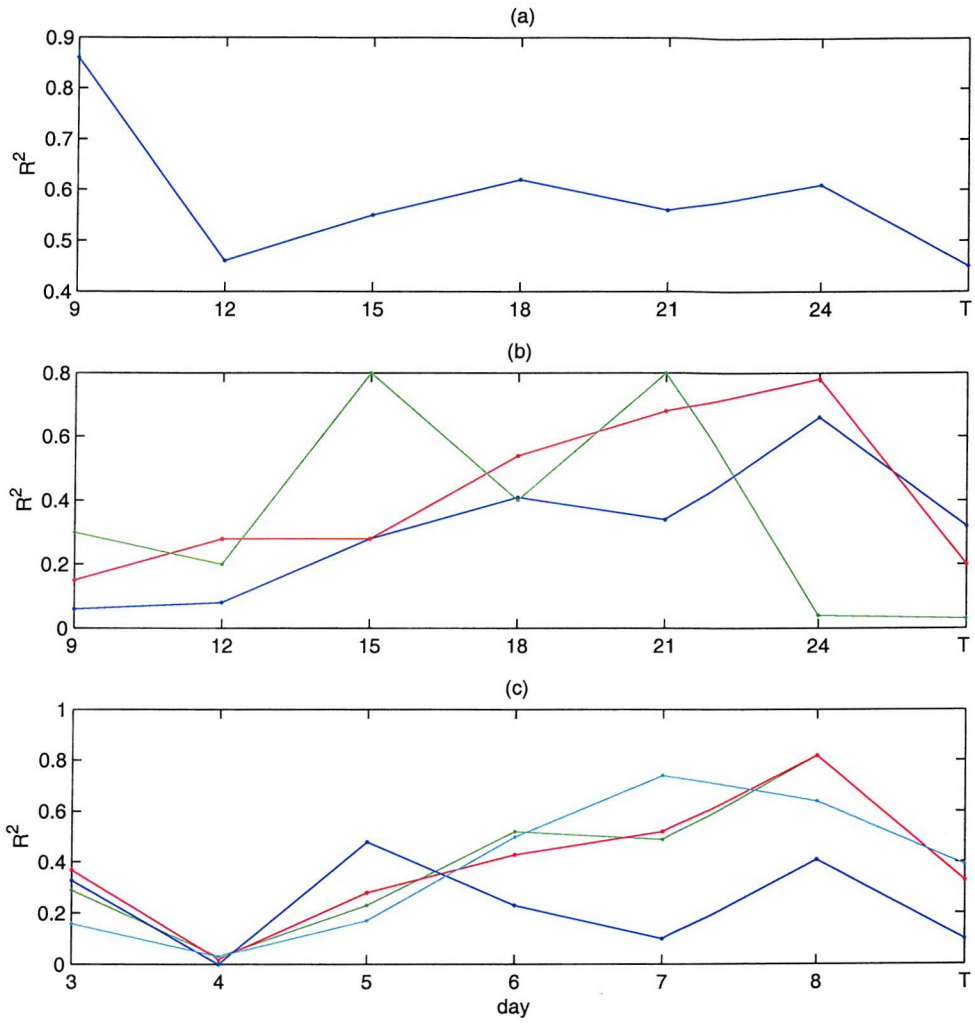

Figure 6.3.3: R^2 value for calculated effective diffusivity to the linear least squares regression of calculated to applied effective diffusivity. R^2 can be taken as an indication of the percentage variability in the data explained by the fit, R^2~0.8 means 80% of the variability is explained by the linear regression. Values for (a) inert tracer; (b) logistically growing tracer: blue: μ=0.1 d^{-1}; red: μ=0.5 d^{-1}; green: μ=1.0 d^{-1}; (c) NPZD model phytoplankton tracer: blue: B.R.(i); red: B.R.(ii); green: B.R.(iii); light blue: B.R.(iv). The x-axis for each is marked in days, T indicating the values for a regression for all data over all preceding days. The different times for phytoplankton compared to the other tracers is due to the different time-scaling used, but times correspond to the same non-dimensional time period.

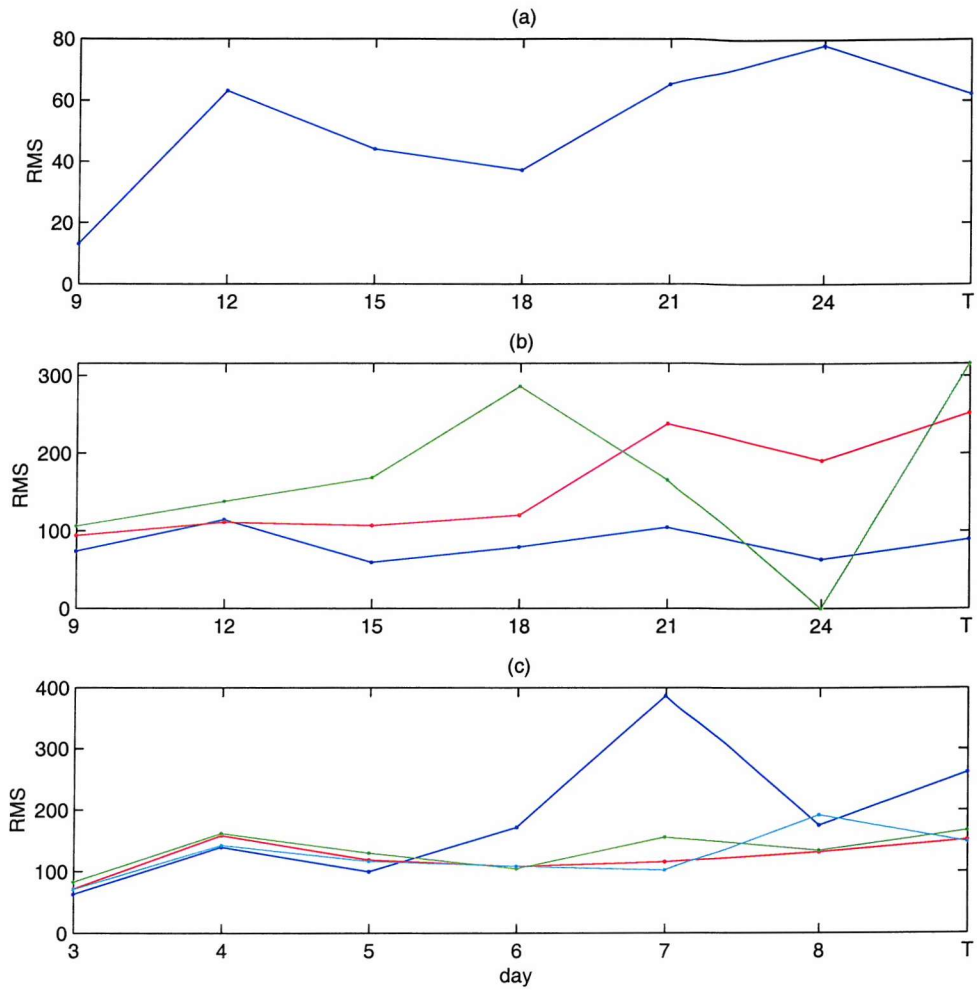

Figure 6.3.4: RMS (root, residual mean square) error (m^2s^{-1}) of calculated effective diffusivity to that predicted by the linear least squares fit of calculated to applied effective diffusivity for (a) inert tracer; (b) logistically growing tracer: blue: μ=0.1 d^{-1}; red: μ=0.5 d^{-1}; green: μ=1.0 d^{-1}; (c) NPZD phytoplankton tracer: blue: B.R.(i); red: B.R.(ii); green: B.R.(iii); light blue: B.R.(iv). The x-axis for each is marked in days, T indicating the values for a regression for all data over all preceding days. The different times for phytoplankton compared to the other tracers are due to the different time-scaling used, but times correspond to the same non-dimensional time period.

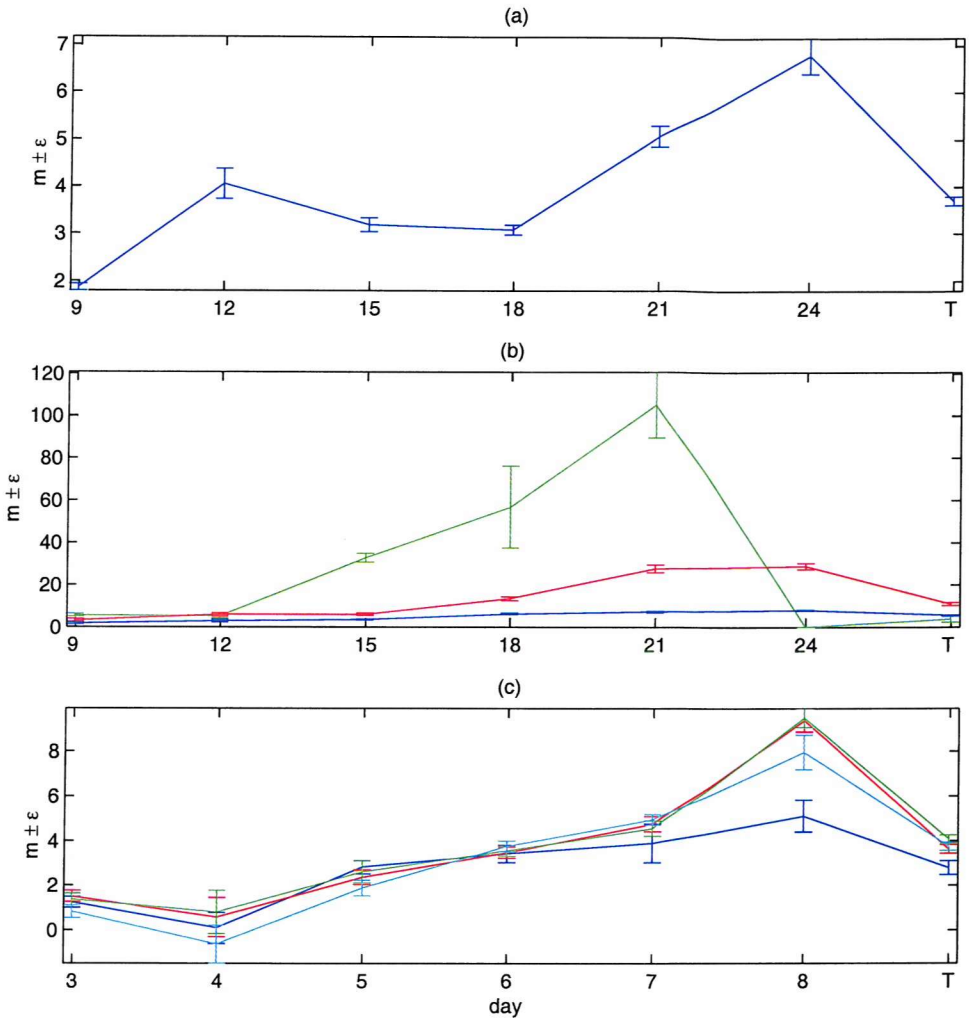

Figure 6.3.5: Gradient(m) plus/minus one standard deviation (ε) for the least squares linear fit of calculated to applied effective diffusivity for (a) inert tracer; (b) logistically growing tracer: blue: μ=0.1 d^{-1}; red: μ=0.5 d^{-1}; green: μ=1.0 d^{-1}; (c) NPZD phytoplankton tracer: blue: B.R.(i); red: B.R.(ii); green: B.R.(iii); light blue: B.R.(iv). The x-axis for each is marked in days, T indicating the values for a regression for all data over all preceding days. The different times for phytoplankton compared to the other tracers is due to the different time-scaling used, but times correspond to the same non-dimensional time period.

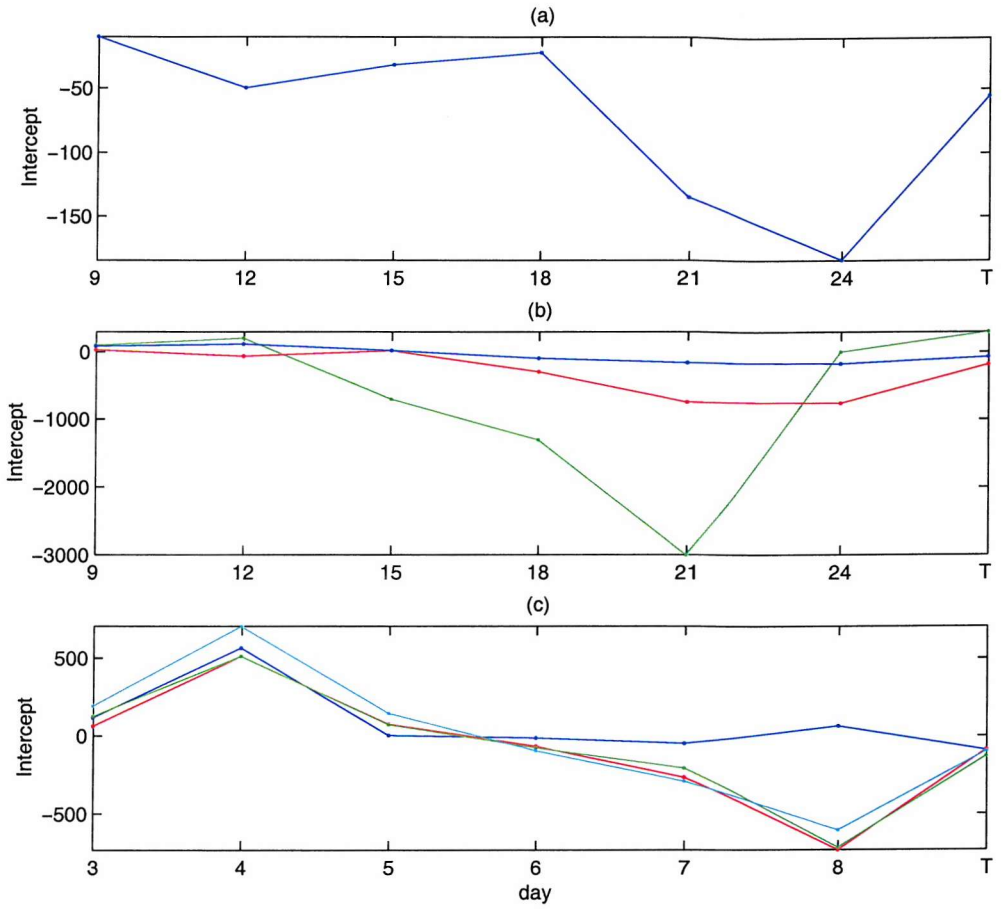

Figure 6.3.6: Intercept (m^2s^{-1}) for the least squares linear fit of calculated to applied effective diffusivity for (a) inert tracer; (b) logistically growing tracer: blue: μ=0.1 d^{-1}; red: μ=0.5 d^{-1}; green: μ=1.0 d^{-1}; (c) NPZD phytoplankton tracer: blue: B.R.(i); red: B.R.(ii); green: B.R.(iii); light blue: B.R.(iv). The x-axis for each is marked in days, T indicating the values for a regression for all data over all preceding days. The different times for phytoplankton compared to the other tracers is due to the different time-scaling used, but times correspond to the same non-dimensional time period.

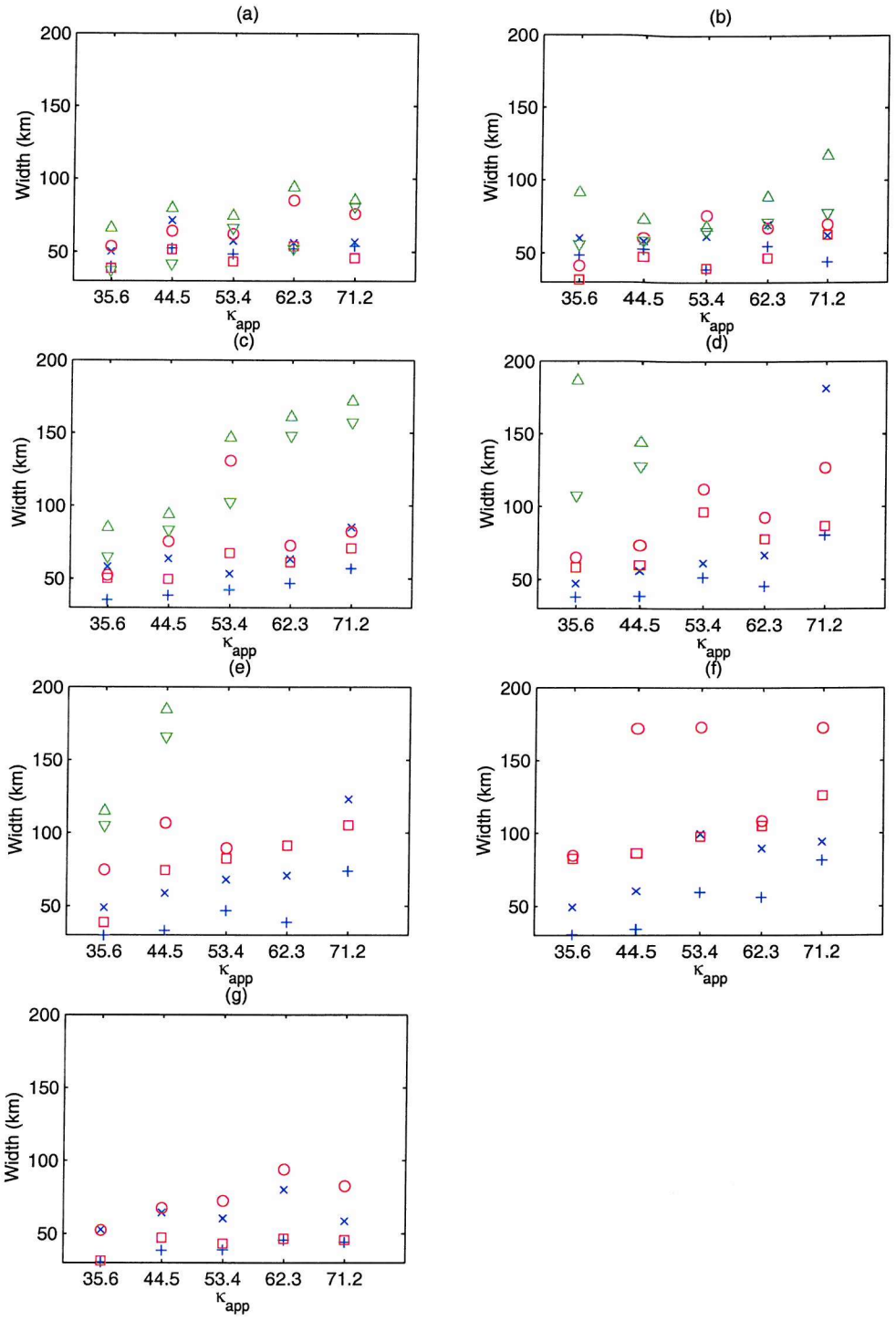

Figure 6.3.7: Variation of minimum and modal logistic tracer widths with applied effective diffusivity (m^2s^{-1}) on: (a) day 9, (b) day12, (c) day 15, (d) day 18, (e) day 21, (f) day 24, (g) average over all above days. The higher value is each colour is the modal value while the lower is the minimum. Blue +/x: μ=0.1 d^{-1}, □/O: μ=0.5 d^{-1}, green ∇/Δ: μ=1.0 d^{-1}, where μ is the maximum tracer growth rate. 'Missing' points for highest growth rate cases are due to lack of filamental structure at later times.

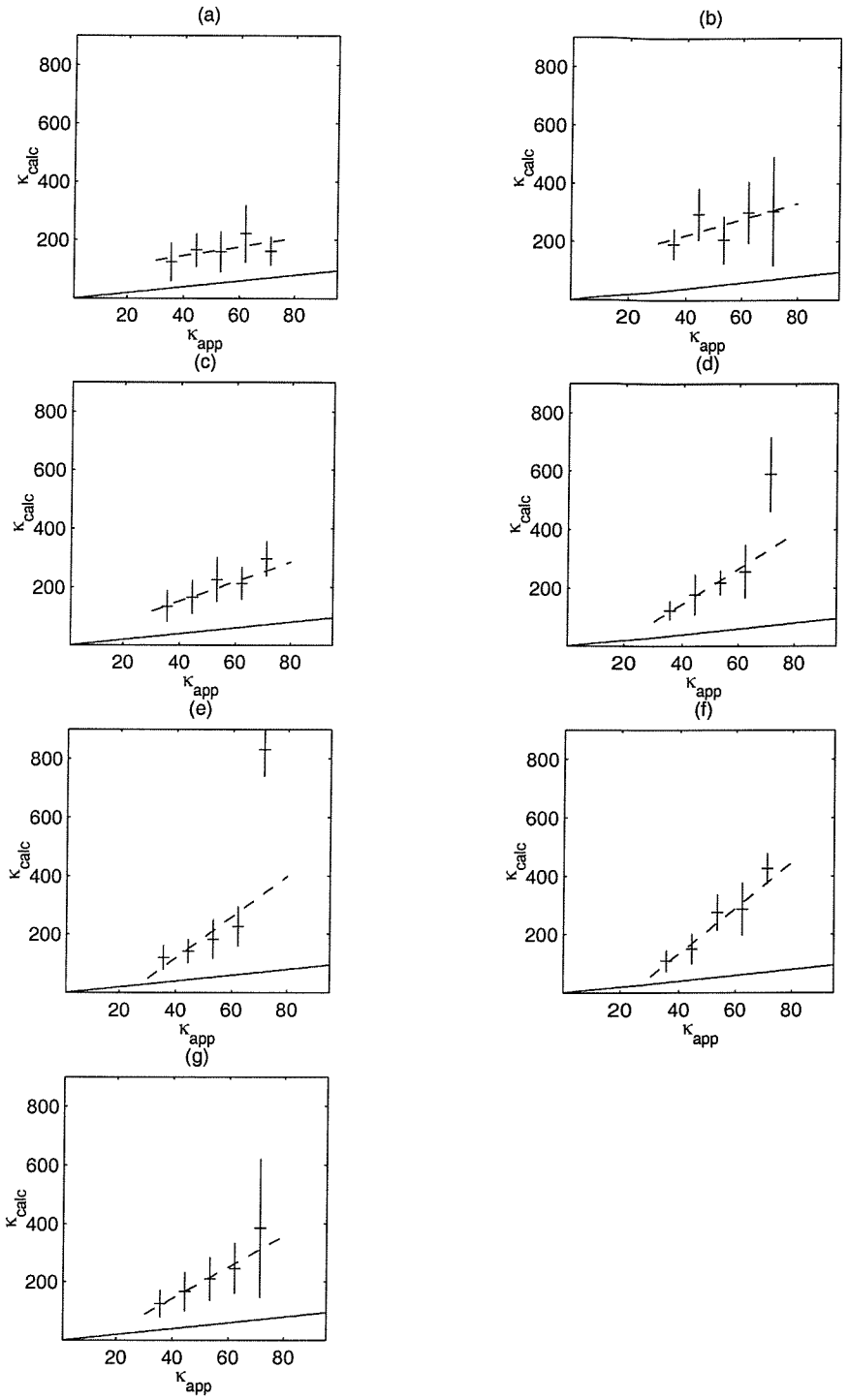

Figure 6.3.8(a): Plot of calculated versus applied effective diffusivity (m^2s^{-1}) for logistic tracer, maximum growth rate $\mu=0.1d^{-1}$. Error bars show mean plus and minus one standard deviation. Solid line indicates a 1:1 fit (expected from one-dimensional, uniform strain, theory), dashed line indicates linear regression. Distribution on (a) day 9, (b) day12, (c) day 15, (d) day 18, (e) day 21, (f) day 24, (g) average over all above days.

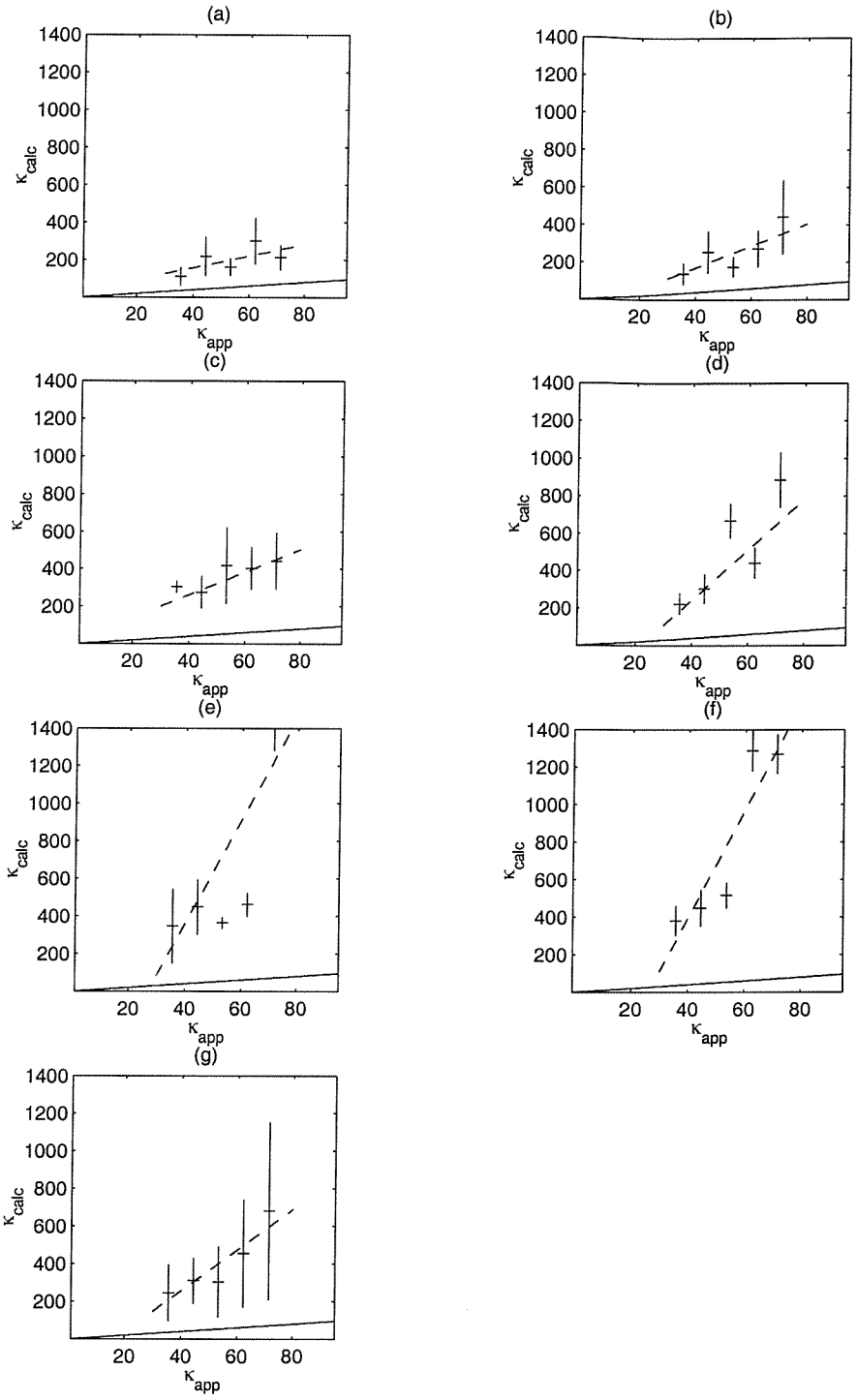

Figure 6.3.8(b): Plot of calculated versus applied effective diffusivity (m^2s^{-1}) for logistic tracer with maximum growth rate μ=0.5 d^{-1}. Error bars showing mean plus and minus one standard deviation. Solid line indicates a 1:1 fit (expected from uniform strain theory), dashed line indicates linear regression. Distribution on (a) day 9, (b) day12, (c) day 15, (d) day 18, (e) day 21, (f) day 24, (g) average over all above days.

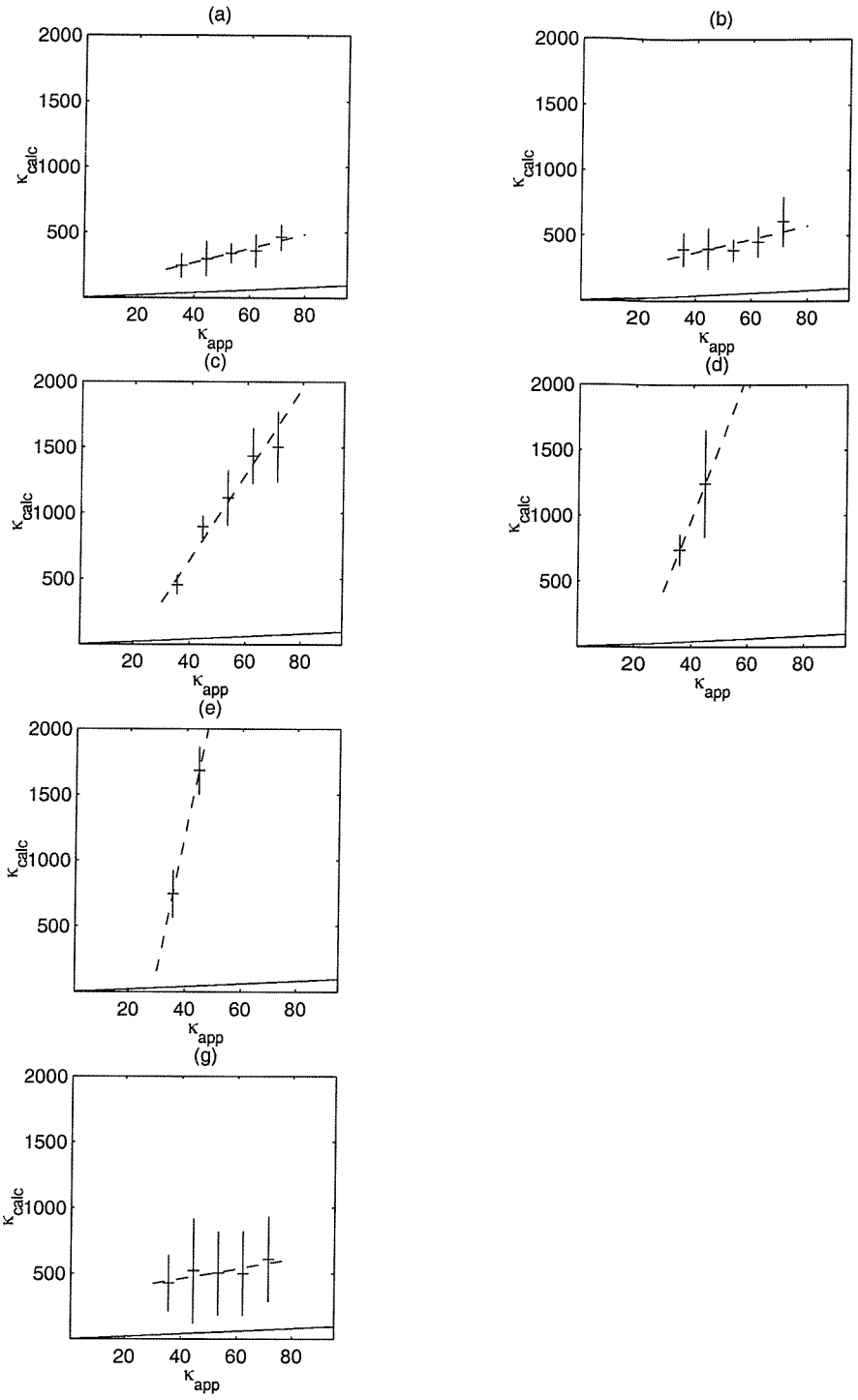

Figure 6.3.8(c): Plot of calculated versus applied effective diffusivity (m^2s^{-1}) for logistic tracer with maximum growth rate μ=1.0d^{-1}. Error bars showing mean plus and minus one standard deviation. Solid line indicates a 1:1 fit (expected from uniform strain theory), dashed line indicates linear regression. Distribution on (a) ~day 9, (b) day12, (c) day 15, (d) day 18, (e) day 21, (g) average over all above days. Missing points (and plot compared to 6.3.8(a) and (b)) are due to no solutions being achieved for the filament at these diffusivities.

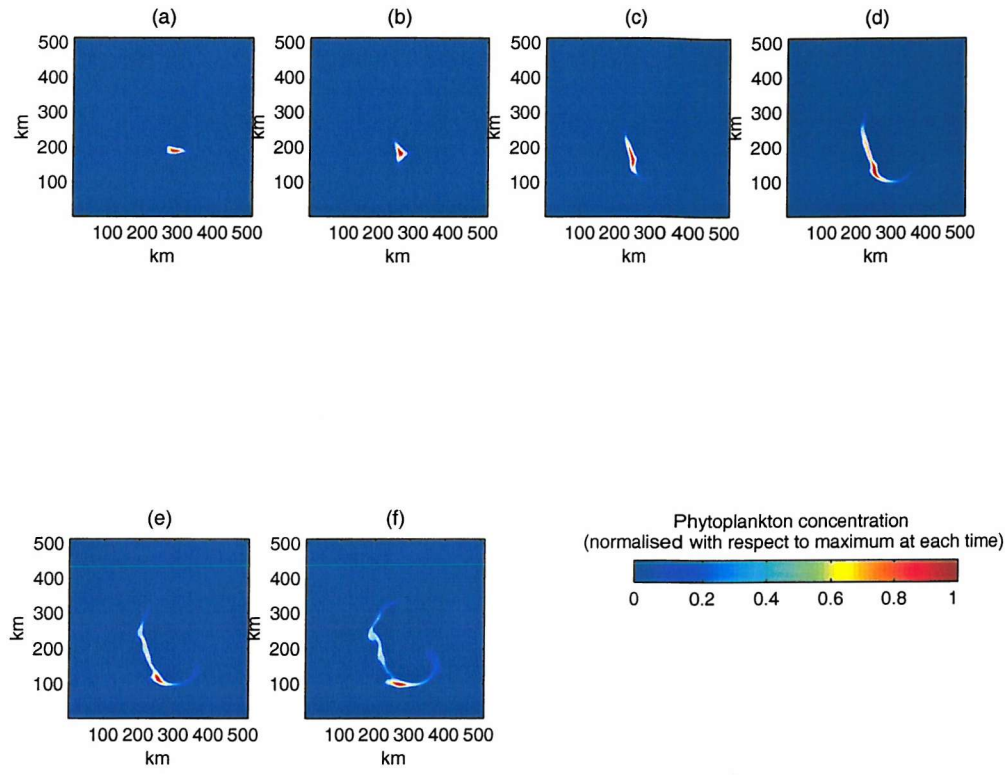

Figure 6.3.9: Evolution of the Phytoplankton filament, Biological Regime: i (hereafter B.R.(i)) N_0=15 mMol N m^{-3}, ε=1.0 (mMol N $m^{-3})^{-2}$ d^{-1}, κ_{app}=107 m^2s^{-1}. Images on day (a) 3, (b) 4, (c) 5, (d) 6, (e) 7, (f) 8. Note visual similarity to inert tracer distribution (figure 4.3.2).

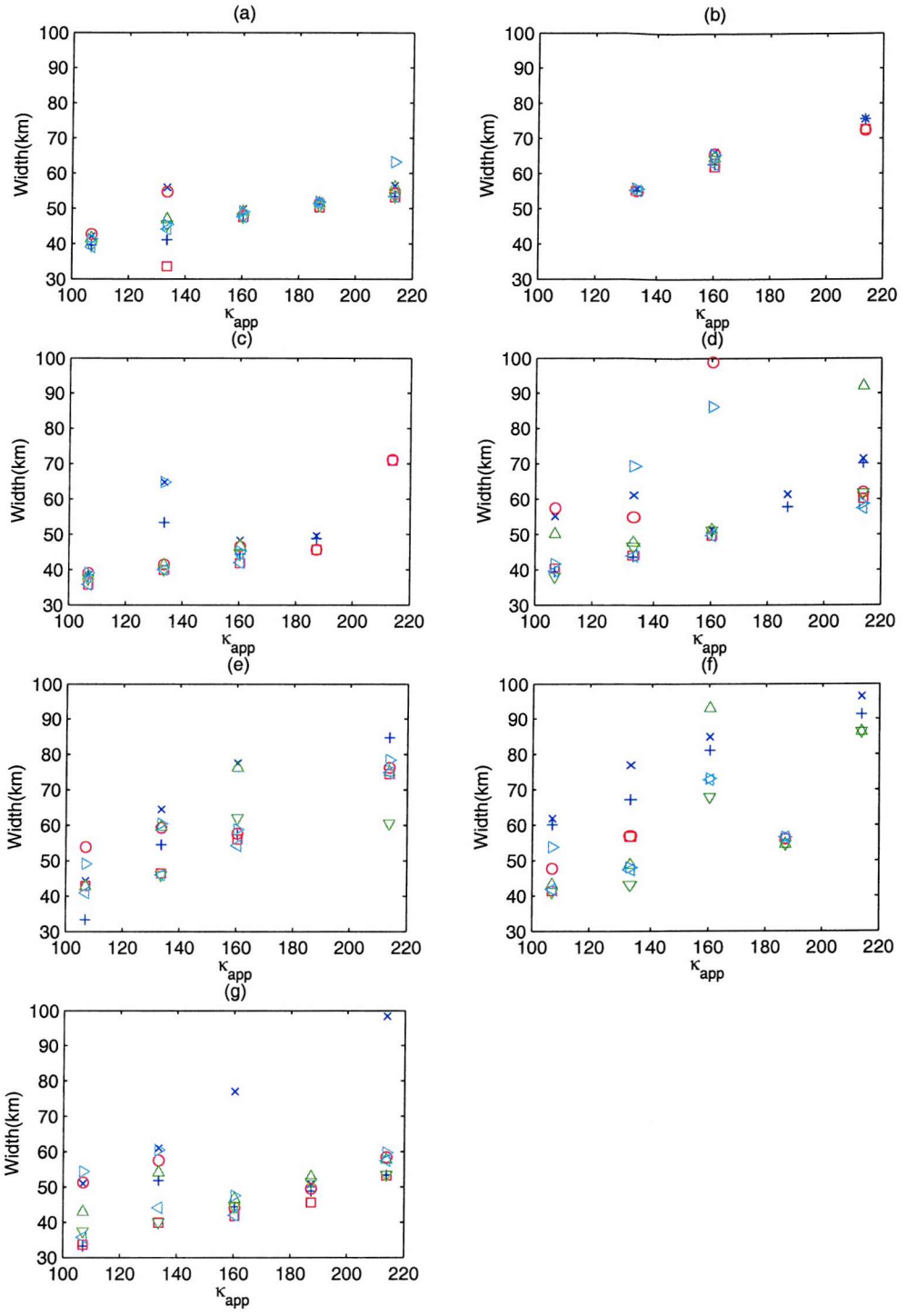

Figure 6.3.10: Variation of minimum and modal P_{NPZD} widths with applied effective diffusivity (m^2s^{-1}) on: (a) ~day 3, (b) day 4, (c) day 5, (d) day 6, (e) day 7, (f) day 8, (g) average over all above days. Blue +/x=B.R.(i), Red □/O=B.R.(ii), green ∇/Δ= B.R.(iii), light blue ◀/▶=B.R.(iv). 'Missing' points are due to lack of sufficiently good curve solutions.

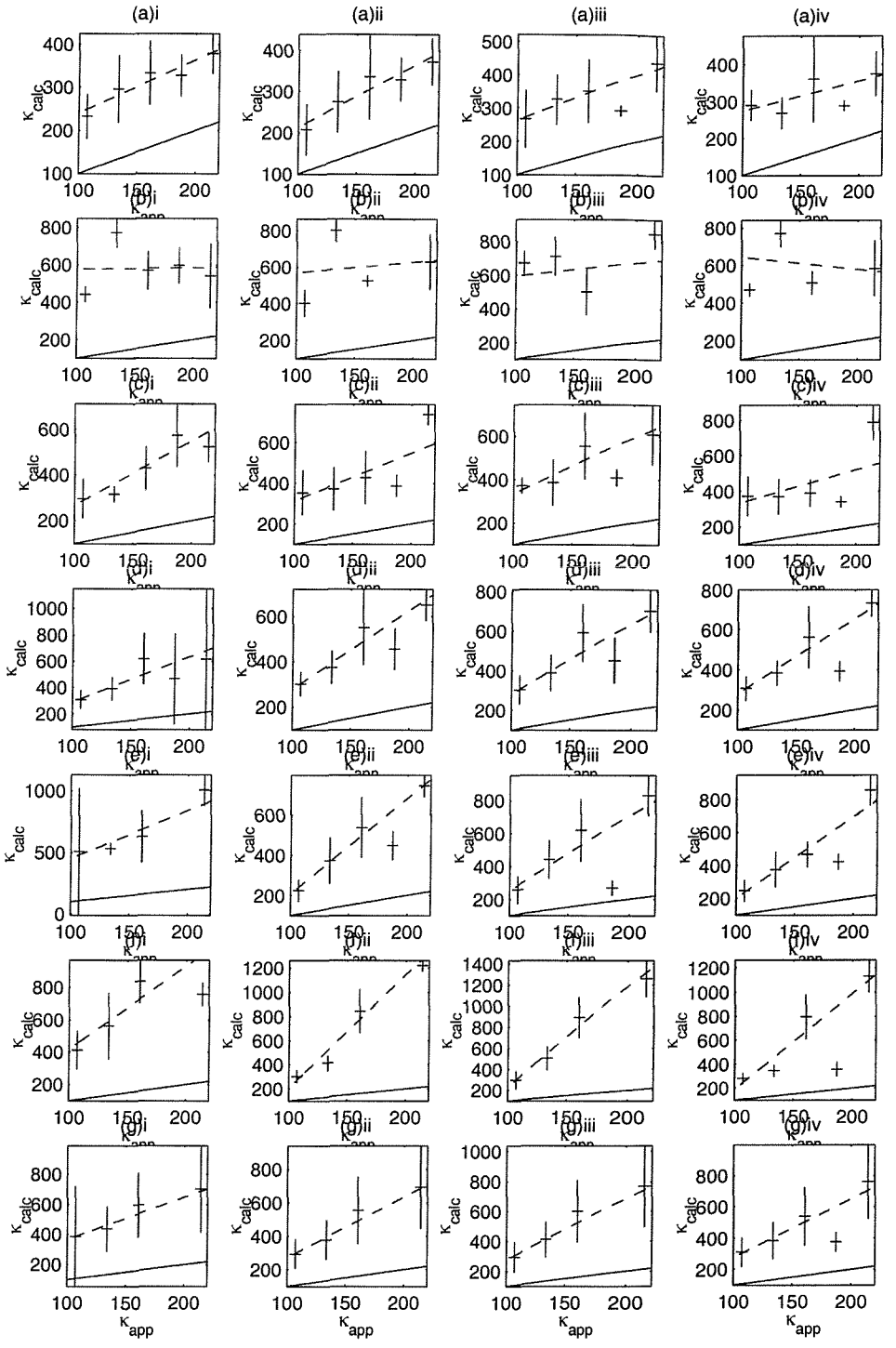

Figure 6.3.11: Plot of calculated versus applied effective diffusivity (m^2s^{-1}) for P_{NPZD}, biological regimes i-iv. Error bar shows mean plus and minus one standard deviation. Solid line indicates a 1:1 fit (expected from one-dimensional, uniform strain theory relating to logistic tracer dispersal), dashed line indicates linear regression. Distribution on (a) day 3, (b) day 4, (c) day 5, (d) day 6, (e) day 7, (f) day 8, (g) average over all above days.

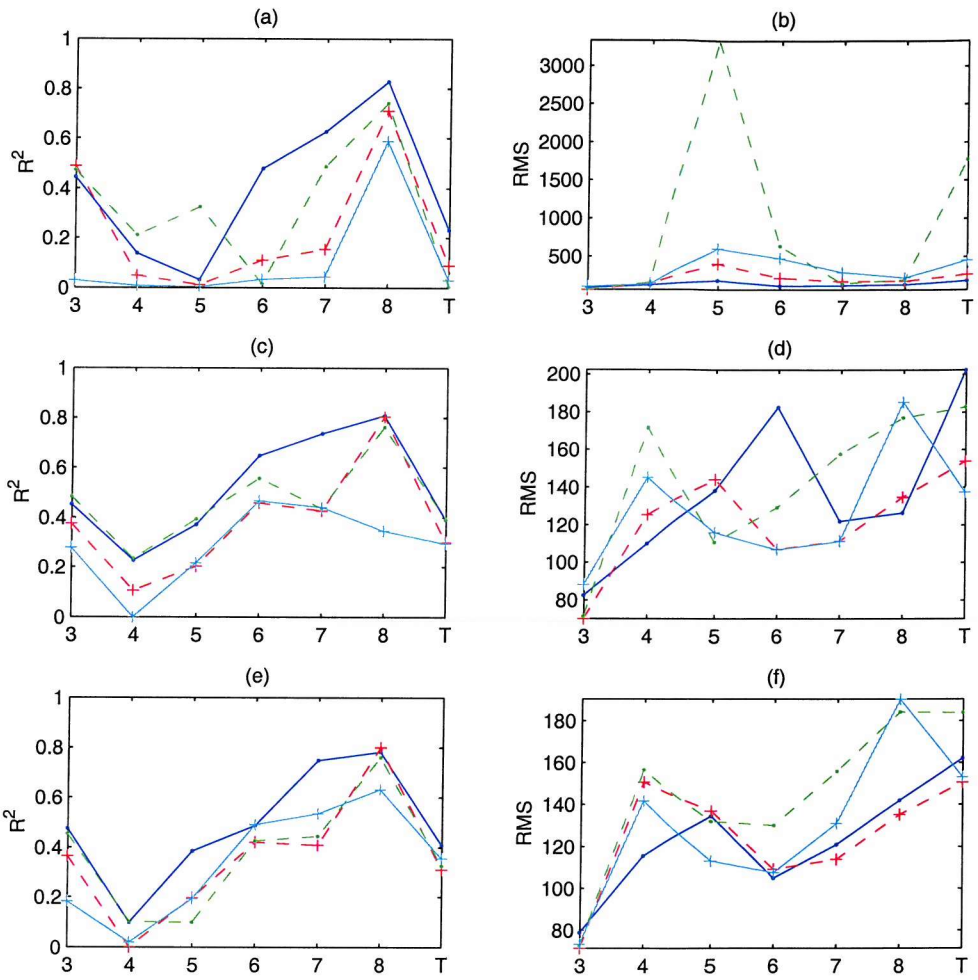

Figure 6.3.12: R^2 and RMS error for a regression of calculated to applied effective diffusivity (m^2s^{-1}) on days 3-8, plus 'T' the regression for values from all times using the widths of (a)/(b) Nutrient, (c)/(d) Zooplankton, and (e)/(f) Detritus. Blue '.' and solid line=B.R.(i), red '+' and dashed line= B.R.(ii), green '.' and dashed line= B.R.(iii), light blue '+' and solid line=B.R.(iv).

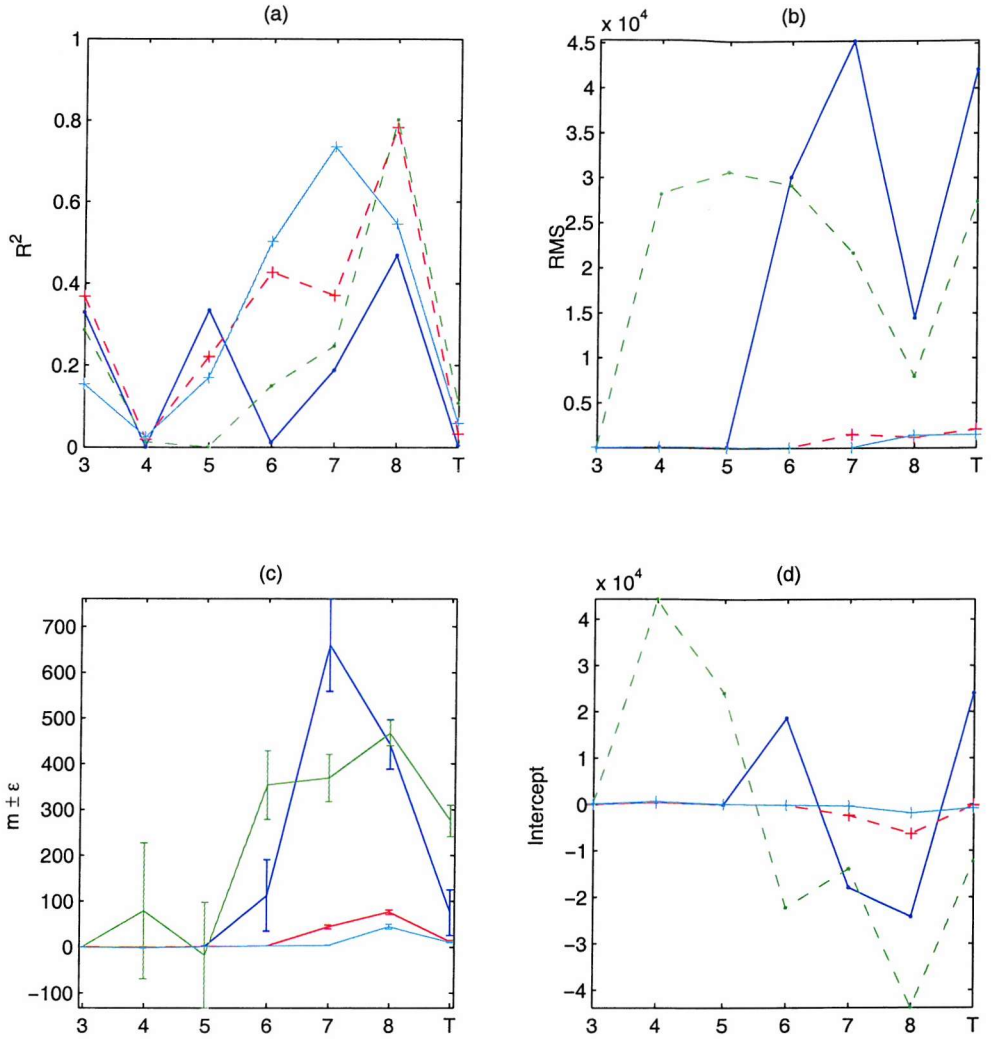

Figure 6.3.13: Results for P_{NPZD} compartment of NPZD ecosystem model using rate of change of biomass as the measure of growth rate. (a)R^2 (b) RMS error, (c) gradient (m) plus/minus one standard deviation (ε) in the gradient, (d) Intercept of the linear fit for a regression of calculated to actual applied effective diffusivity on days 3-8, plus 'T' the regression for values from all times. Blue '.' and solid line=B.R.(i), red '+' and dashed line= B.R.(ii), green '.' and dashed line= B.R.(iii), light blue '+' and solid line=B.R.(iv).

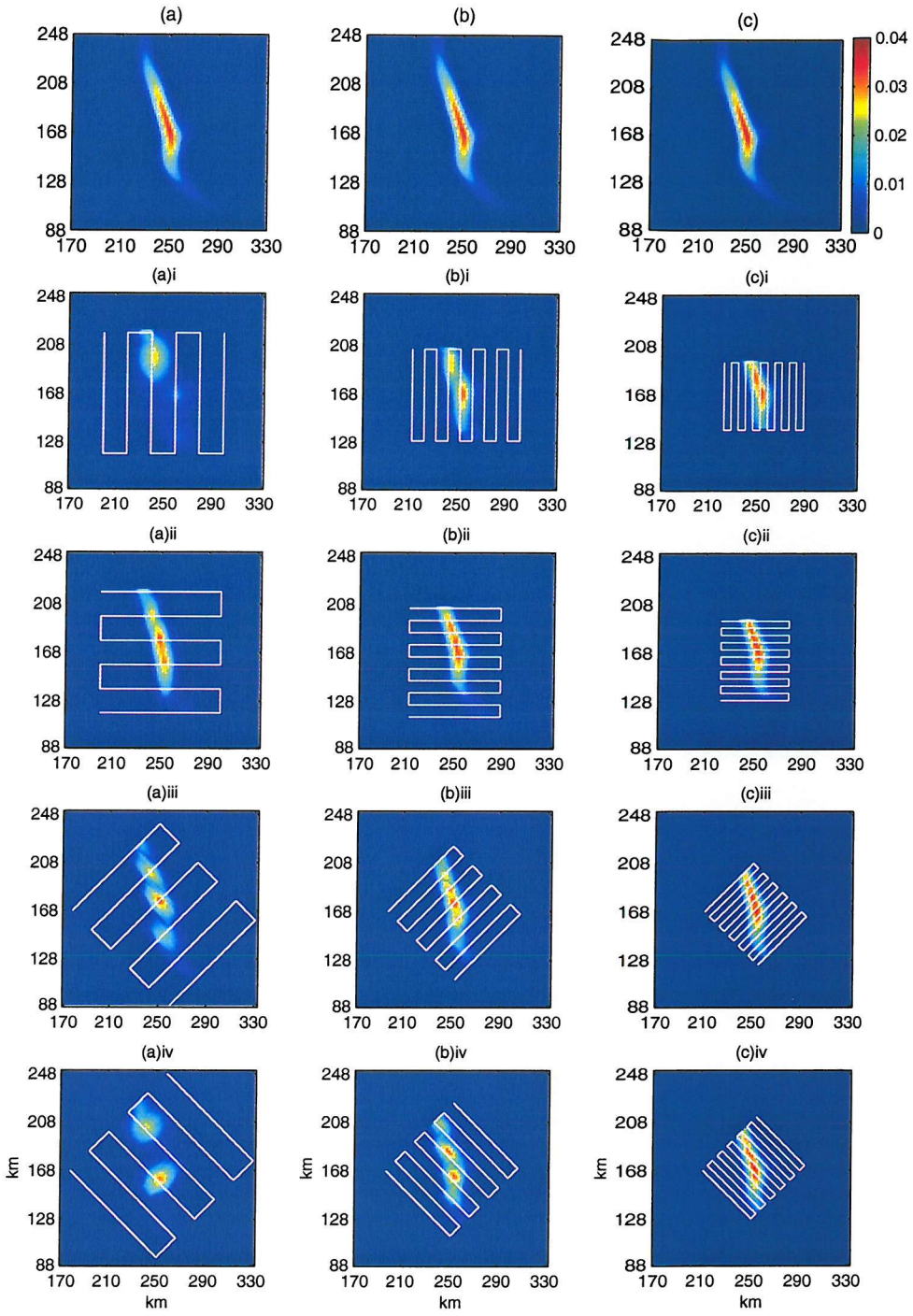

Figure 7.3.1: Original and gridded inert tracer fields for survey track spacing of (a) 20Km, (b) 10Km, and (c) 5Km, at orientations i-iv. Gridded field shown overlain with the respective sampling strategy. Both axes show distance in kilometres. Colour bar (tracer concentration in mMol m^{-3}) shown in the top right applies to all plots.

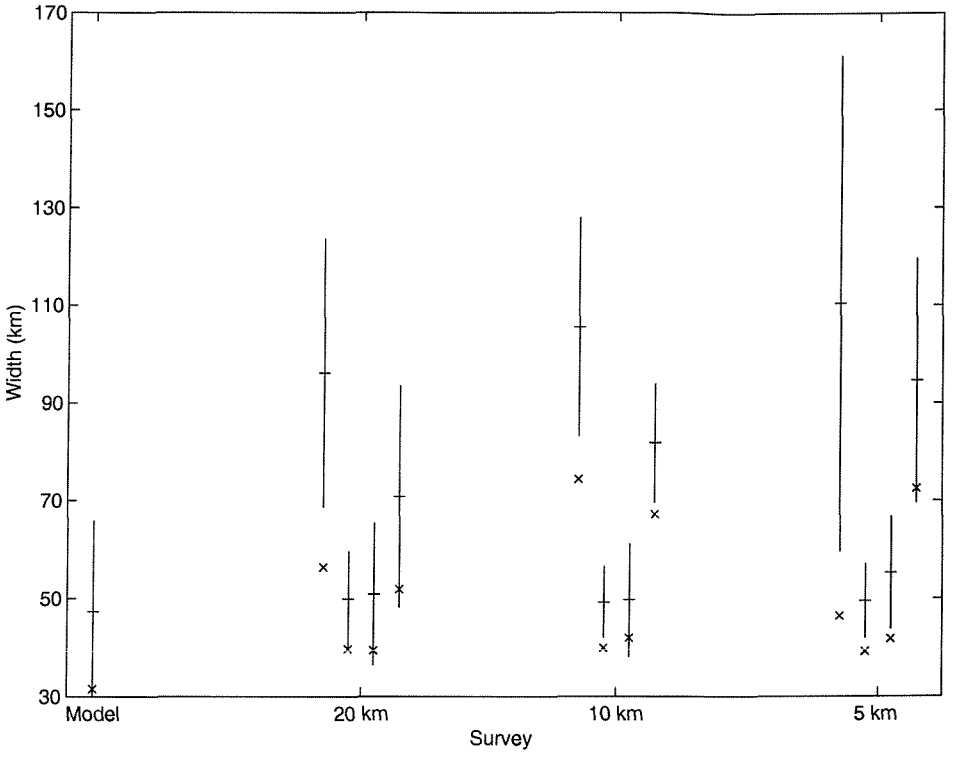

Figure 7.3.2: Minimum width (×), and mean (+) plus/minus one standard deviation (bars) for width of an inert tracer for the model "truth" analysis, plus each size and orientation of survey. Track spacing as labelled. Orientations (i-iv) plotted in numerical order, left to right, for each size survey.

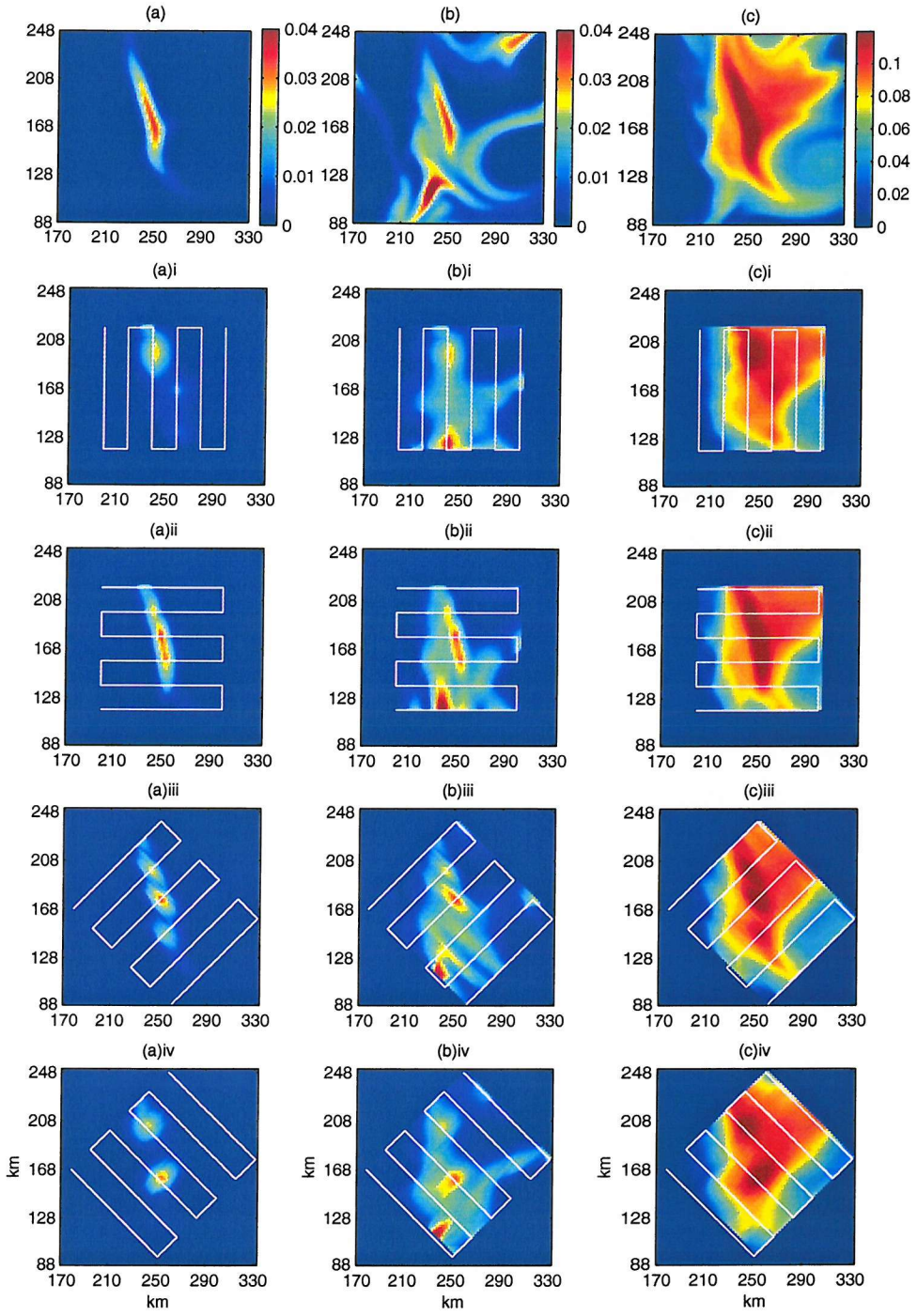

Figure 7.3.3: Original and re-gridded tracer fields for inert tracer interference experiment. Tracer initialised in (a) single patch, (b) multiple patches, and (c) single patch above a background level. 20Km survey track spacing in orientations, i-iv. Re-gridded tracer field shown overlain with respective survey track. Colour bar (mMol m^{-3}) applies to all plots within subsets (a)-(c).

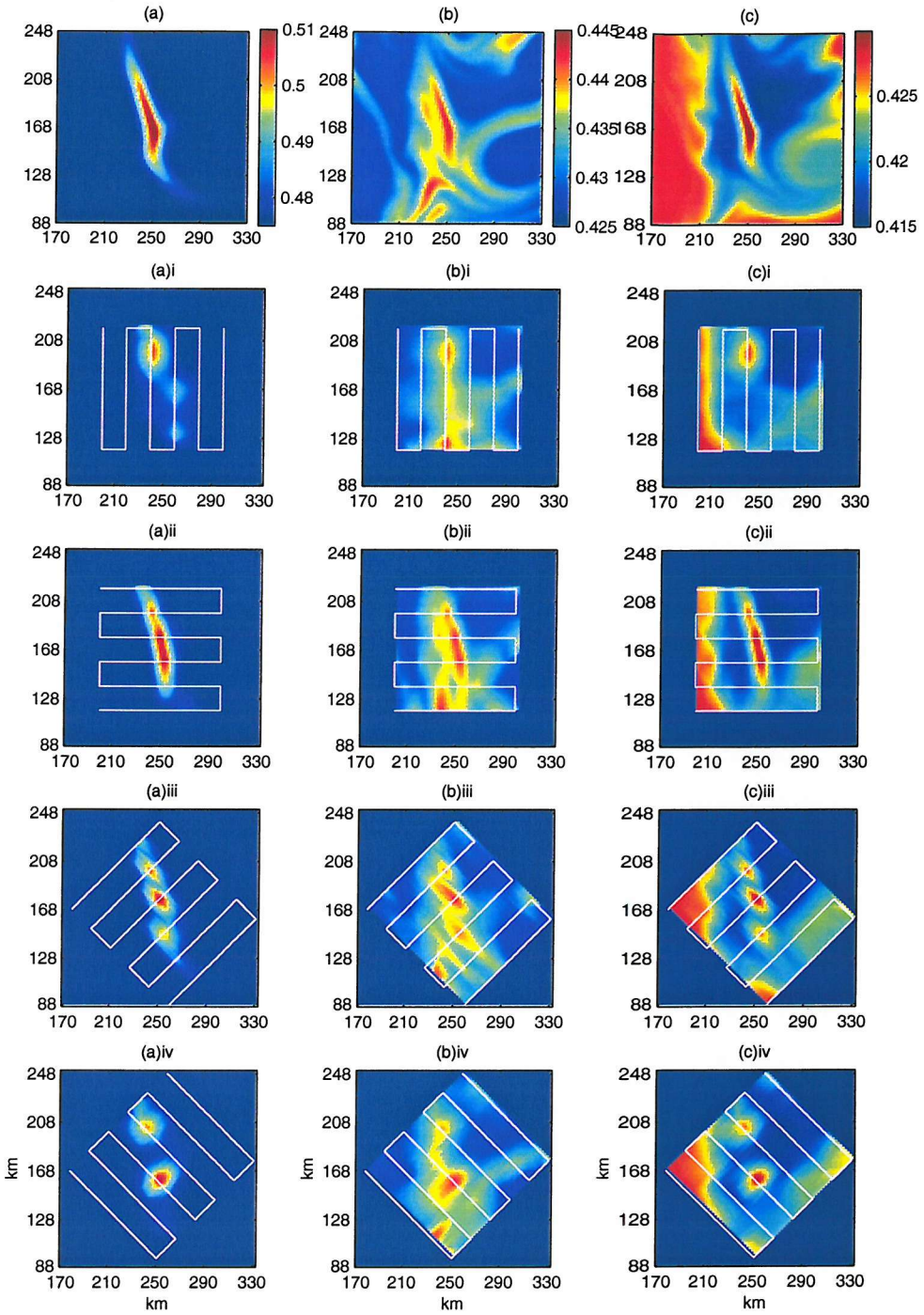

Figure 7.3.4: Original and re-gridded phytoplankton fields for interference experiment. Distributions induced from a spiking in the nitrate field initialised in (a) single patch, (b) multiple patches, and (c) patch above a non-equilibrium level. 20Km track spacing in orientations, i-iv. Re-gridded fields are shown overlain with respective survey track. Colour bar (mMol N m^{-3}) applies to all plots within subsets (a)-(c).

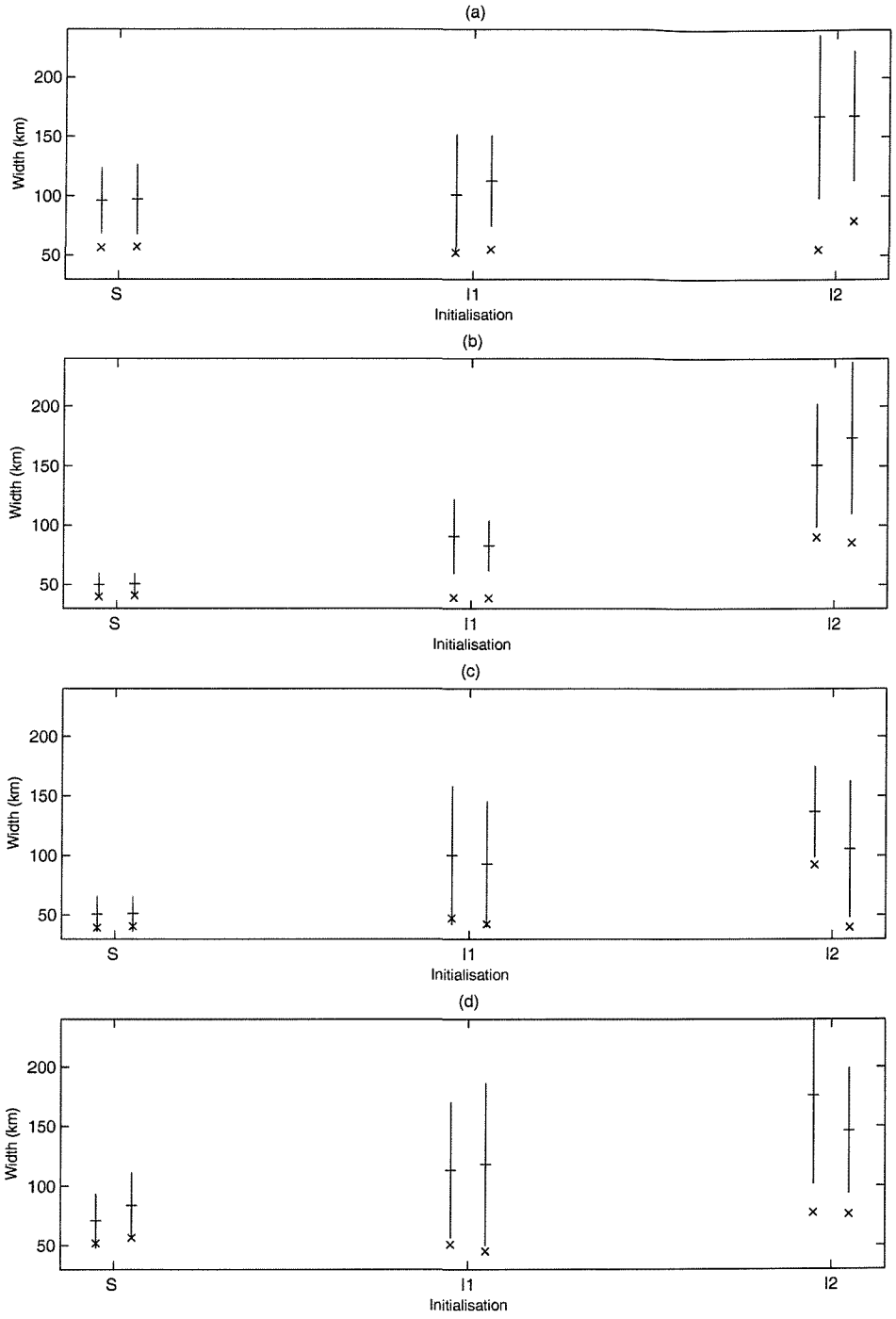

Figure 7.3.5: Minimum width (×), and mean (+) plus/minus one standard deviation (bars) of all measured widths in interference experiment. Results for 'S' the single release, 'I1' multiple releases, and 'I2' release above a background level. For each initialisation the first lines correspond to results for an inert tracer, the second to the Phytoplankton component of an NPZD model. Track orientations (a) i, (b) ii, (c) iii, and (d) iv